LEVEL

1

AIR FORCE INSTITUTE OF TECHNOLOGY

AIR UNIVERSITY
UNITED STATES AIR FORCE

SCHOOL OF ENGINEERING

WRIGHT-PATTERSON AIR FORCE BASE, OHIO

AFIT/GAE/AA/78M-14

EVALUATION OF THE THREE PARAMETER WEIBULL DISTRIBUTION FUNCTION FOR PREDICTING FRACTURE PROBABILITY IN COMPOSITE MATERIALS.

THESIS

AFIT/GAE/AA/78M-14 Dennis Schneider
Capt USAF

AFIT/GAE/AA/78M-14

EVALUATION OF THE THREE PARAMETER WEIBULL DISTRIBUTION FUNCTION FOR PREDICTING FRACTURE PROBABILITY IN COMPOSITE MATERIALS

THESIS

Presented to the Faculty of the School of Engineering
of the Air Force Institute of Technology
in Partial Fulfillment of the
Requirements for the Degree of
Master of Science

by

Dennis R. Schneider, B.S.A.E.
Captain USAF
Graduate Aeronautical Engineering

March 1978

Approved for public release; distribution unlimited.

Preface

The Weibull distribution function has been widely used as a statistical tool for predicting the fracture probability in structural materials. Application of this statistical method to composite materials addressing nonuniform stress distributions and the three parameter form of the theory has been very limited. I have performed an evaluation of the three parameter Weibull distribution function applied to a composite material under both uniform and nonuniform stress distributions which includes establishment of a parameter determination methodology as well as the evaluation of the theory's ability to predict fracture across a variety of failure modes.

I am deeply indebted to several individuals who assisted in the conduct of this thesis. I am very grateful to my thesis advisor, Dr. Anthony N. Palazotto, for his guidance, encouragement and counseling which aided immensely throughout this study; to Dr. James Whitney and Mr. Marvin Knight of the Air Force Materials Laboratory for their support and assistance in providing the experimental data required to conduct this thesis. A special thanks to my family for their patience during this trying time, and especially to my wife, Jean, for her many hours of dedicated typing support.

Dennis R. Schneider

Contents

List of Figures

*including strain gaged specimen ** without strain gaged specimen

*including strain gaged specimen **without strain gaged specimen

*including strain gaged specimen **without strain gaged specimen

List of Tables

List of Symbols

B	risk of rupture
b	width of specimen in y-direction, in.
E_{11}, E_{22}	modulus of a unidirectional composite in the longitudinal and transverse direction of the fiber axes, respectively, lb/in^2.
$\bar{E}$	effective bending modulus of a laminated beam, lb/in^2.
G_{12}	shear modulus of a unidirectional composite in the 1-2 plane, lb/in^2.
h	thickness of specimen, in.
h_k, h_{k-1}	distance from the neutral axis to the two outer edges of the k th lamina within a laminated plate, in.
I	beam area moment of inertia, in^4.
k	lamina number within a laminated plate.
K_x, K_y, K_{xy}	curvature in a plate.
L	specimen length, in.
m	flaw density exponent (shape parameter).
$\bar{m}$	interger less or equal to m.
M	bending moment applied to a beam, lb-in.
M_x	bending moment per unit length of plate surface, lb-in/in.
N	axial force per unit length of plate surface, lb.
P	load on specimen, lb.
p	lamina in which $\sigma = \sigma_u$ occurs.
$Q_{ij}, \bar{Q}_{ij}$	terms in the composite laminate stiffness matrix in the material and load axes, respectively, lb/in^2.
r	dummy variable used in series notation.

S	probability of fracture.
u,v,w	displacements of a specimen in the x,y,z directions, respectively, in.
V	volume of a specimen, in^3.
x,y,z	load axis of a specimen.
$1,2,3$	material property axis of a specimen.
	fractional portion of the term m.
$\epsilon_1,\epsilon_2,\epsilon_{12}$	strains in the material axis, in/in.
$\epsilon_x,\epsilon_y,\epsilon_{xy}$	strains in the load axis, in/in.
$\epsilon_x^o,\epsilon_y^o,\epsilon_{xy}^o$	strains in the mid surface of a plate, in/in.
	Poisson's ratio in the longitudinal and transverse material directions, respectively.
$\sigma_1,\sigma_\sigma,\sigma_{12}$	stresses in the material axis, lb/in^2.
$\sigma_x,\sigma_y,\sigma_{xy}$	stresses in the load axis, lb/in^2.
σ	stress in a specimen, lb/in^2.
σ_b	bending stress in a specimen, lb/in^2.
σ_m	mean failure stress of a distribution, lb/in^2.
σ_o	scale parameter, lb/in^2.
σ_{ot}	scale parameter for tension normalized for volume, lb/in^2.
σ^*_{ot}	scale parameter for tension normalized for the distribution, lb/in^2.
σ_{o3pt}	scale parameter for three-point loading normalized for volume, lb/in^2.
σ_u	zero probability strength parameter (location parameter), lb/in^2.

Abstract

This thesis is an evaluation of the three parameter Weibull distribution function for predicting fracture in a composite material subjected to failure under both uniform and nonuniform stress distributions. The specific forms of the three parameter Weibull equations for these failure modes are derived for a general laminated composite and simplified for the special case of a unidirectional composite. An analysis into a parameter determination methodology which is mathematically reproducible is presented. The resulting expressions and methodology are applied to experimental bending, tension and three-point loading failure data for 0-degree and 90-degree unidirectionally laminated graphite-epoxy specimens. Weibull parameter sets are derived from both the bending and tension experimental data. Each set is then used to evaluate the theory's ability to predict the probability of failure throughout the three failure modes and thereby to establish a single set characteristic of the material. Although a set of parameters peculiar to each failure distribution was obtained, a characteristic set of values capable of predicting failure across the variety of failure modes was not found for this composite material.

EVALUATION OF THE THREE PARAMETER WEIBULL DISTRIBUTION FUNCTION FOR PREDICTING FRACTURE PROBABILITY IN COMPOSITE MATERIALS

I. Introduction

Background

The classical theory of strength can readily be shown to be incompatible in material failure prediction when compared with experimental measurements. This is most easily demonstrated by the dispersions in ultimate strength which occur in experimental measurements.

In the past this variability of ultimate strength has generally been treated as relatively unimportant, since it could easily be taken into account through the use of large factors of safety. However, with requirements for greater economy, weight restrictions, and increased performance, significant effort towards the development of more accurate failure prediction techniques is being expended. To bridge the inconsistencies between the theoretical strength predictions and experimental data, statistical theories of fracture have become a widely used tool.

The most widely accepted statistical theory of fracture is that based on the Weibull distribution function [6,2]. This theory is based on a weakest-link failure concept and relates the probability of fracture to the actual

stress observed at fracture [2]. To fit the physical facts of the experimental variability, the theory has been corrected to a semi-empirical distribution based on experimental data [2]. Two basic criteria of fracture; size and normal tensile stress, are used in the theory, and it is postulated that failure in an isotropic, homogeneous material is fully described by three material dependent parameters; the zero probability strength (location parameter), the flaw density exponent (shape parameter) and a scale parameter [7]. Within the validity of these criteria, the theory can describe failure for any type of stress distribution [6].

Use of this theory has been applied to a large variety of materials, from ceramics to laminated composites. Daniel and Weil [6] investigated the effects of a stress gradient on the fracture characteristics of brittle materials; Bortz and Weil [2] investigated the applicability of Weibull's semi-empirical distribution function to ceramic oxides, deriving the Weibull material parameters under various condition of test temperature, heat treatment, surface conditions as well as specimen size; Kaminski [11] studied the effects of specimen geometry on the predictability of the strength of a composite material; and Knight and Hahn [12] performed experiments on randomly-distributed short fiber composites, looking at the statistical characteristics of the experimental data by use of the Weibull distribution

function.

Most of the efforts investigating fracture using statistics have dealt with homogeneous isotropic materials, with a lesser emphasis towards composite materials. However, with present day interest, especially within the aerospace industry, being placed on such factors as weight, strength, and performance, the composite material has taken on an important role in the development of lighter-weight high-strength aerospace structures. Even though modern manufacturing procedures of this material allow for carefully controlled manufacturing conditions, its precise breaking strength cannot be accurately predicted [9]. The variability of breaking strengths in a composite is identical in nature to that found for other materials, even when specimens are tested under assumed identical test conditions. It is this variability among a controlled population which necessitates accurate statistical approaches to the fracture process.

The Weibull distribution function can be applied to experimental data in either a two parameter or three parameter form. Each characterization has been investigated using both uniform and nonuniform stress distributions.

A discussion of the parametric equations and related functions is provided in Section II of this thesis, however, it is important at this point to mention some previous efforts relative to the Weibull theory.

Daniel and Weil [6] addressed in detail the three parameter form of the Weibull equation for both uniform and nonuniform stress distributions. Columbia Resin (CR-39) was used as the experimental material. The theoretical derivations for different stress fields are presented based on elementary beam theory applied to a prismatic beam under four-point loading. The resulting set of statistical equations provides a means with which the probability of fracture can be predicted for a variety of loading conditions and stress distributions assuming the three material parameters are known. The hypothesis in their development is that the three parameters are in fact "material" constants. This is substantiated by graphically confirming a close correlation between theoretical and experimental data. Although a set of three material parameters was established and verified for one set of experimental data, no verification of this set of parameters with data from different stress distributions was provided. Similar efforts have since been completed using composite materials, however, detailed theoretical validation is very limited.

Daniel and Weil also developed analytical means for determining the unknown material parameters from a given set of experimental data. Their method involved the simultaneous solution of a system of three equations with three unknowns. However, due to computational difficulties which were experienced, the graphic method devised by Weibull [16]

proved to be much easier for parameter determination.

Since the composite material provides a material with unique characteristics when compared to conventional structural materials, the applicability of the approach developed by Daniel and Weil is of significant interest. Furthermore, the verification of whether a given set of material parameters will allow the prediction of fracture probability throughout a variety of loading conditions would confirm that the parameters are in fact material related. More important, this evidence could provide a significant cost savings in terms of the number tests required to determine general fracture characteristics of a material.

Purpose

There are four separate purposes to be investigated in this thesis.

The first purpose is to establish the basic forms of the Weibull equation for a composite lamina under uniform and nonuniform stress distributions using the approach developed by Daniel and Weil for a homogeneous isotropic beam [6]. Classical laminate theory is expanded in the Weibull equation form for bending, tension and three-point loading conditions. The equations are derived using general composite material notation and then reduced to a simplified, single lamina form, for the specific specimen being used in this study. Composites with only unidirectional ply orientations (0-degree and 90-degree) are investigated.

The second purpose is to obtain experimental fracture data for graphite-epoxy to allow validation of the above equations. The material parameters are derived from experimental pure bending data gathered to form the characteristic fracture distribution of the material. Twenty-five tests will form this distribution. Both the analytical methods described in [7] as well as the trial and error graphical method recommended by Weibull [16] are used to determine the material parameters. Procedures to permit reproducibility of the parameters and parameter associated sensitivities are addressed.

The third purpose of this thesis is to investigate the extendability of the three parameters found from bending tests to other failure modes. This will investigate the hypothesis that the parameters are in fact material related numbers. A minimum of 25 tests for both tension and three-point loading will establish the fracture distributions for each. The theoretical equations developed for the first purpose of this study will be solved using the three parameters found from the bending test distribution. The criteria for conformance is the closeness of fit between each experimental distribution and theoretical prediction. Methods of obtaining additional accuracy of fit will also be evaluated.

The fourth purpose is to compare the three parameter and two parameter Weibull function in prediction accuracy.

The two parameter model also considers nonuniform stress, however the third parameter, the location parameter, is assumed to be zero. Factors in comparison include the mathematical difficulty of establishing the three parameter model and variations in fit accuracy when compared to the two parameter model. In addition, suitability of each model across the variety of failure modes is to be addressed.

II. Theory

The theory development for this investigation is presented in three sections. The first two sections will provide a brief background into the basic Weibull theory and classical composite theory. The third section will provide the derivations and equations used in this thesis, which are a combination of the theories described in the first two sections.

Weibull Distribution Function

This section is intended to provide a background of the theoretical considerations of the Weibull theory for the prediction of fracture [6,16] as well as its extension to a variety of stress distributions.

The Weibull theory [16] is based on the concept that brittle materials contain a large number of flaws, which tend to lower the fracture stress of a material below the theoretical rupture stress [2]. These flaws are assumed to be of a random size and distribution throughout the body, and to be the cause of the scatter which is found in experimental fracture data. Two basic critera of failure used in the Weibull distribution function are size and normal tensile stress. For a uniaxial stress field in a homogeneous isotropic material, the probability of fracture for a volumetric flaw distribution is given by

$$S = 1 - e^{-B} \qquad (1)$$

where

$$B = \int_V \left(\frac{\sigma - \sigma_u}{\sigma_o}\right)^m dV \qquad (2)$$

and

B is the risk of rupture

σ_u is the zero probability strength (location parameter)

σ_o is the scale parameter

m is the flaw density exponent (shape parameter)

Equation (1) shows that no special allowance is made for nonuniformity of stress. Each elemental volume with a normal tensile stress is added to form the overall risk of rupture for the specimen. To address the question of nonuniformity [6], one can look at specific case derivations using a prismatic beam under desired loading conditions or stress distributions. The three loading conditions which are investigated in this thesis are; pure bending, three-point loading and tension.

The development of equations accounting for tensile stress gradients can be accomplished using elementary beam theory. Figure 1 shows a prismatic beam under four-point loading and the resulting extreme fiber stress distribution. The section between the minor span is assumed to be in pure bending, while the section between the minor and major span has the type of stress distribution found in a three-point loading condition. These sections can now be addressed separately.

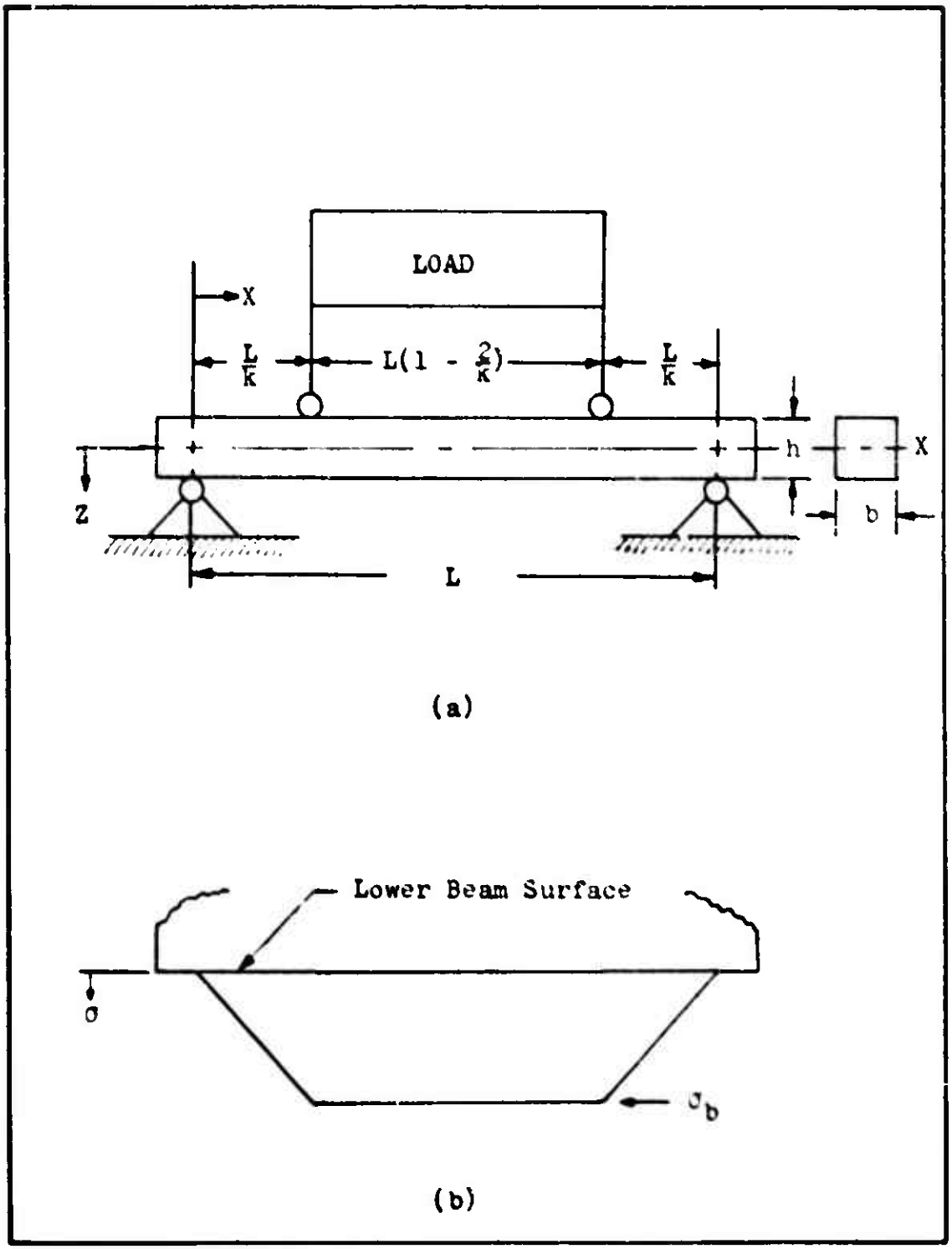

Fig. 1. (a) Four-point Loading Arrangement

(b) Extreme Fiber Stress Distribution

For a pure bending failure, let (k) in Figure 1 be equal to infinity, thereby placing the total length of the beam under pure bending. Using elementary beam theory, the stress distribution within the beam is described by

$$\sigma = \frac{2\sigma_b}{h} Z \tag{3}$$

this assumption can be realized in a four-point bending test using only failures occurring between the minor span as the data samples.

The risk of rupture, Equation (2) can now be rewritten in integral form as follows

$$B = \int_0^b \int_0^L \int_{Z_u}^{h/2} \left(\frac{\frac{2\sigma_b Z}{h} - \sigma_u}{\sigma_0} \right)^m dV \tag{4}$$

where

$$Z_u = \frac{\sigma_u h}{2\sigma_b} \tag{5}$$

Equation (5) is necessary since the three parameter form of the Weibull equation is being used, thereby making the assumption that a stress value exists below which the probability of fracture is zero. A physical interpretation of Z_u is shown in Figure 2 in which the shaded area represents the region where the zero probability failure parameter, (σ_u), is exceeded. The stress gradient for pure bending is as shown for every point along the x - axis. Integrating Equation (4) results in the risk of rupture equation for pure bending

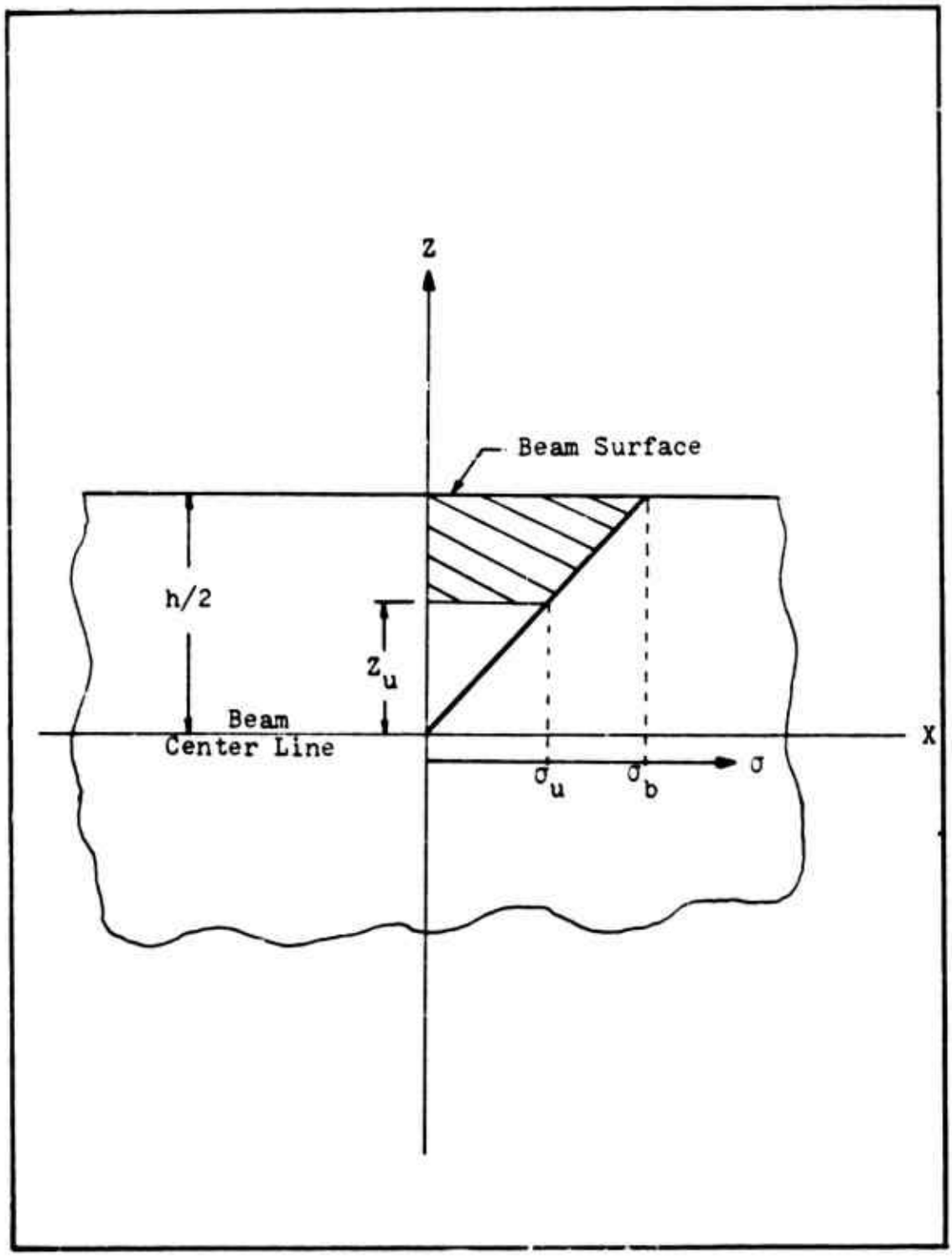

Fig. 2. Stress Distribution - Pure Bending

$$B = \frac{V}{2(m+1)} \frac{(\sigma_b - \sigma_u)^{m+1}}{\sigma_b \sigma_o^m} \tag{6}$$

where V is a dimensionless number expressing the quantity of unit volumes subjected to a uniform tensile stress [2]. Using Equation (6) in Equation (1) the probability of fracture for a beam subjected to pure bending can be found.

The derivation of the risk of rupture for a center or three-point loading condition requires that (k) in Figure 1 be equal to two. This is representative of a beam with a varying moment as shown in Figure 3. According to elementary beam theory, the stress distribution within the beam is described by

$$\sigma = \frac{4\sigma_b}{hL} XZ \qquad 0 \le X \le \frac{L}{2} \tag{7}$$

Equation (2) can now be rewritten using this definition and the following integral limits

$$B = 2 \int_0^b \int_{z_u}^{h/2} \int_{x_u}^{L/2} \left(\frac{\frac{4\sigma_b}{hL} XZ - \sigma_u}{\sigma_o} \right) dV \tag{8}$$

where

$$X_u = \frac{\sigma_u hL}{4\sigma_b Z} \tag{9}$$

and Z_u is given in Equation (5). The limit expressed by Equation (9) represents the point in the x - direction at which the stress reaches the value σ_u. A physical interpretation of x_u is shown in Figure 4. The superimposed

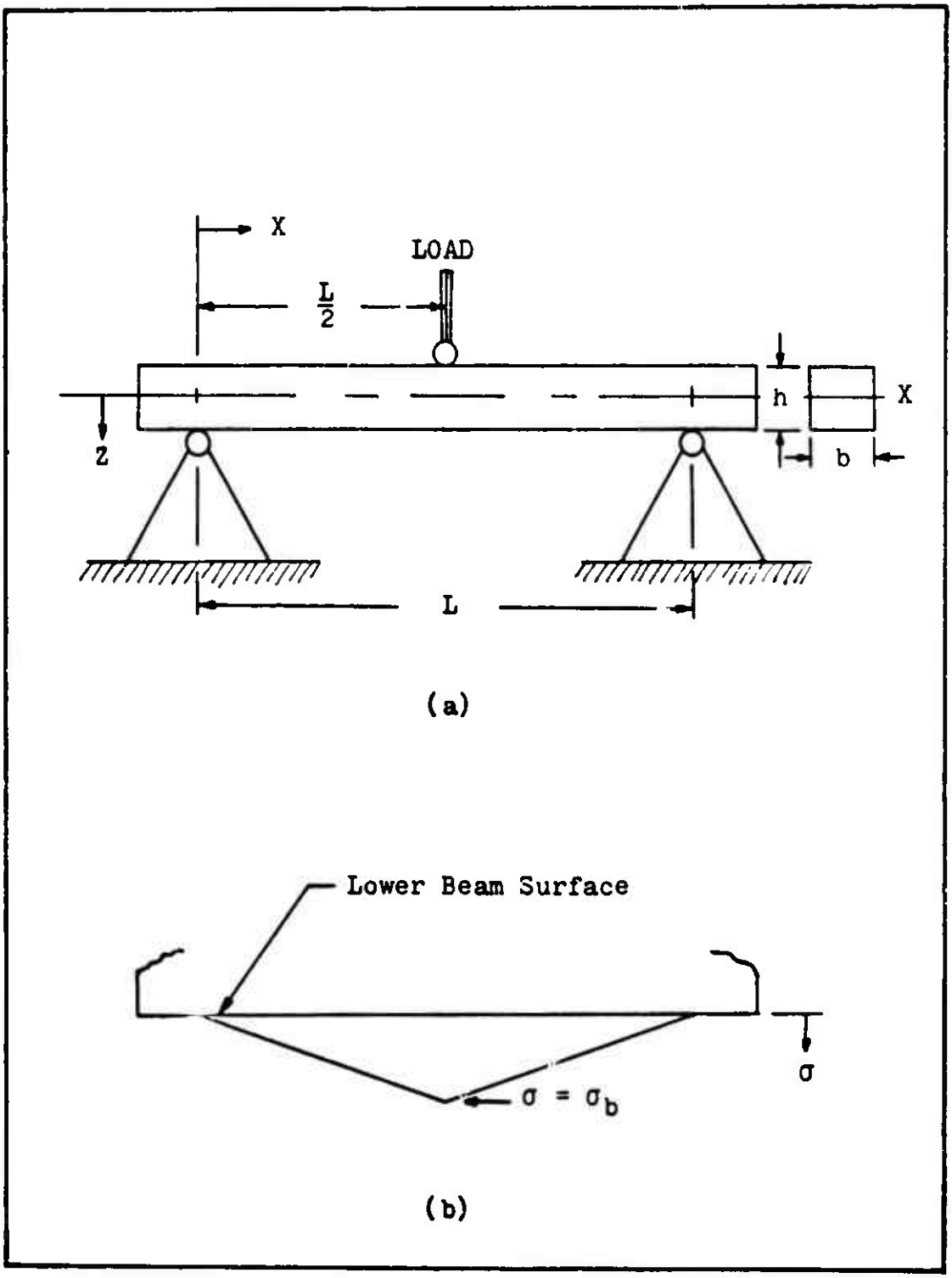

Fig. 3. (a) Third-point Loading Arrangement

(b) Extreme Fiber Stress Distribution

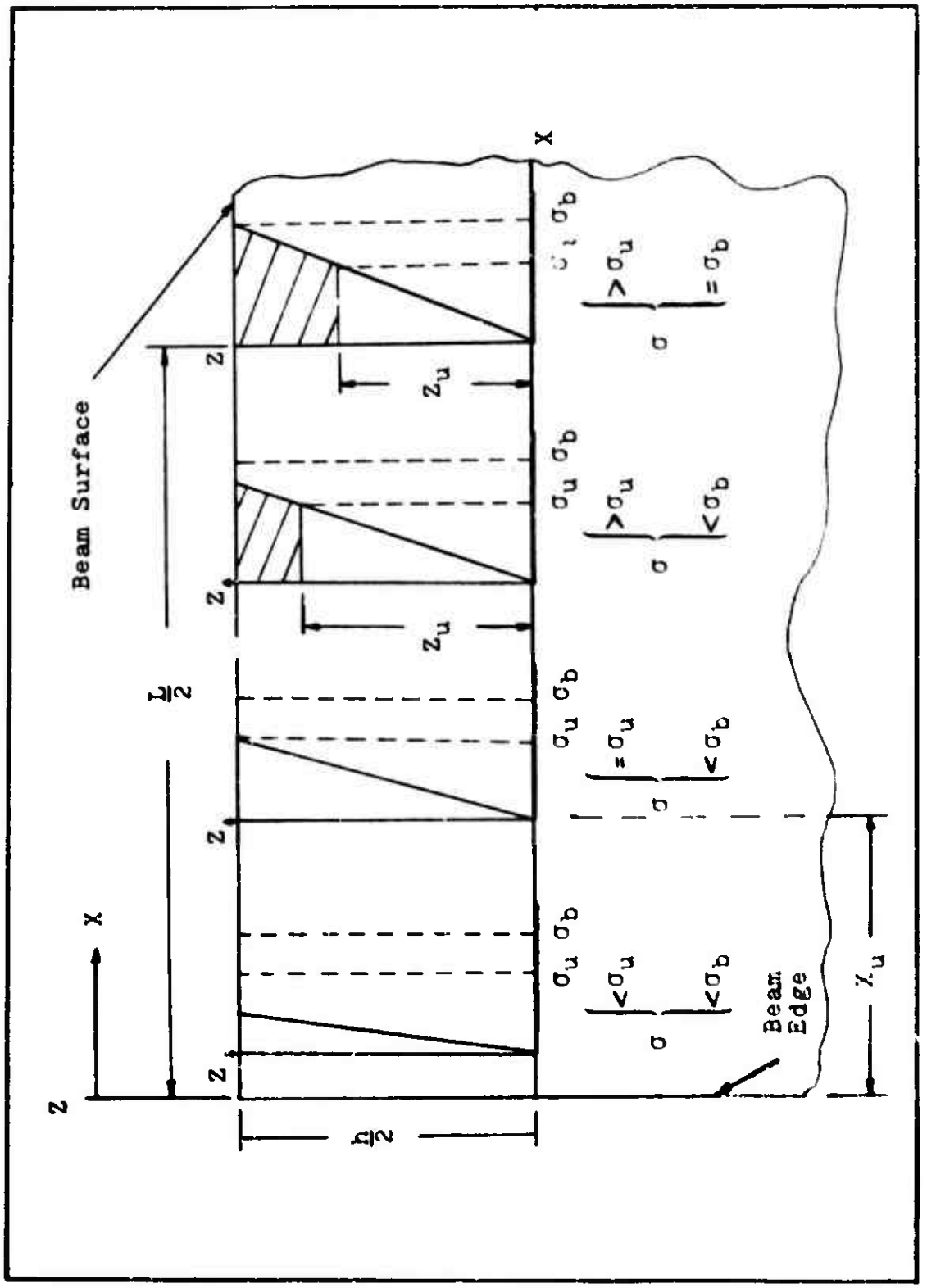

Fig. 4. Three-point Loading Stress Distribution

stress curves show how the stress gradient and extreme fiber stress varies with respect to the x and y axis for this loading condition. Using simple proportions it can be shown that

$$\frac{\sigma_u / Z}{X_u} = \frac{\sigma_b / h/2}{L/2} \tag{10}$$

from which Equation (9) is derived. Integrating Equation (8) results in the risk of rupture equation for a third-point loading condition

$$B = \frac{V}{2(m+1)\,\sigma_b\,\sigma_0^{m}} \left\{ (\sigma_b - \sigma_u)^{m+1} \sum_{r=1}^{\bar{m}} \frac{1}{m+1-r} \left(1 - \frac{\sigma_b}{\sigma_u}\right)^{-r} + (-\sigma_u)^{\bar{m}+1} \int_{z_u}^{h/2} \frac{\left(\frac{2\sigma_b}{h} Z - \sigma_u\right)^{\alpha}}{Z} dz \right\} \tag{11}$$

where

$$m = \bar{m} + \alpha \tag{12}$$

and $(\bar{m})$ is the largest integer less than or equal to (m) and (α) is the decimal fractions of (m). The term (r) is introduced as a dummy variable for the summation term.

Due to the complexity of the mathematics involved in the derivation of Equation (11), a detailed derivation is provided in Appendix A.

The derivation for the risk of rupture under tension loading is the simplest of the three loading conditions being investigated. Figure 5 shows that the stress distribution for this loading results in a uniform stress over the entire thickness of the beam and therefore is expressed as

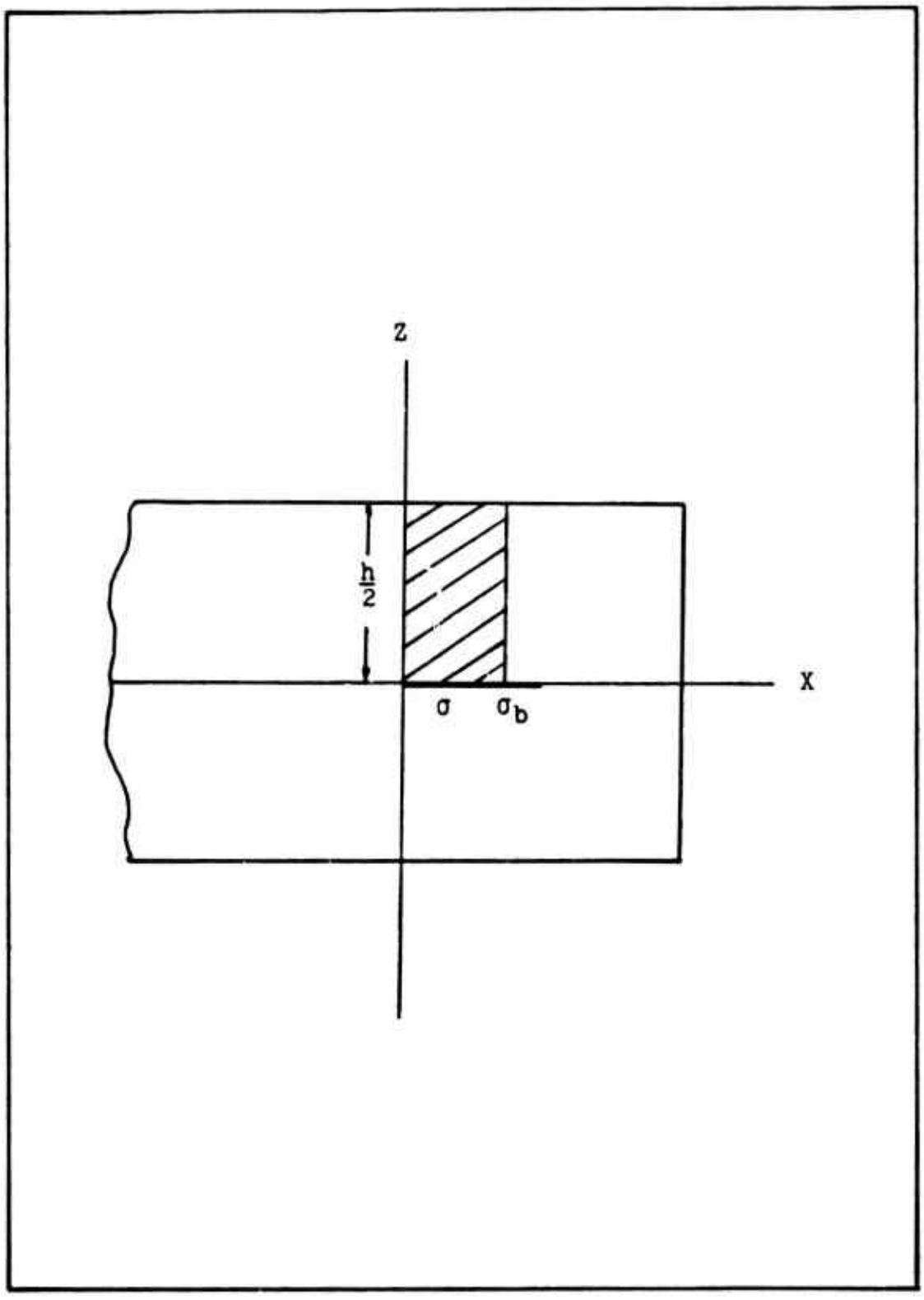

Fig. 5. Stress Distribution for Tension

$$\sigma = \sigma_t \tag{13}$$

The risk of rupture equation therefore becomes

$$B = \int_{-h/2}^{h/2} \int_{0}^{L} \int_{0}^{b} \left(\frac{\sigma_t - \sigma_u}{\sigma_0} \right)^m dV \tag{14}$$

Integrating Equation (14) results in the risk of rupture for tension loading

$$B = V \left(\frac{\sigma_t - \sigma_u}{\sigma_0} \right)^m \tag{15}$$

Once the failure distribution of a material has been established, another characteristic of interest is the distribution mean. Once the three material parameters m, σ_u and σ_0 have been established, the mean failure stress σ_m can be determined and used as a further check on the use of the Weibull theory for a given set of data [2].

$$\sigma_m = \sigma_u + \int_{\sigma_u}^{\infty} e^{-B} d\sigma \tag{16}$$

Equations (6), (11) and (15) represent the basic approach and format of the risk of rupture expressions which will be extended to composite materials.

Classical Composite Theory

This section outlines some of the basic laminated plate relationships (for background see [1,3,10]. Figure 6 indicates the axis system relationships which are used in the derivations, as well as some of the geometry of a laminated composite.

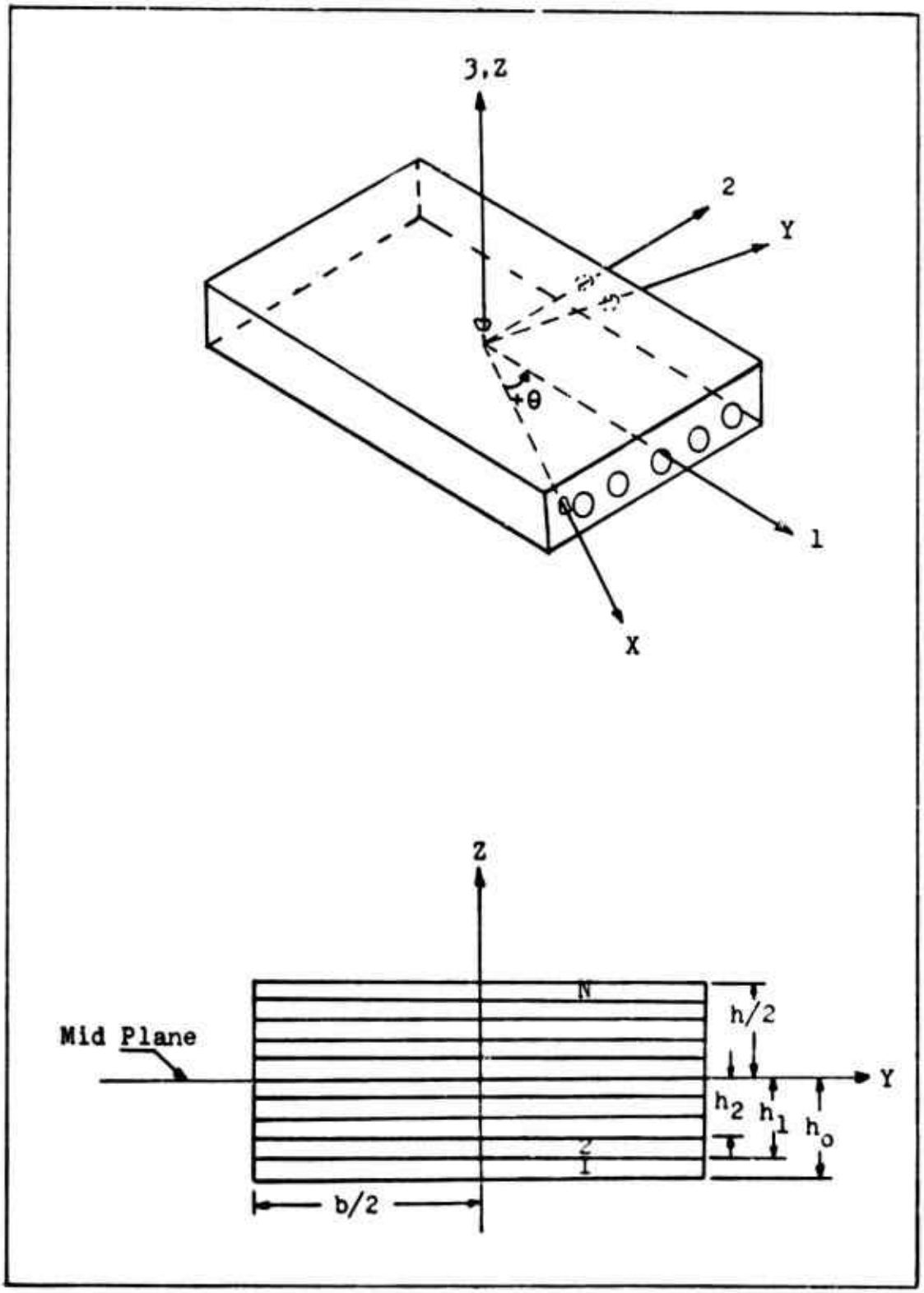

Fig. 6. Lamina Axis System and Cross Section Geometry

The stresses in an orthotopic composite plate, or lamina, can be calculated with the following relationships

$$\begin{Bmatrix} \sigma_1 \\ \sigma_2 \\ \sigma_{12} \end{Bmatrix}_K = \begin{bmatrix} Q_{11} & Q_{12} & Q_{16} \\ Q_{12} & Q_{22} & Q_{26} \\ Q_{16} & Q_{26} & Q_{66} \end{bmatrix}_K \begin{Bmatrix} \epsilon_1 \\ \epsilon_2 \\ \epsilon_{12} \end{Bmatrix}_K \tag{17}$$

where (Q_{ij}) is referred to as the lamina stiffness matrix and whose components are

$$\begin{aligned} Q_{11} &= E_{11} / (1 - \nu_{12}\nu_{21}) \\ Q_{22} &= E_{22} / (1 - \nu_{12}\nu_{21}) \\ Q_{66} &= G_{12} \\ Q_{12} &= \nu_{12} E_{22} / (1 - \nu_{12}\nu_{22}) = \nu_{21} E_{11} / (1 - \nu_{12}\nu_{21}) \\ Q_{16} &= Q_{26} = 0 \end{aligned} \tag{18}$$

and (k) the k th lamina within a laminated composite. The matrix of Equation (17) provides the equations for finding the stress due to loading the material axis. If the stress is desired due to loading in other than the material axis, (x,y,z in Figure 6), rotated some angle θ off the material axis, the stress is found using the following relationship

$$\begin{Bmatrix} \sigma_x \\ \sigma_y \\ \sigma_{xy} \end{Bmatrix}_K = \begin{bmatrix} \bar{Q}_{11} & \bar{Q}_{12} & \bar{Q}_{16} \\ \bar{Q}_{12} & \bar{Q}_{22} & \bar{Q}_{26} \\ \bar{Q}_{16} & \bar{Q}_{26} & \bar{Q}_{66} \end{bmatrix}_K \begin{Bmatrix} \epsilon_x \\ \epsilon_y \\ \epsilon_{xy} \end{Bmatrix}_K \tag{19}$$

where

$$\begin{aligned} \bar{Q}_{11} &= Q_{11}\cos^4\theta + 2(Q_{12}+2Q_{66})\sin^2\theta\cos^2\theta + Q_{22}\sin^4\theta \\ \bar{Q}_{22} &= Q_{11}\sin^4\theta + 2(Q_{12}+2Q_{66})\sin^2\theta\cos\theta + Q_{22}\cos^4\theta \\ \bar{Q}_{66} &= (Q_{11}+Q_{22}-2Q_{12}-2Q_{66})\sin^2\theta\cos^2\theta + Q_{66}(\sin^4\theta+\cos^4\theta) \\ \bar{Q}_{12} &= (Q_{11}+Q_{22}-4Q_{66})\sin^2\theta\cos^2\theta + Q_{12}(\sin^4\theta+\cos^4\theta) \\ \bar{Q}_{16} &= (Q_{11}-Q_{12}-2Q_{66})\sin\theta\cos^3\theta + (Q_{12}-Q_{22}+2Q_{66})\sin^3\theta\cos\theta \\ \bar{Q}_{26} &= (Q_{11}-Q_{12}-2Q_{66})\sin^3\theta\cos\theta + (Q_{12}-Q_{22}+2Q_{66})\sin\theta\cos^3\theta \end{aligned} \tag{20}$$

The convention used for positive rotation is shown in Figure 6.

The strain components can be obtained from the following relationships

$$\begin{Bmatrix} \epsilon_x \\ \epsilon_y \\ \epsilon_{xy} \end{Bmatrix} = \begin{Bmatrix} \epsilon^\circ_x \\ \epsilon^\circ_y \\ \epsilon^\circ_{xy} \end{Bmatrix} + Z \begin{Bmatrix} K_x \\ K_y \\ K_{xy} \end{Bmatrix} \tag{21}$$

where the ($^\circ$) superscript refers to the midplane strains of a laminated composite. The components of Equation (21) are as follows

$$\begin{Bmatrix} \epsilon^\circ_x \\ \epsilon^\circ_y \\ \epsilon^\circ_{xy} \end{Bmatrix} = \begin{Bmatrix} \partial u^\circ/\partial x \\ \partial v^\circ/\partial y \\ \partial u^\circ/\partial y + \partial v^\circ/\partial x \end{Bmatrix} \tag{22}$$

and

$$\begin{Bmatrix} K_x \\ K_y \\ K_{xy} \end{Bmatrix} = \begin{Bmatrix} -\partial^2 w/\partial x^2 \\ -\partial^2 w/\partial y^2 \\ -2\partial^2 w/\partial x \partial y \end{Bmatrix} \tag{23}$$

where u, v, and w are displacements in the x, y, and z direction respectively. If one uses the relationships of Equations (21), (22) and (23), Equation (19) can be written as

$$\{\sigma\}_k = [\bar{Q}]_k \{\epsilon^\circ\} + Z[\bar{Q}]_k \{K\} \tag{24}$$

For convenience, a simpler system of forces and moments is now introduced which are defined as force resultants and moment resultants. The force resultant (N_x) is defined as a force per unit width and the moment resultant (M_x) as a moment per unit length. In general then, these values

can be given in terms of the stress vector as follows

$$\{N_i\} = \int_{-h/2}^{h/2} \{\sigma_i\}\, dZ = \sum_{k=1}^{N} \left\{ [\bar{Q}]_k \{\epsilon_i^\circ\} \int_{Z_{k-1}}^{Z_k} dZ + [\bar{Q}]_k \{K_i\} \int_{Z_{k-1}}^{Z_k} Z\, dZ \right\}$$

$$\{M_i\} = \int_{-h/2}^{h/2} \{\sigma_i\} Z\, dZ = \sum_{k=1}^{N} \left\{ [\bar{Q}]_k \{\epsilon_i^\circ\} \int_{Z_{k-1}}^{Z_k} Z\, dZ + [\bar{Q}]_k \{K_i\} \int_{Z_{k-1}}^{Z_k} Z^2\, dZ \right\}$$

where

$$i = (X, Y, XY)$$

By rewriting these equations, a shorter notation can be obtained

$$\{N\} = [A]\{\epsilon^\circ\} + [B]\{K\}$$
$$\{M\} = [B]\{\epsilon^\circ\} + [D]\{K\} \qquad (27)$$

where

$$A_{ij} = \sum_{k=1}^{N} [\bar{Q}_{ij}]_k (h_k - h_{k-1})$$
$$B_{ij} = \frac{1}{2} \sum_{k=1}^{N} [\bar{Q}_{ij}]_k (h_k^2 - h_{k-1}^2) \qquad (28)$$
$$D_{ij} = \frac{1}{3} \sum_{k=1}^{N} [\bar{Q}_{ij}]_k (h_k^3 - h_{k-1}^3)$$

and

[A] - extensional stiffness

[B] - coupling stiffness

[D] - bending stiffness

and $(h_k - h_{k-1})$ represent the individual lamina thicknesses.

When the laminate is symmetric in <u>both</u> geometry and material properties about the mid-plane, Equation (27) simplifies considerably. Due to the symmetry, the thickness terms cause the coupling stiffness (B_{ij}) to go to zero [10].

For the uncoupled axial and moment loads, Equation (27) can be written as

$$\{N\} = [A]\{\epsilon^0\}$$
$$\{M\} = [D]\{K\} \qquad (29)$$

Whitney, Browning and Mair [17] further simplified the moment resultant equation as follows: since from Equation (29)

$$\{K\} = [D]^{-1}\{M\} \qquad (30)$$

Thus, for a pure bending moment this can be written as

$$\begin{Bmatrix} K_x \\ K_y \\ K_{xy} \end{Bmatrix} = \begin{Bmatrix} -\partial^2 W/\partial x^2 \\ -\partial^2 W/\partial y^2 \\ -2\,\partial^2 W/\partial x \partial y \end{Bmatrix} = \begin{bmatrix} D_{11}^{-1} & D_{12}^{-1} & D_{16}^{-1} \\ D_{12}^{-1} & D_{22}^{-1} & D_{26}^{-1} \\ D_{16}^{-1} & D_{26}^{-1} & D_{66}^{-1} \end{bmatrix} \begin{Bmatrix} M_x \\ 0 \\ 0 \end{Bmatrix} \qquad (31)$$

M_x is the moment resultant defined by

$$M_x = \frac{M}{b} \qquad (32)$$

If one assumes that the specimen has a high length-to-width ratio then

$$W = W(X)$$

and

$$\partial^2 W/\partial x^2 = -\frac{M}{\bar{E}I} \qquad (33)$$

where

$$\bar{E} = 12/h^3 D_{11}^{-1}$$

which is of the same form as classical beam theory with the isotropic modulus (E) replaced by an effective bending modulus ($\bar{E}$). Stress can now be obtained as

$$\{\sigma\}_k = [\bar{Q}]_k Z \{K\} \qquad (34)$$

or

$$\sigma_{xk} = Z f_{1k} \frac{M}{I}$$
$$\sigma_{yk} = Z f_{2k} \frac{M}{I} \qquad (35)$$
$$\sigma_{zk} = Z f_{3k} \frac{M}{I}$$

where

$$\{f_i\}_k = [\bar{Q}_{im}] \{S_{im}\}$$
$$i = 1,2,3$$
$$m = 1,2,6 \qquad (36)$$
$$Q_{im} = Q_{mi}$$
$$S_{im} = D^{-1}_{im} h^3/12$$

Equation (36) then represents an equation applicable to a general class of symmetric laminates, derived by considering a beam as a special case of a laminated plate.

The axial stress equation, when considering only the normal force resultant N_x, can be derived as follows

$$\{\epsilon^\circ\} = [A]^{-1} N_x \qquad (37)$$

where

$$N_x = \frac{P}{b} \qquad (38)$$

Since symmetric specimens will be used the equation for tension only is

$$\{\epsilon^\circ\} = \{\epsilon\} = [A]^{-1} N_x \qquad (39)$$

the normal stress can then be expressed as

$$\sigma_{xk} = \bar{Q}_{11k} \epsilon_x + \bar{Q}_{12k} \epsilon_y + \bar{Q}_{16k} \epsilon_{xy}$$
$$= \left[\bar{Q}_{11k} A^{-1}_{11} + \bar{Q}_{12k} A^{-1}_{12} + Q_{16k} A^{-1}_{16}\right] N_x \qquad (40)$$

Weibull Equation for Composite Materials

This section deals with the extension of the Weibull distribution function forms, presented for a beam in Equations (6), (11) and (15), to composite materials. Derivations are based on the composite theory equation forms presented in the previous section. The final equations are then presented both in composite notation as well as in a simplified form applicable to the specific experimental specimens being analyzed in this study.

Since the Weibull theory is based on fracture due to normal tensile stress in materials containing random flaw distributions, the composite is also assumed to contain volumetric flaws and to be subject to normal tensile stress fracture. The derivation of the composite bending equations can be modified with this assumption, and Equation (35) reduces to

$$\sigma_{xk} = Z f_{1k} \frac{M}{I} \tag{41}$$

or

$$\sigma_{xk} = Z \left[\bar{Q}_{11k} D'_{11} + \bar{Q}_{12k} D'_{12} + \bar{Q}_{16k} D'_{16} \right] \frac{M}{b} \tag{42}$$

if we now define

$$C_k = \left[\bar{Q}_{11k} D'_{11} + \bar{Q}_{12k} D'_{12} + \bar{Q}_{16k} D'_{16} \right] \frac{M}{b} \tag{43}$$

for simplified notation, then the stress in a laminate subjected to bending can be expressed as

$$\sigma_k = Z C_k \tag{44}$$

where (z) is the distance from the neutral axis.

The laminate specimen used in this investigation will consist of only unidirectional ply orientations and therefore act like a single lamina with respect to stress distribution. Equations (45) through (49) provide some basic definitions for later theory development and are graphically presented for a unidirectional laminate in Figure 7

$$h_{\sigma_u} = \left\{ h_{p-1} + \left(\frac{\sigma_{up} - \sigma_{up-1}}{\sigma_p - \sigma_{p-1}} \right) (h_p - h_{p-1}) \right\} \tag{45}$$

where the subscript (p) refers to the p-th lamina which is the lamina in which $\sigma = \sigma_u$. The stress in the p-th lamina is defined as

$$\sigma = C_p Z = \left[Q_{11p} D_{11} + Q_{12p} D_{12} + Q_{16p} D_{16} \right] \frac{M}{b} \tag{46}$$

also

$$\sigma_{up} = C_p h_{\sigma_u} \tag{47}$$

$$\sigma_{p-1} = C_p h_{p-1} \tag{48}$$

$$\sigma_p = C_p h_p \tag{49}$$

With the use of these equations the evaluation of the risk of rupture becomes

$$B = \int_0^b \int_0^L \int_{h_{\sigma_u}}^{h_p} \left(\frac{C_p Z - \sigma_{up}}{\sigma_0} \right)^m dV + \sum_{k=p+1}^{n} \int_0^b \int_0^L \int_{h_{k-1}}^{h_k} \left(\frac{C_k Z - \sigma_{uk}}{\sigma_0} \right)^m dV \tag{50}$$

where the first triple integral represents the number of unit volumes in the lamina in which the stress partially exceeds σ_u. The second triple integral represents the summation of this quantity for all other lamina in which the

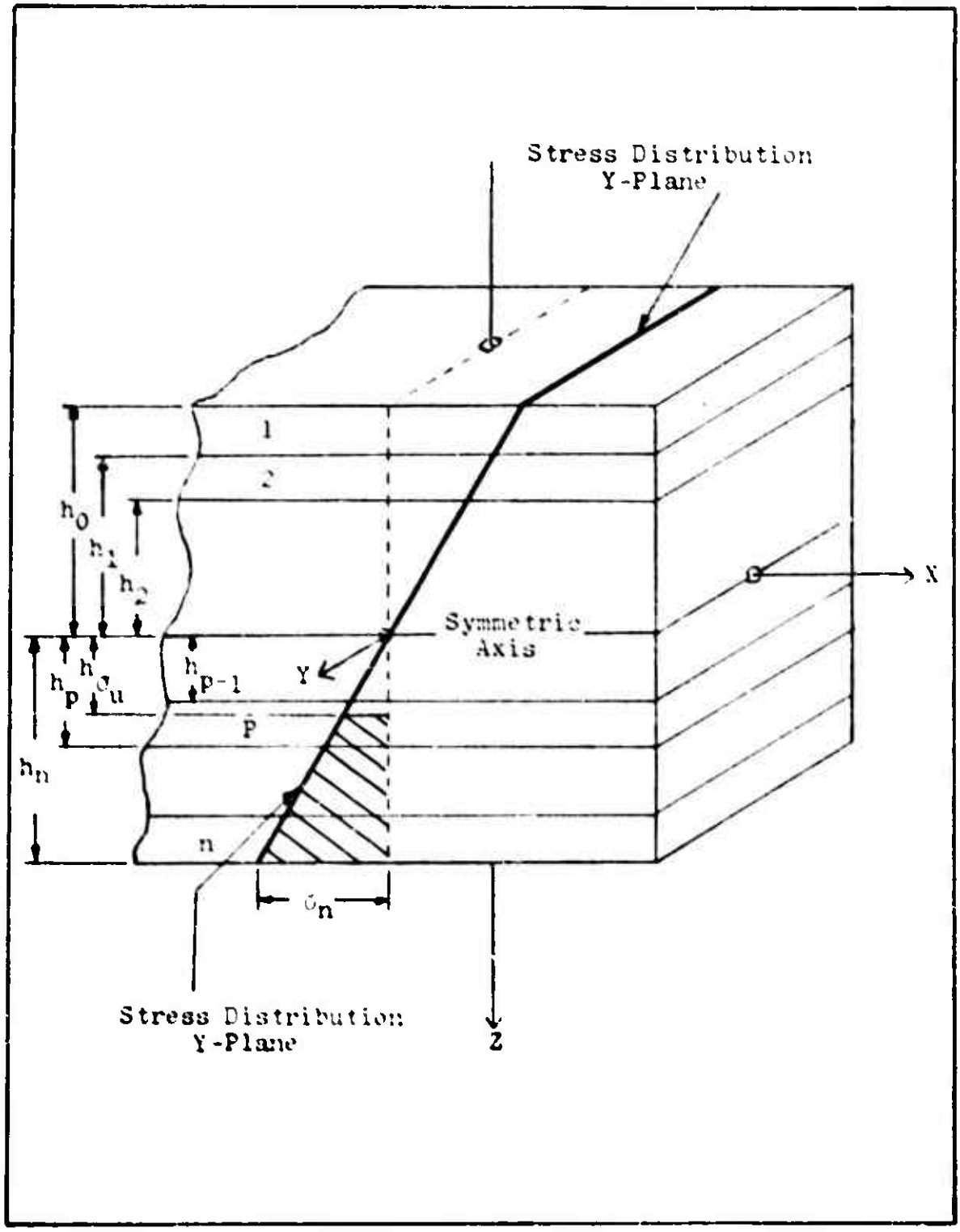

Fig. 7. Typical Stress Distribution - Composite with Unidirectional Ply Orientation

stress exceeds σ_u. Subscripts are provided to σ_u to account for variations of this value in multi-directionally oriented specimens and as such make this term ply dependent. The equation in this form represents the risk of rupture for pure bending of a general laminated composite. For a unidirectionally laminated composite, as that being used in this thesis, σ_u is assumed to be identical for all plies and consequently subscripts are dropped from subsequent equations. Integrating this equation results in the expression for the risk of rupture for a unidirectionally laminated composite subjected to pure bending.

$$B = \frac{Lb}{\sigma_o^m (m+1)} \left\{ \left[\frac{(C_p h_p - \sigma_u)^{m+1}}{C_p} \right] + \sum_{k=p+1}^{n} \left[\frac{(C_k h_k - \sigma_u)^{m+1} - (C_k h_{k-1} - \sigma_u)^{m+1}}{C_p} \right] \right\} \qquad (51)$$

This equation can be simplified further by use of the characteristics peculiar to the specimens being incorporated into this thesis. For unidirectional fiber orientations

$$C_p = C_k = C \qquad (52)$$

because the terms in the lamina stiffness matrix $\bar{Q}_{ij}$ are identical for each lamina. This reduces Equation (51) to

$$B = \frac{Lb}{(m+1)} \frac{(Ch_n - \sigma_u)}{C} \left(\frac{Ch_n - \sigma_u}{\sigma_o} \right)^m \qquad (53)$$

Equation (53) can also be written in terms of the extreme fiber stress as was Equation (6). The stress distributions for these composite specimens are linear, and therefore can be expressed as

$$\sigma = \frac{2\sigma_n}{h} Z = \frac{\sigma_n}{h_n} Z \tag{54}$$

since

$$C_n\left(h/2\right) = C\left(h/2\right) = \sigma_n \tag{55}$$

therefore

$$B = \frac{Lb}{(m+1)} \left(\frac{\sigma_n - \sigma_u}{C}\right) \left(\frac{\sigma_n - \sigma_u}{\sigma_o}\right)^m \tag{56}$$

where

$$C = \sigma_n\left(2/h\right) \tag{57}$$

now

$$B = \frac{Lbh}{2(m+1)} \left(\frac{\sigma_n - \sigma_u}{\sigma_n}\right) \left(\frac{\sigma_n - \sigma_u}{\sigma_o}\right)^m \tag{58}$$

where

$$Lbh = V$$

Equation (58) is identical to Equation (6) as is expected for the type of composite being considered, and therefore represents the risk of rupture equation for pure bending loading tests in the thesis. A similar approach is used in the derivation of the risk of rupture equation for three-point loading. Some of the previously defined terms must, however, be modified to allow for a varying moment. The moment equation for three-point loading is

$$M = \left(P/2\right) X \tag{59}$$

where (P) is the applied load. Equation (42) can now be written

$$\sigma_k = Z\left[\bar{Q}_{11k}\bar{D}'_{11} + \bar{Q}_{12k}\bar{D}'_{12} + \bar{Q}_{16k}\bar{D}'_{16}\right]\frac{P}{2b}X \qquad (60)$$

defining

$$C'_k = \left[Q_{11k}D_{11} + Q_{12k}D_{12} + Q_{16k}D_{16}\right]\frac{P}{2b} \qquad (61)$$

then

$$\sigma_k = C'_k Z X \qquad (62)$$

since the specimens are unidirectional, the lamina subscript can be dropped. Figure 3b shows the extreme fiber stress distribution, and from this we define

$$\sigma_b\,(\text{beam}) = \sigma_n\,(\text{composite}) = C'\frac{h_n L}{2} \qquad (63)$$

or

$$C' = \frac{\sigma_n 2}{h_n L} \qquad (64)$$

where σ_n is the maximum extreme fiber stress, and h_n is defined in Figure 7. Using Equation (62) in Equation (2) results in the expression

$$B = 2\int_0^b \int_{x_{\sigma u}}^{L/2} \int_{Z_u}^{h/2} \left(\frac{C'_k Z X - \sigma_u}{\sigma_0}\right)^m dV \qquad (65)$$

which when integrated takes the form

$$B = \frac{2b}{C'\sigma_0^m(m+1)}\left\{\left[\sum_{r=0}^{\bar{m}} \frac{(C'L/2\,h_n - \sigma_u)^{m+1-r}}{m+1} + (-\sigma_u)^{-r}\right] + (-\sigma_u)^{\bar{m}+1}\int_{Z_u}^{h/2} \frac{(C'L/2Z - \sigma_u)^{\alpha}}{Z} dZ\right\} \qquad (66)$$

which can be put in terms of the maximum extreme fiber stress σ_n by use of Equation (64). Using this definition

the final risk of rupture for a composite under three-point loading then becomes identical to Equation (11).

The risk of rupture for a composite under tension is derived from Equations (25) and (27). In this case only the tension loading and extensional stiffness is considered. Using Equations (2) and (40) the integral equation for the risk of rupture under tension is

$$B = \sum_{k=1}^{n} \int_{0}^{b} \int_{0}^{L} \int_{h_{k-1}}^{h_k} \left(\frac{\sigma_{xk} - \sigma_u}{\sigma_0} \right)^m dV \tag{67}$$

which integrates to

$$B = Lb \sum_{k=1}^{n} \left(\frac{\sigma_{xk} - \sigma_u}{\sigma_0} \right)^m (h_k - h_{k-1}) \tag{68}$$

If one incorporates the unidirectional properties of the specimen as related to this thesis in addition to

$$\sigma_{xk} = \sigma_t = \text{Constant} \tag{69}$$

Equation (68) reduces to Equation (15).

This study will utilize Equations (15), (58) and (66) in predicting the risk of rupture for graphite-epoxy under the loading conditions for which each of the equations was derived, and then use these values in establishing the probability of fracture from Equation (1).

III. Experimental and Analytical Procedures

This section provides an overview of the methodology developed to obtain the material parameters in the Weibull distribution function. A description of experimental equipment and procedures as well as the analytical process used in manipulating the experimental data is provided. Also postulated in this section is some analysis theory directed at data evaluation and interpretation. A sensitivity analysis is provided in an attempt to show the dependency of the resulting theoretical equations on the specific experimental data being analyzed.

Material, Equipment and Test Procedures

Graphite-epoxy specimens are used exclusively in the experiments. Specimens were constructed of both sixteen and eight ply graphite fibers impregnated in epoxy. Fiber orientations were unidirectional within each specimen. The specimens were cut from a single 24 inch by 24 inch sheet, thereby obtaining both 0-degree and 90-degree oriented test samples from the same layup. A description of the specimens is provided in Figure 8. Two laminate thicknesses are used due to limitations on specimen size; sixteen ply specimen for both four-point and three-point loading tests and eight ply specimens for the tension tests. The lower ply specimens were chosen for tension so the necessary fracture loads would not deform or separate the end-tabs from the

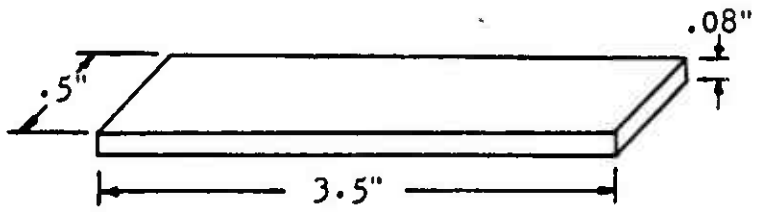

Typical 16 Ply 90 & 0 degree Specimen
(Pure Bending & 3-point Loading)

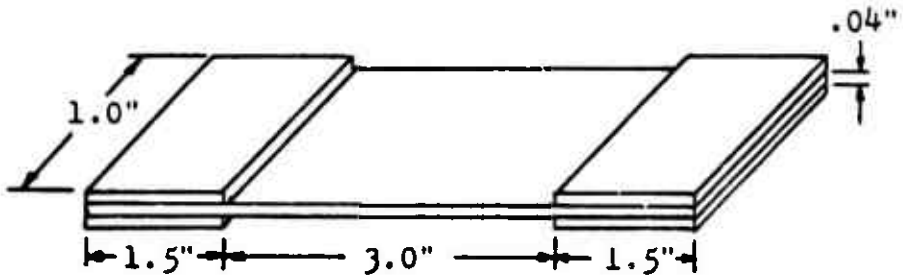

Typical 8 Ply 90-degree Tension Specimen

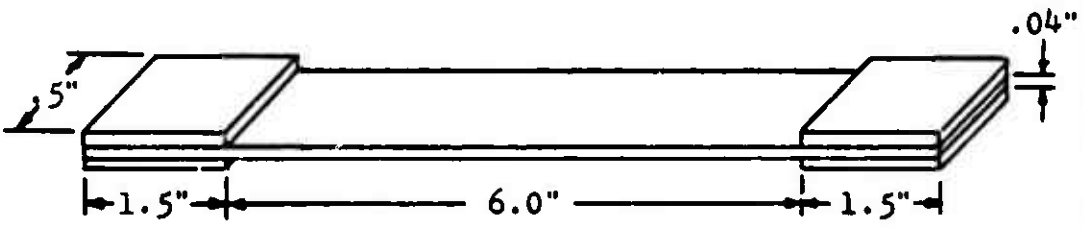

Typical 8 Ply 0-degree Tension Specimen

Fig. 8. Test Specimen Geometry

specimen, thereby inducing measurement inaccuracies.

A standard Instron testing machine was used to conduct all testing. For each four-point and three-point loading test, the load was applied at .05 in/min. The tension tests were conducted with a stroke rate of .02 in/min. The application of loading continued until castastrophic failure or load resistance went to zero. A chart recorder recorded deflection versus load for each specimen. Approximately 20% of the specimens were equipped with strain gages. For these specimens strain versus load was recorded.

Accurate volumes were obtained for each individual specimen by conducting, individually, three measurements of thickness and width. These measurements were then averaged to obtain an average width and thickness per specimen. All testing followed in accordance with standard test procedures. In order to obtain a region of pure bending within the four-point loading tests, the cross-sectional dimensions were controlled to a span to depth ratio of 32 to 1 for each specimen. A minimum of 25 specimens were tested for each ply orientation and loading condition.

The succeeding paragraphs provide the steps followed by the author in arriving at the final procedures of deriving the material parameters using published information. With the accumulated experience obtained in the methodology process, a final technique is developed and presented.

Material Parameter Determination

Once the basic equations for the Weibull distribution

function are established, experimental data is gathered to validate the theory. The problem that now arises is the development of those values of the material parameters which make the theoretical probability of fracture curve fit the experimental data best.

Daniel and Weil [6] used as a suitable criterion the analytical method of minimization of the sum of the mean squares differences. In their procedure, experimental data obtained from pure bending tests was used in the parameter determination.

The procedure combines Equation (1) and (6). Taking the double log of Equation (1) yields

$$Y_n = \operatorname{Ln}\operatorname{Ln}\frac{1}{1-S_n} = \operatorname{Ln} B = \operatorname{Ln}\frac{V}{2} - \operatorname{Ln}(m+1) + (m+1)\operatorname{Ln}(\sigma_n - \sigma_u) - \operatorname{Ln}\sigma_n - m\operatorname{Ln}\sigma_o \tag{70}$$

The corresponding (estimated value for the probability of fracture obtained experimentally is

$$S_n = \frac{n}{N+1} \tag{71}$$

from which

$$y_n = \operatorname{Ln}\operatorname{Ln}\frac{N+1}{N+1-n} \tag{72}$$

where N = total number of specimens tested

n = specimen number when specimens are arranged in ascending order of stress

The least squares method requires

$$\sum_{n=1}^{N} (Y_n - y_n)^2 = \text{MINIMUM} \tag{73}$$

The necessary conditions for this minimization also require that the derivatives of Equation (73) when taken with respect to σ_u, σ_o and m to be set equal to zero.

This then results in three equations with three unknowns which can be solved simultaneously. Convergence to zero results in the determination of a unique parameter set.

Although mathematically correct, convergence of these equations was found difficult to obtain. A possible reason being their highly non-linear nature [2].

Another more widely used approach is one suggested by Weibull [6]. This method is a trial and error procedure in which the experimental data is linearized. The recommended procedure is to rearrange equation (70) into the form of the equation of a straight line

$$Y = mX + b \tag{74}$$

this is accomplished as follows

$$LNLN\frac{N+1}{N+1-n} + LN\,\sigma_n = (m+1)LN(\sigma_n - \sigma_u) + LN\frac{V}{2(m+1)} - m\,LN\sigma_0 \tag{75}$$

Two axes (x and y) can now be established where

$$Y = LNLN\frac{N+1}{N+1-n} + LN\,\sigma_n \tag{76}$$

and

$$X = LN(\sigma_n - \sigma_u) \tag{77}$$

The correct value of σ_u is obtained through a trial and error procedure. Various σ_u values are picked until a straight line results from the plot of Equations (76) versus (77). If σ_u is too low, a curve concave down will result,

if too high the result will be a curve concave up [16]. The slope of the resulting straight line then becomes $(m + 1)$. Once m and σ_u are established, all values of Equation (70) are known except for σ_o. This value can now be determined by substituting the known values back into Equation (70).

This procedure was also employed by Daniel and Weil when their analytical method proved impractical. One drawback found during their experimentation showed that generally a very large number of guesses are required to finally obtain the desired linear result. Consequently they devised a process in which the upper and lower end slopes of the concave curves resulting from several estimates of σ_u are plotted against σ_u. This procedure is illustrated in Figure 9. Connecting the end slope points with a straight line results in a plot as shown in Figure 9d. The intersecting point provides the desired values for m and σ_u. This procedure significantly reduces the total number of estimates to identify σ_u.

The development of the methodology for the parameter determination for this study was based on two sets of experimental data, each with established material parameters. One data set was for a ceramic material and the other for a composite material.

The least squares analytical method of parameter determination was not investigated due to the findings by Daniel and Weil [7]. A detailed analysis, however, was conducted

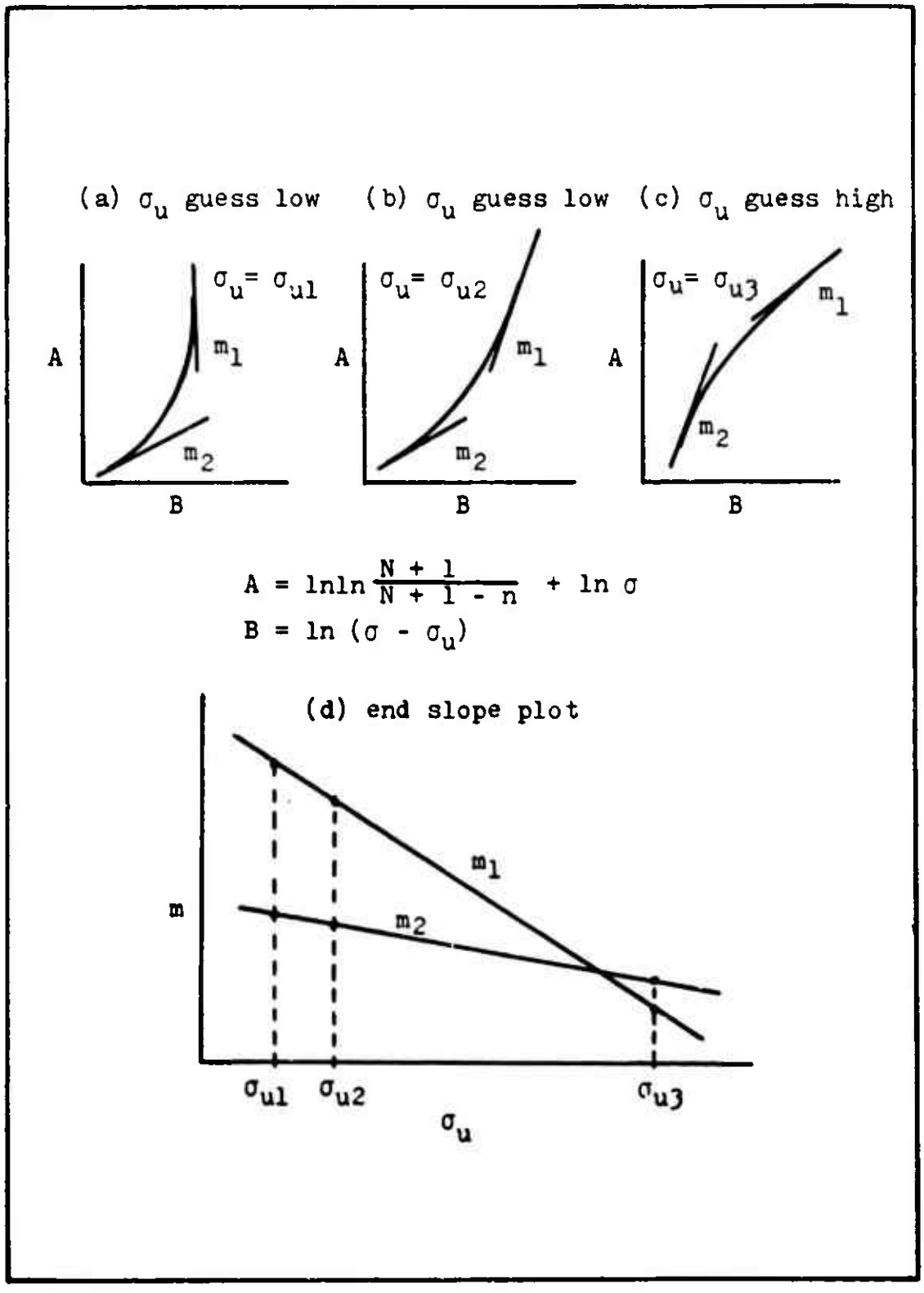

Fig. 9. Parameter Determination Method

to establish an effective way to use the graphical approach. The ceramic material fracture data was used exclusively in this effort due to its more manageable magnitudes in stress values. The composite data allowed for additional verification of the final procedures.

The basic approach of the analysis followed the procedures outlined by Weibull, with modifications made as required. The following paragraphs outline the sequence of events and the rationale which led to the final methodology for determining the material parameters.

From the outset of the analysis, a variety of σ_u values were plotted using Equations (76) and (77) as plot coordinates. The resulting graphical data, however, showed refinement to the method was required. For all values of σ_u chosen, no singularly definable straight line or identifiable concavity could be established. Figure 10 shows a typical case of the experimental data when plotted using Equations (76) and (77).

To improve the method, a smoothed curve was fitted to the experimental data. Plotting the values along this curve instead of the individual data points, resulted in a definably straight line from which σ_u and m could be obtained. The problem with this technique, however, is the arbitrary approach used in fitting a smooth line to the experimental data. This became more evident when the published material parameters for the data could not be duplicated.

A more regimented approach for data smoothing was in-

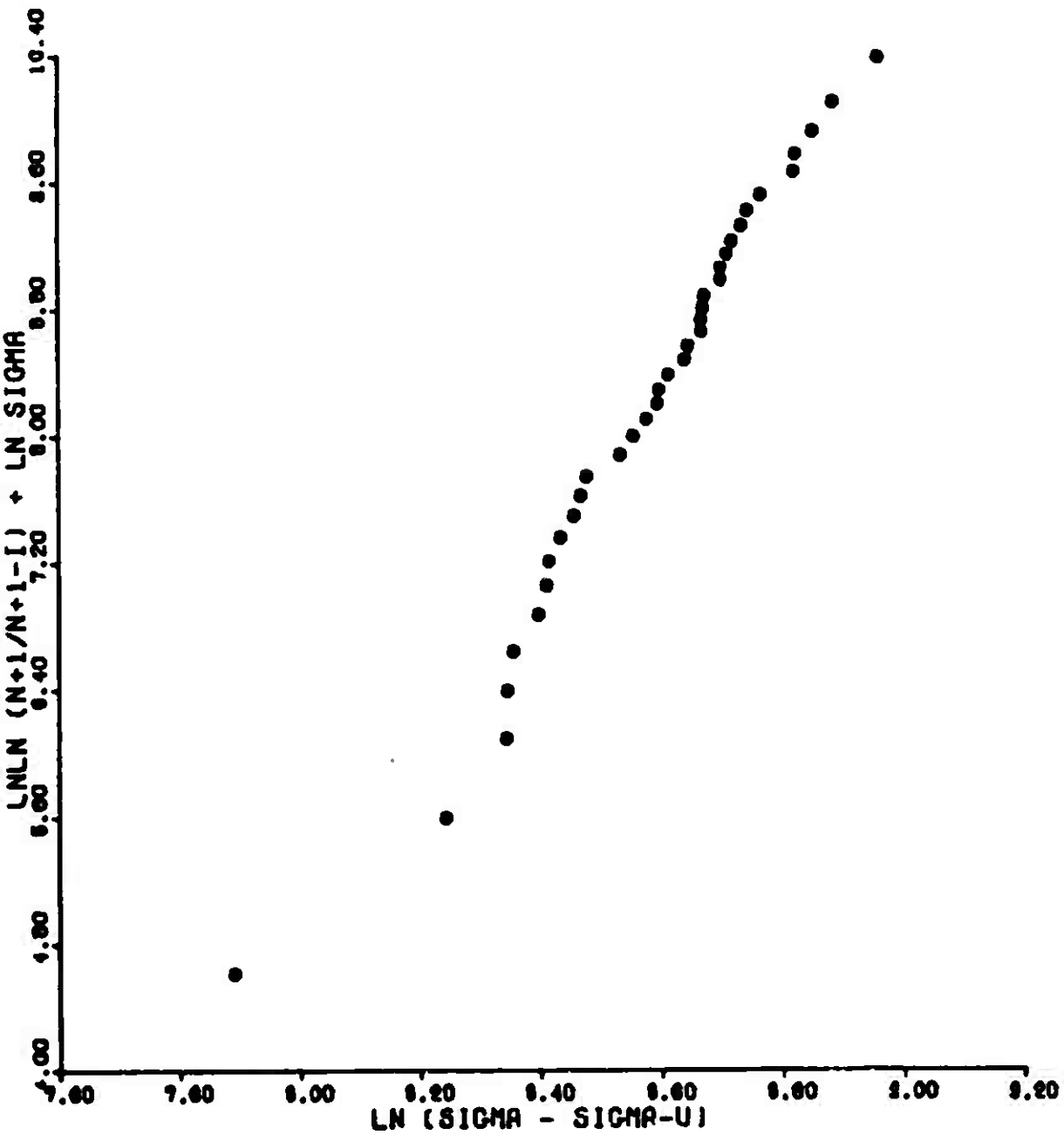

Fig. 10. Typical Example of
Weibull Parameter Determination Plot

stituted through the use of the least squares principle and thus various degree polynomial equations were studied which adequately approximated the data. This required a decision as to which degree polynomial provided the best results. A mathematical best fit could not be used since this would necessarily be a high degree polynomial, resulting therefore in an irregular curve rather than the desired smooth curve. Rather than limit the flexibility of this method, numerous polynomials were incorporated to approximate the data, and then evaluated with respect to the vaiability in the Weibull parameters. Although all higher degree polynomials produced distinctive values for m and σ_u, each polynomial resulted in distinctively different values. The published parameters were again not duplicated.

Analysis of the characteristics of each polynomial curve revealed an invariance in the curves in the region beyond the first three to six data points. A very high variability was found, however, in fitting these first few points. Figure 11 depicts this area. The characteristics of smoothing within this zone resulted in the following; a smoothed curve which flared as shown by curve 1 in Figure 11, resulted in σ_u values near zero or even negative, curves within the shaded area resulted in values falling between zero and the lowest failure data point depending on whether the curve fit was chosen in the upper or lower portion of this shaded section, finally if a fit approximated curve 2,

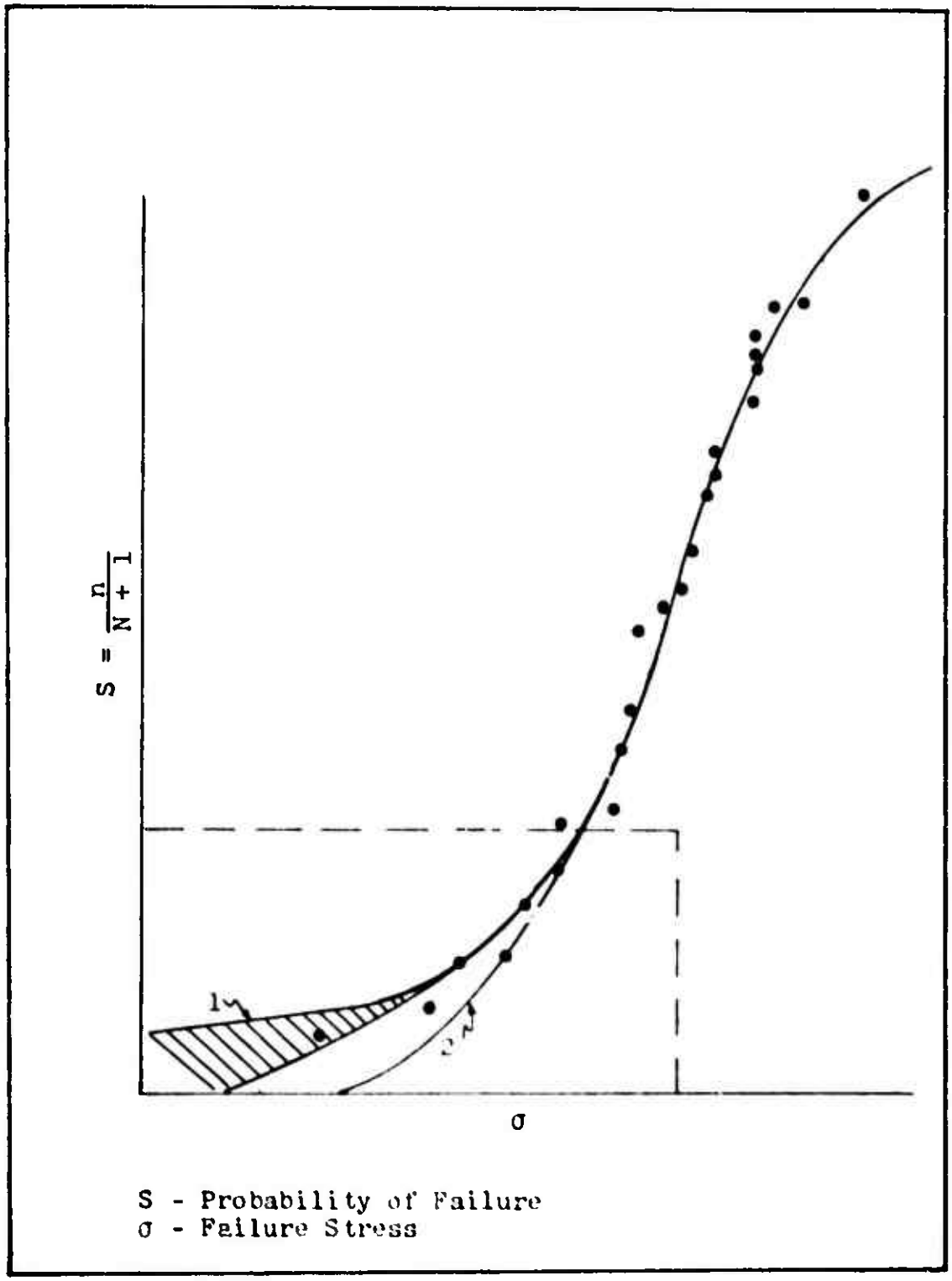

Fig. 11. Area of Curve Smoothing Sensitivity

values of σ_u greater than the lowest failure data point were required to obtain a straight line plot using Equations (76) and (77). As a result of these characteristics and due to its physical significance within the Weibull equation, σ_u was chosen as a bounding value. The lower limit of σ_u was chosen to be zero based on the physical interpretation that stress below this value must result in a probability of fracture equal to zero. The lowest experimental failure stress determined the upper limit for σ_u, thereby specifying that a finite probability of fracture exists above this value.

Using various degree least square polynomials a variety of σ_u's and m's were established within these limits of σ_u. If these values are displayed in graphical form a linear relationship results as shown in Figure 12. This data implied that an infinite number of combinations of both m and σ_u existed within the set limits, any of which could be used to theoretically duplicate the experimental data. The published material parameters for the sample data were also located on this line. Based on these interesting results, this technique had provided the means of duplicating the published material parameters as one of a very large set.

To verify that each set of values resulted in a valid theoretical prediction of the experimental distribution, randomly picked parameter sets were plotted using the Weibull equation and overlayed on the experimental data. Vis-

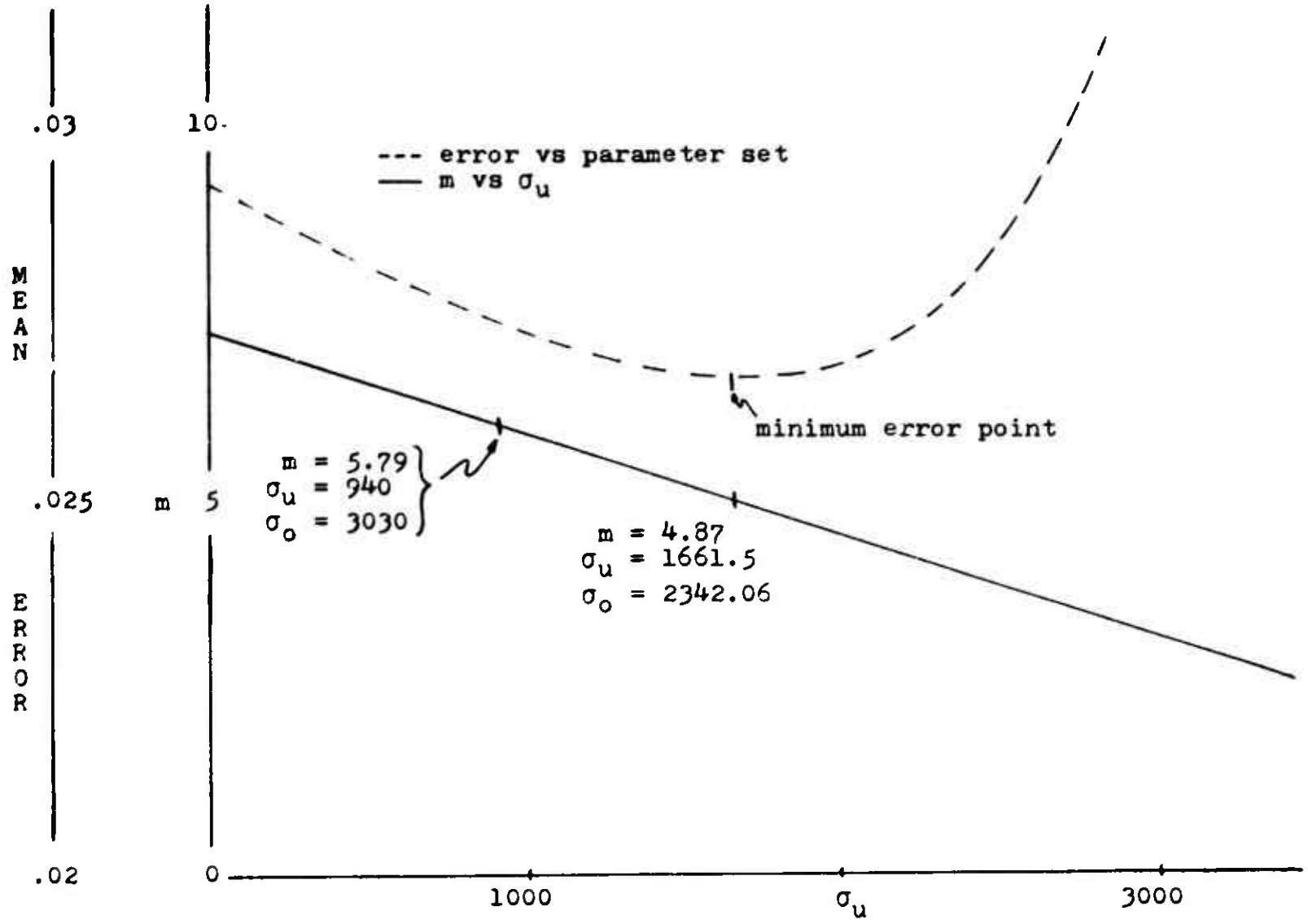

Fig. 12.
Optimum Parameter Determination

ually adequate fit was achieved with all sets. However, it was noted that sets with values of σ_u near zero or near the lowest fracture data point did not match the experimental data as well as those with intermediate σ_u values. It appeared therefore that a "best" set of parameters existed which could be mathematically isolated.

The mathematical analysis to isolate the best set of parameters employed the least squares method of summing the squares of the mean difference between the experimental data and theoretical Weibull equations. The error between these two models was calculated and plotted for a variety of material parameter sets. The dashed line shown in Figure 12 represents this sum of the mean difference squared plotted against the corresponding m and σ_u values. As can be seen, a "best" set of parameters does exist among the family of sets represented by the straight line when analyzed in this manner. Eventhough the set which resulted from this procedure did not match the published set of parameters, the magnitude of the overall error in fit difference is very small. Figures 13 and 14 provide a graphical representation of the experimental data points overlayed using the published material parameters (Figure 13) and the best set determined by the aforementioned procedure.

The final step in establishing the procedures for the parameter determination was to check the sensitivity of fit accuracy between the experimental data and theoretical curve

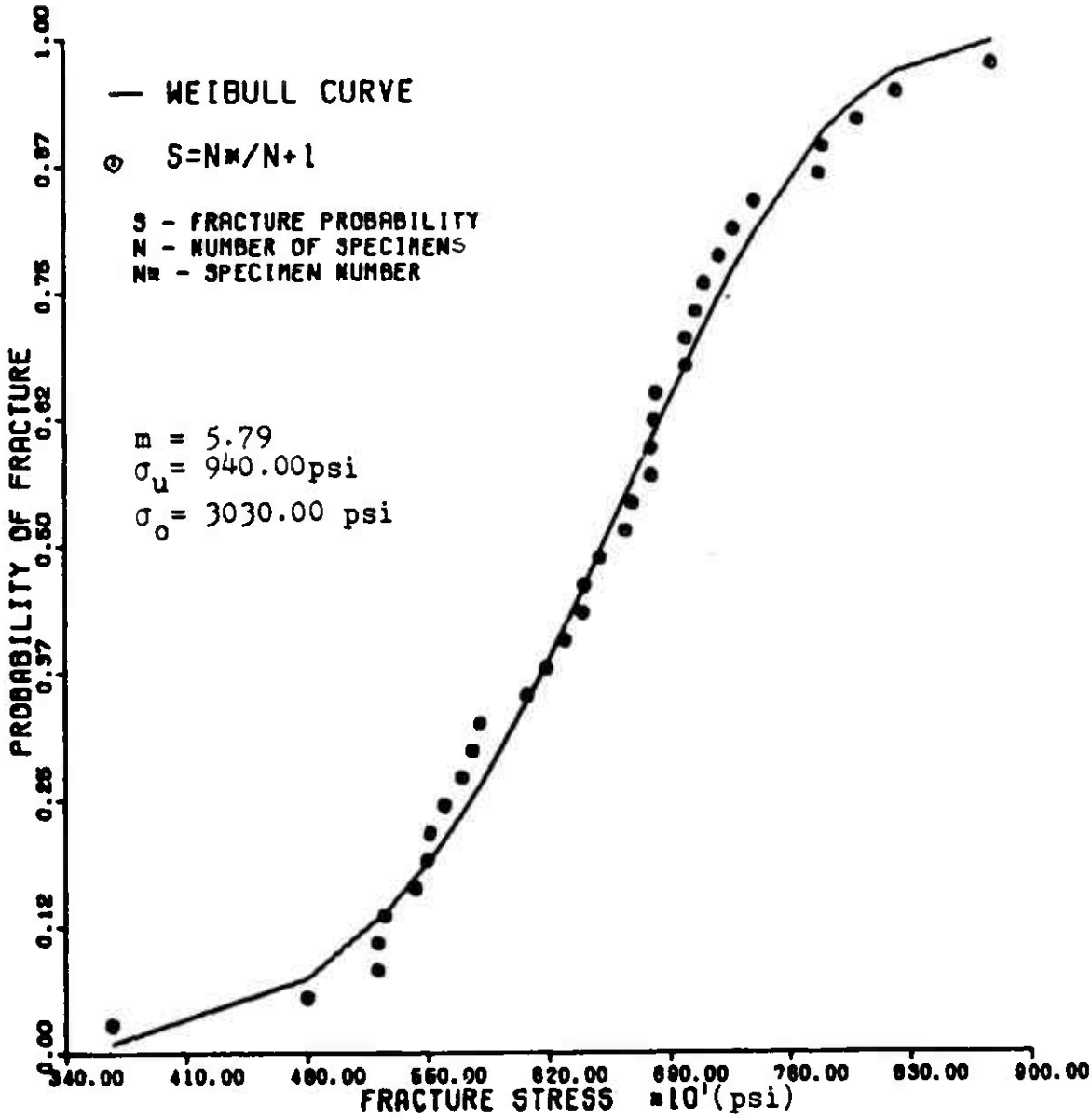

Fig. 13. Comparison of Sample Experimental Data and Theoretical Cumulative Distribution Function Using Published Parameters

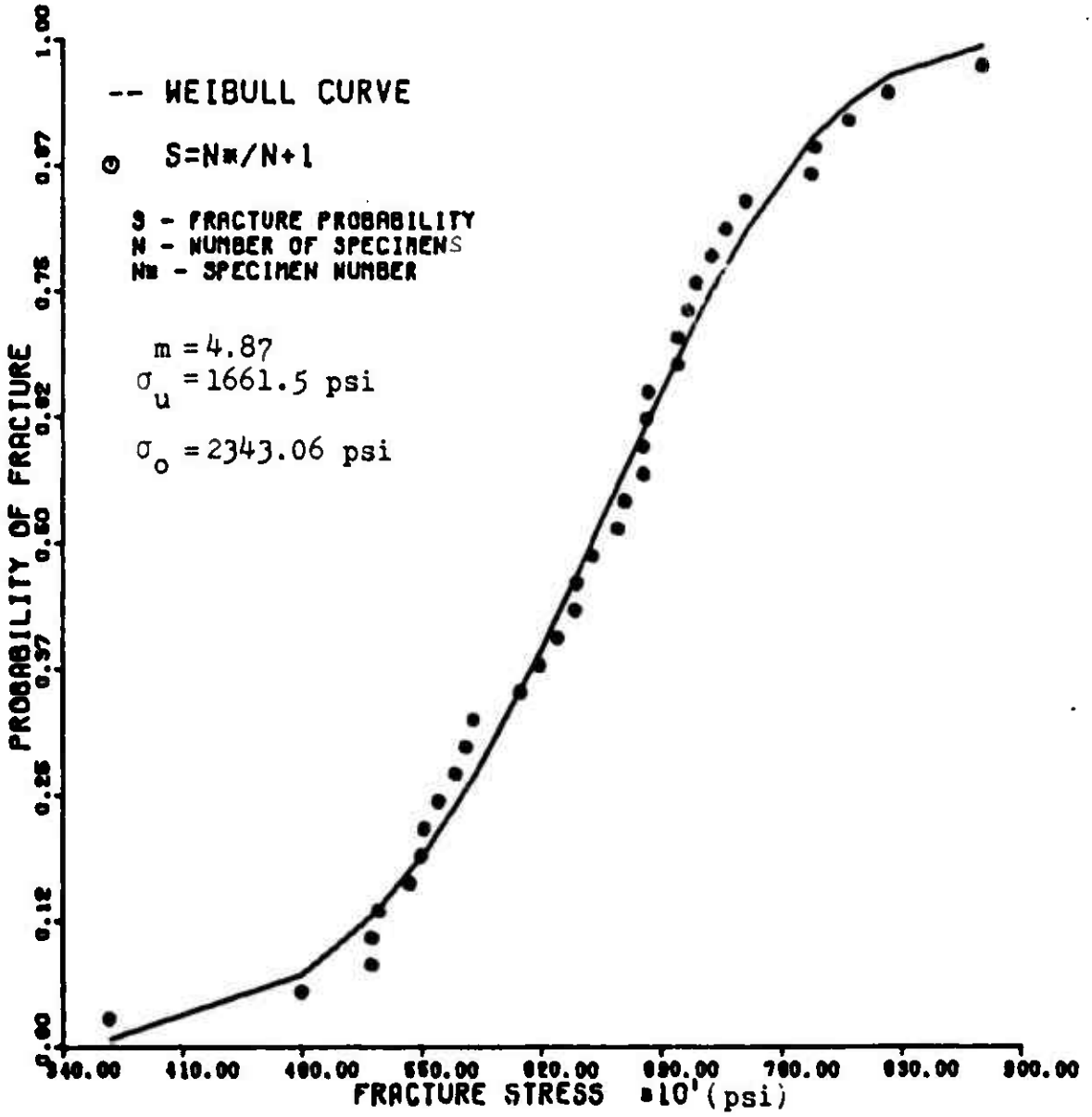

Fig. 14. Comparison of Sample Experimental Data and Theoretical Cumulative Distribution Function Using Derived Parameters

due to small changes in each parameter of the Weibull distribution function. The results showed that all changes to σ_u and m would cause an increase in fit error. However, if σ_o is made the variable at a fixed m and σ_u the author was able to find values which decreased the fit error. The cause of this lies in the methodology used in the derivation of this parameter. The procedure, which is used to find σ_o, evaluates Equation (75) for each stress/probability value and establishes as many σ_o values as there are data points. These values of σ_o are then averaged to obtain the final σ_o. This final number therefore is very data sensitive since the addition of another failure value would generally result in a change to σ_o.

Based on this information, the value of σ_o for each set of m and σ_u was allowed to vary approximately plus and minus one percent, and a new fit error was calculated for each resulting new set of parameters. Although the reduction in error is extremely small in overall magnitude (.02655698) versus (.02655657) the resulting set of "best" parameters is changed significantly (m = 4.868, σ_u = 1661.5 σ = 2342.06 versus m = 4.856, σ_u = 1670, σ_o = 2333.52).

Due to this sensitivity found in the σ_o parameter, the procedure of graphically establishing m and σ_u was revised. The writing of a computer program became necessary, incorporating the experimental data in conjunction with Equation (76) and (77), to allow a numerical refinement for various

values of σ_u. From this numerical data, initial values of m could then be obtained. For each σ_u, the values of m and σ_o are allowed to vary until a combination of the three values is found which provides a minimum fit error to the experimental data. Figure 15 is a three dimensional representation of the physical interpretation of this error minimization process. This procedure greatly simplifies the more involved and subjective graphical method. It also provides immediate mathematical comparisons. The computerization verified the high sensitivity of fit accuracy to variations in σ_o when establishing an accurate theoretical model for an experimental failure distribution.

Since the above methodology demonstrated that for given values of σ_u, the fit error could be minimized, the analytical method of maximums and minimums should also be able to predict this point. Therefore an analytical check of these procedures was also conducted. The minimum error expression can be written as

$$\epsilon = \sum_{n=1}^{N} \left(S - S_n\right)^2 = \text{MINIMUM} \tag{78}$$

were

$$S = \frac{n}{N+1} \tag{79}$$

and S_n = Equations (1) and (6).

Taking the derivative of this equation with respect to the variables yields the following expressions

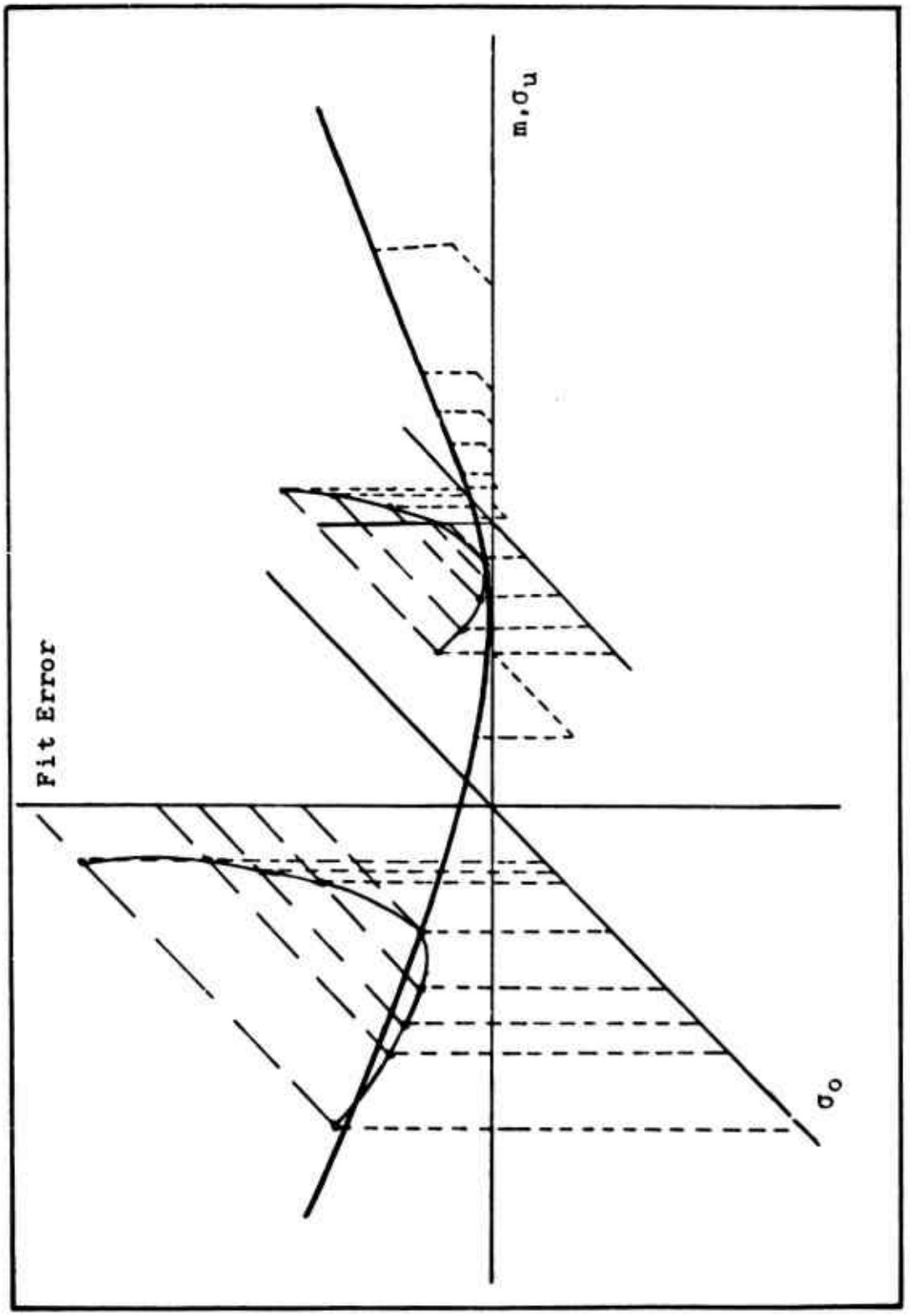

Fig. 15. Error Minimization Process

$$\sum_{n=1}^{N} (S - S_n)\,\partial S_n/\partial m = 0$$
$$\sum_{n=1}^{N} (S - S_n)\,\partial S_n/\partial \sigma_u = 0 \qquad (80)$$
$$\sum_{n=1}^{N} (S - S_n)\,\partial S_n/\partial \sigma_o = 0$$

Convergence of these equations was verified for all parameters evaluated.

The computerized analysis method which resulted from the refinement of the graphical trial and error procedure is used in analysing the data gathered for this thesis. The methodology is mathematically reproducible for a fixed set of experimental data, and therefore less subject to many inherent inaccuracies of graphical analysis techniques.

IV. Results

This section contains a compilation of results from the various analyses and data evaluations comprising this thesis. The discussion is divided into three subsections. The first two parts present the results obtained from the Weibull parameter determination analysis and the theoretical equation validation using the experimentally obtained failure distribution. Peculiarities, which are reported in the first two efforts, led to a supplemental data analysis to further investigate the usability of the Weibull theory. The findings of this evaluation are discussed in the last part of this section. The detailed data from the experimental phase of this study are presented in tabular form in Appendix B.

Due to the complexity in describing the large assortment of analysis variations which occurred during the conduct of this thesis, the author feels it is necessary to present the reader with an overview of the total effort at the outset of this section. This is presented in Table 1. Also, a factor which must be pointed out at this time is a peculiarity which was discovered during the analysis of the 90-degree flexure specimen. It was discovered that all specimen which had been equipped with strain gages had failed at an above average stress. Consequently, it was decided to analyze this data as comprised of two independent samples: one containing 21 samples, the other containg 26. All 90-

Table I.

Summary Correlation Chart

Parameters Derived from	Experimental Data checked for Correlation	Resulting Correlation X-Correlation --no/poor Correlation
0° Bending	0° Bending	X
	0° Tension	X
	0° 3-Point	--
90° Bending*	90° Bending*	X
	90° Tension	--
	90° 3-Point	--
90° Bending**	90° Bending**	X
	90° Tension	--
	90° 3-Point	X
0° Tension	0° Bending	X
	0° Tension	X
	0° 3-Point	--
90° Tension	90° Bending*	--
	90° Bending**	--
	90° Tension	X
	90° 3-Point	--
0° 3-Point $\sigma_u = o$	0° 3-Point	X
90° 3-Point $\sigma_u = o$	90° 3-Point	X

* 26 Specimen Data Sample
** 21 Specimen Data Sample

degree bending data will be analized in this manner.

Parameter Determination

The flexure data shown in Tables IX and X of Appendix B is used for the basic parameter determination. The computerized methodology described in Section III was employed in this analysis. Figures 16, 18, and 20 present the final sets of m and σ_u values for the 0 degree and two sets of 90-degree specimen[6] respectively. Additionally, Figures 17, 19 and 21 provide the values of σ_o which correspond to these values. Superimposed on Figures 16, 18 and 20 are the fit error values which result from the correlation between the experimental and theoretical distributions when using the sets of m, σ_u and σ_o. Table II is a summary of the best parameter values obtained as well as comparison of the experimental mean compared to the theoretical mean using the respective parameters.

Table II.

Weibull Parameters Using Bending

Specimen Type	m	σ_u psi	σ_o psi	σ_m psi Experimental/ Theoretical
0-degree	18.70	0	180010.26	249405.50 249307.14
90-degree*	.90	8498	1.30	9792.25 9736.34
90-degree**	.91	8175	2.95	10173.09 9981.98

* 21 Specimen Data Sample ** 26 Specimen Data Sample

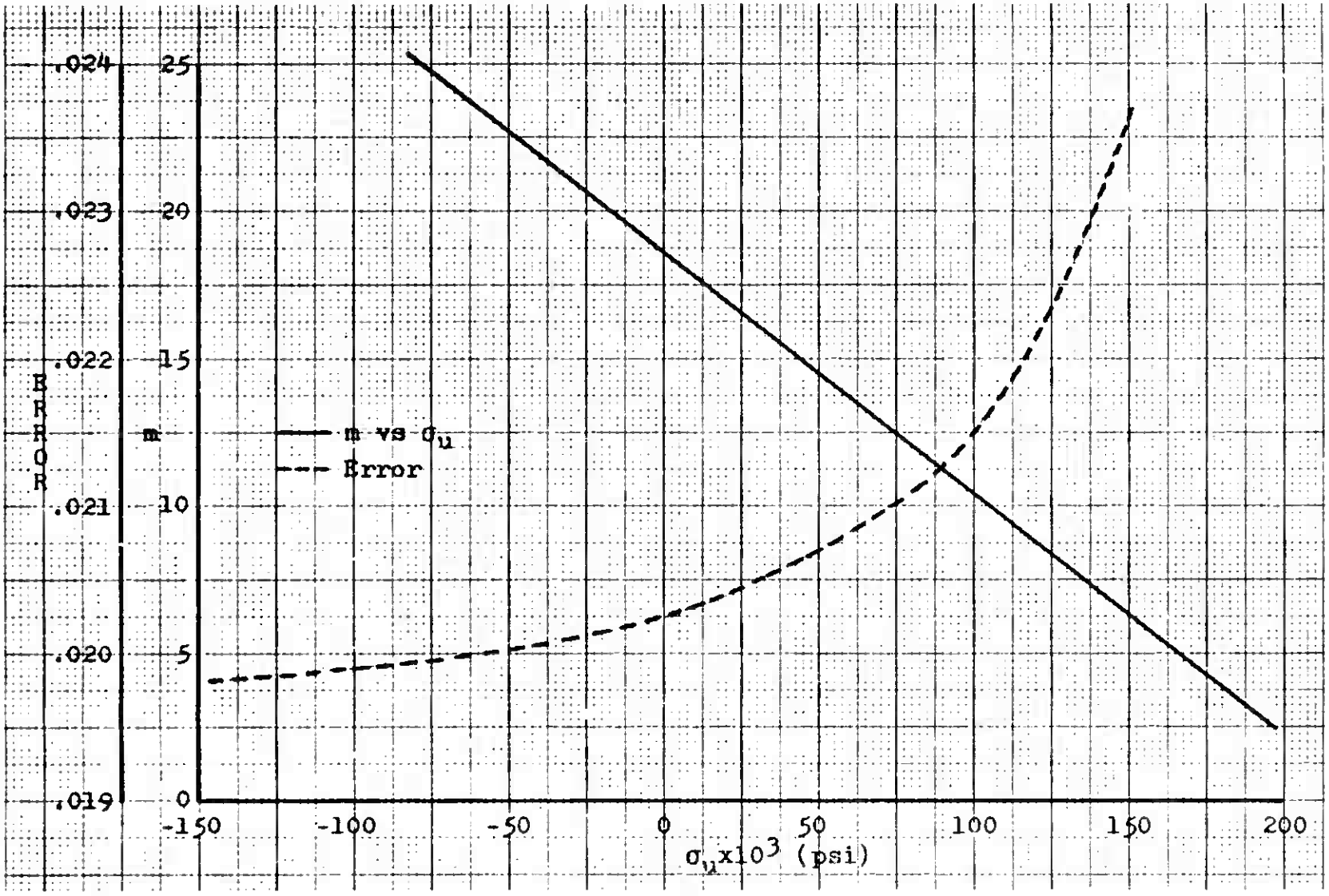

Fig. 16. 0-degree Pure Bending Parameters

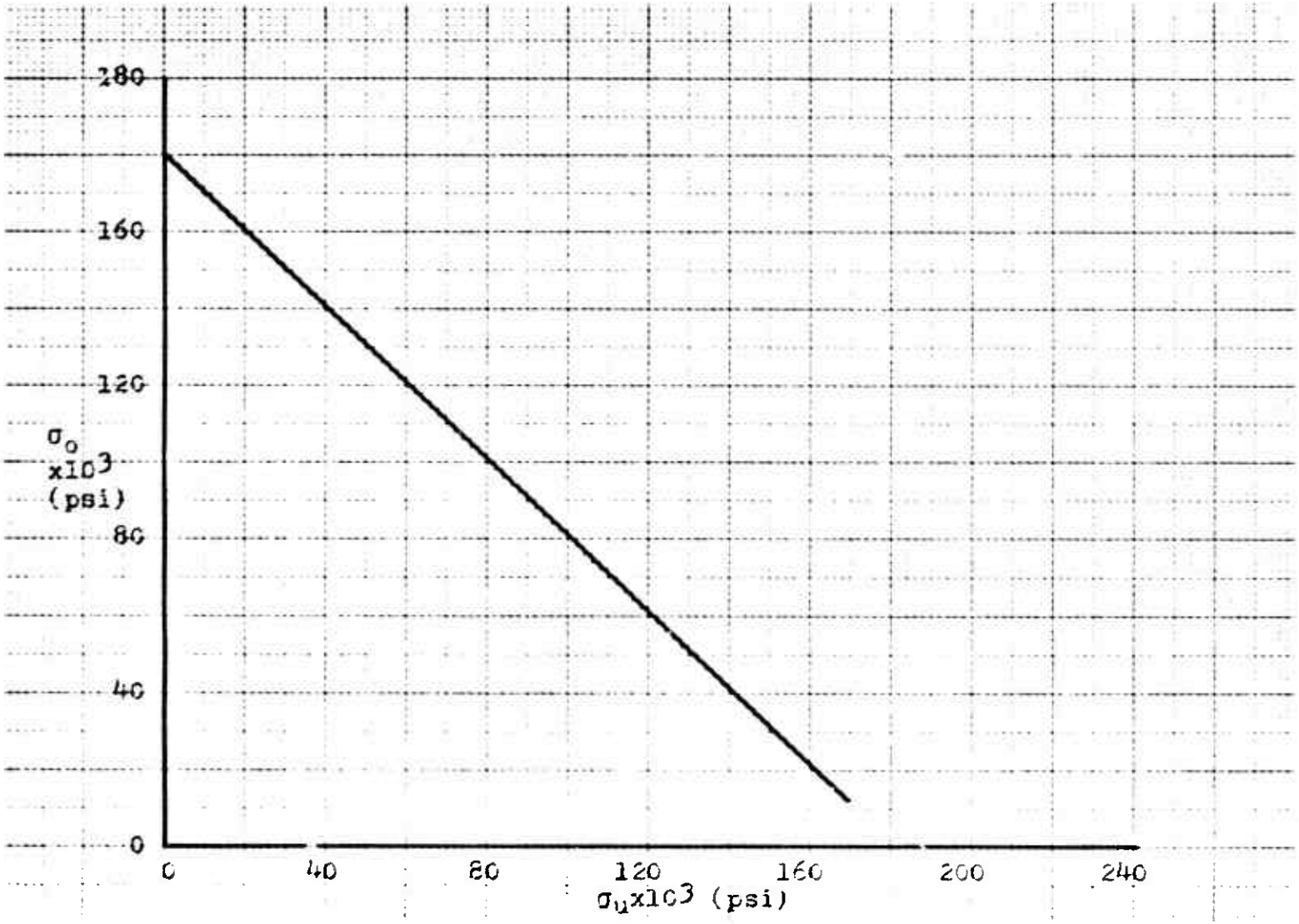

Fig. 17. 0-degree Pure Bending Parameters

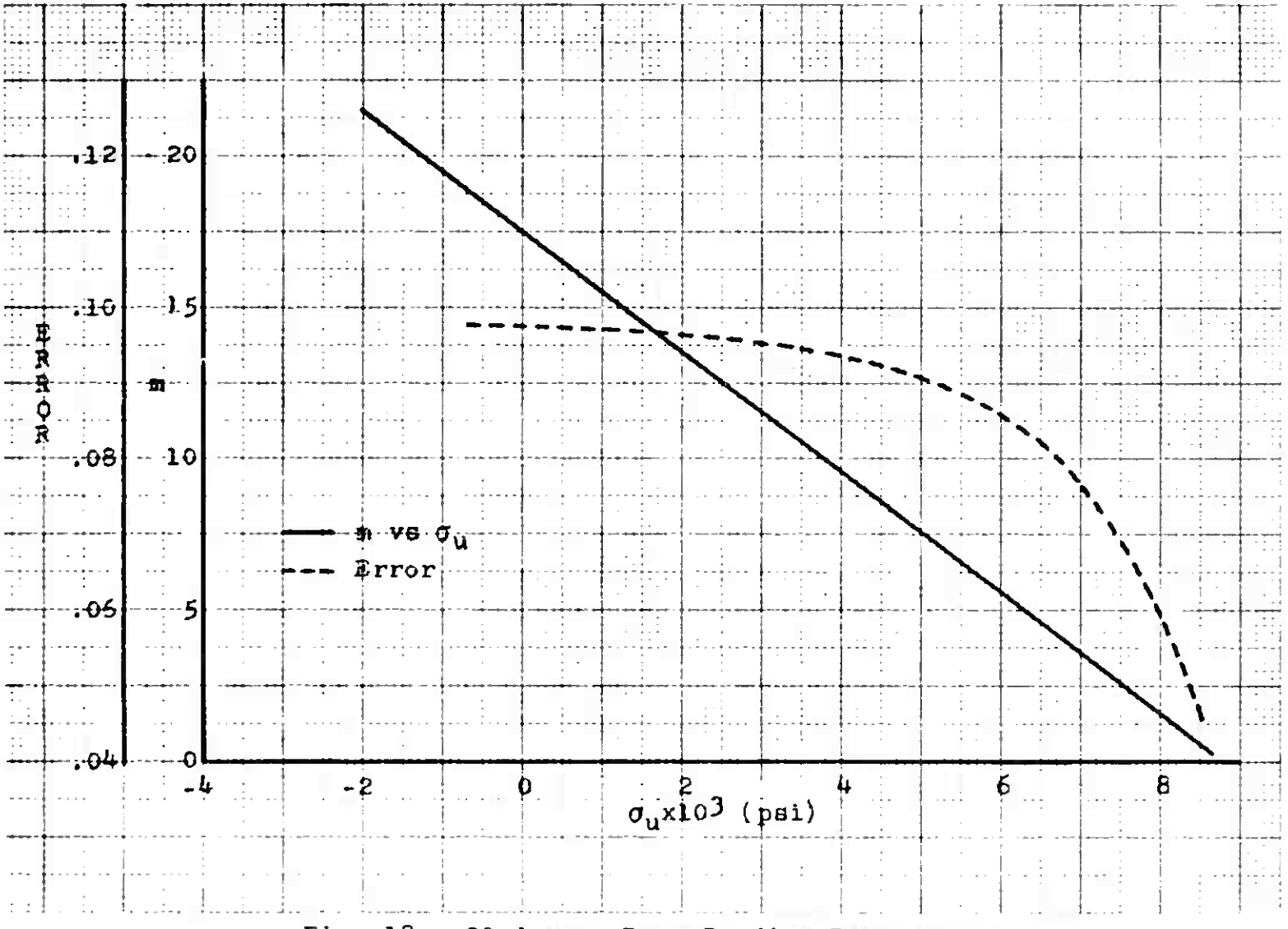

Fig. 18. 90-degree Pure Bending Parameters
(without strain gaged specimen)

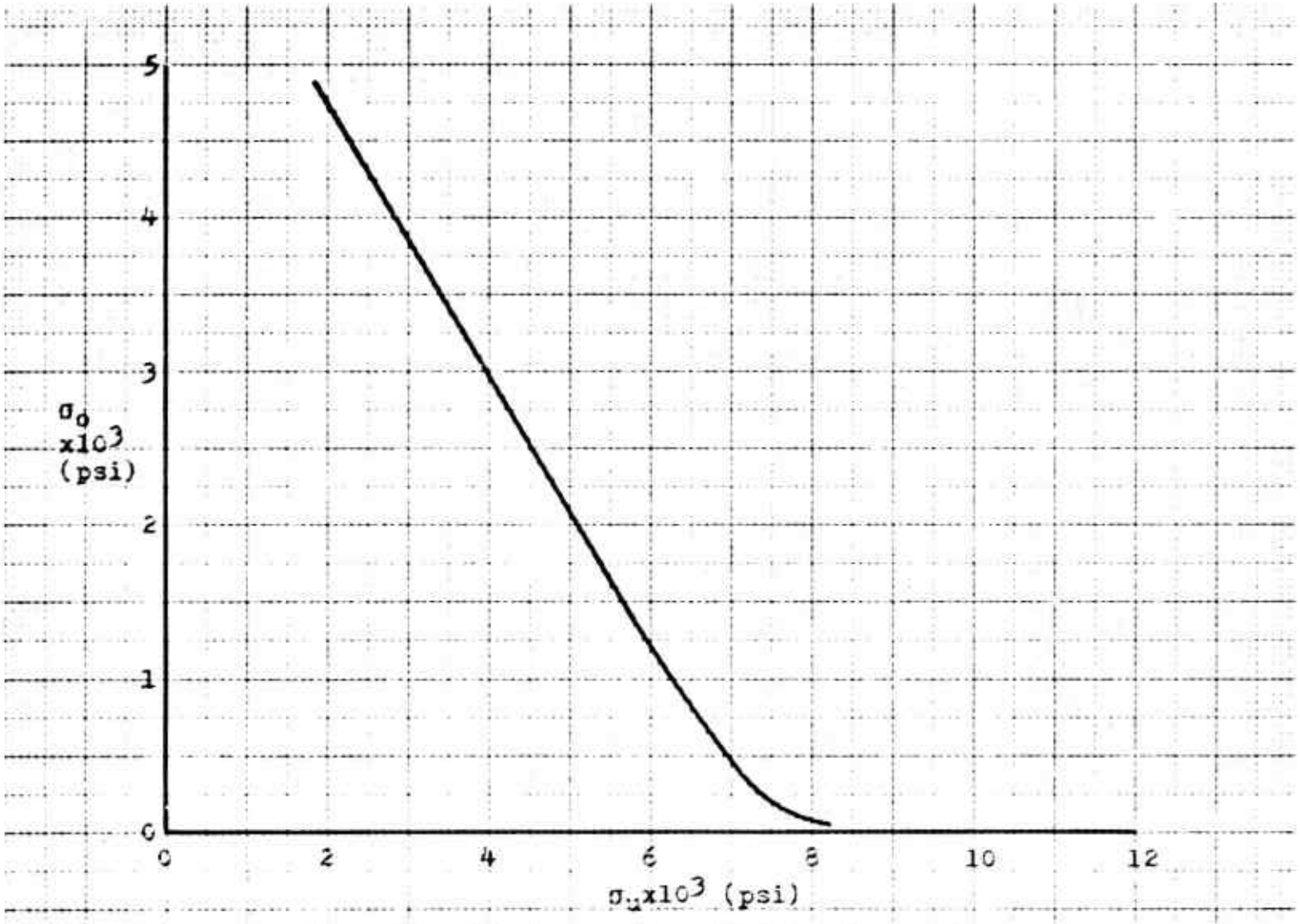

Fig. 19. 90-degree Pure Bending Parameters
(without strain gaged specimen)

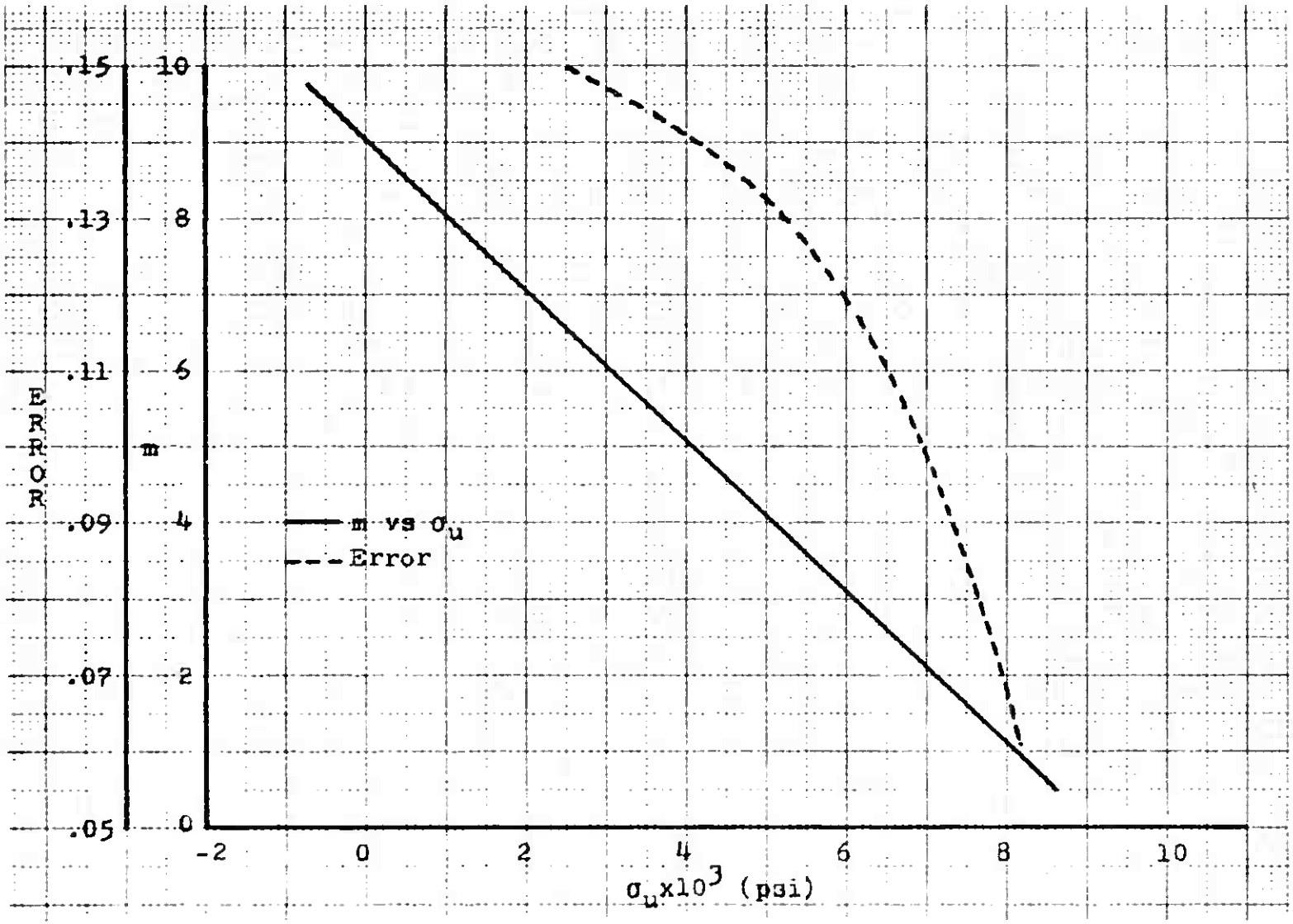

Fig. 20. 90-degree Pure Bending Parameters (including strain gaged specimen)

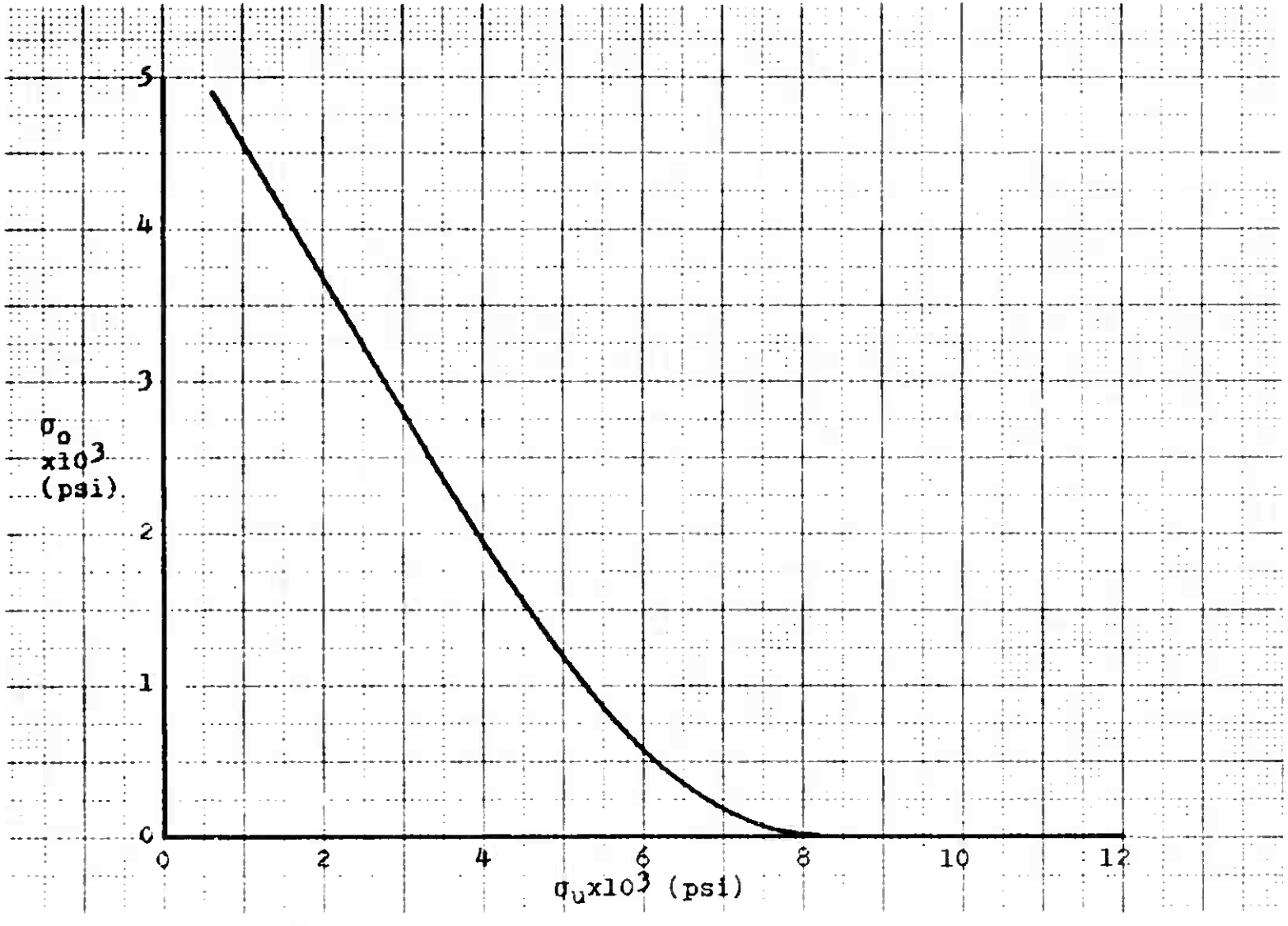

Fig. 21. 90-degree Pure Bending Parameters (including strain gaged specimen)

These values are determined based on a fit error convergence factor of .0001 using the least squares method. Table III. gives the fit error values corresponding to the parameters shown in Table II.

Table III.

Bending Data Fit Error

Specimen Type	Fit Error
0-degree	.02198
90-degree	.04589
90-degree	.06114

The author questioned the difference in fit resulting between the 21 specimen and 26 specimen 90-degree parameters, but one has to realize the relationship of the parameters in the Weibull equation and the significant change in the shape of the distribution curve caused by the addition of the 5 instrumented specimen to the top of the distribution.

Computations became some-what erratic as estimates of σ_u approached the lowest failure data point where probability of failure values predicted by the Weibull expression became very sensitive to very small variations in the individual parameters. The author has attempted to attain as high an accuracy as possible, but practical considerations required the establishing of tolerances. As a consequence of this, the following minimums where placed on the param-

eter variation increments: $\sigma_u \pm 1.0$ psi; $m \pm .01$; $\sigma_o \pm .1$ psi and ± 1.0 psi. Two minimums were placed on σ_o due to the magnitudes of this parameter for the 0-degree specimens. Error variation per unit change in σ_o for the 0-degree data was less than .00001.

Figures 22, 23 and 24 show the experimental pure bending data and the Weibull equation plotted using the values shown in Table II. For comparative purposes additional plots with various parameter sets chosen from Figures 16, 18, and 20 are provided in Figures 1C through 8C of Appendix C.

The determining factor for the best 0-degree specimen parameters is the lower limit previously placed on σ_u. Mathematically, however, a better fit can be achieved using negative values of σ_u. The minimum fit error occured at $\sigma_u = -290{,}000$ psi. This value is approximate since a detailed analysis into establishing this exact value was not conducted. Figure 2C in Appendix C verifies that using negative values does provide a mathematically accurate fit to the experimental data. Within the physical interpretation of this parameter as the zero probability failure value, this of course cannot occur. The reason for the increased accuracy using a negative σ_u value is again due to the mathematical relationship of the three parameters within the Weibull bending equation. This of course also points to the fact that placing a physical significance onto the σ_u parameter as it appears in the Weibull equation, may be incorrect.

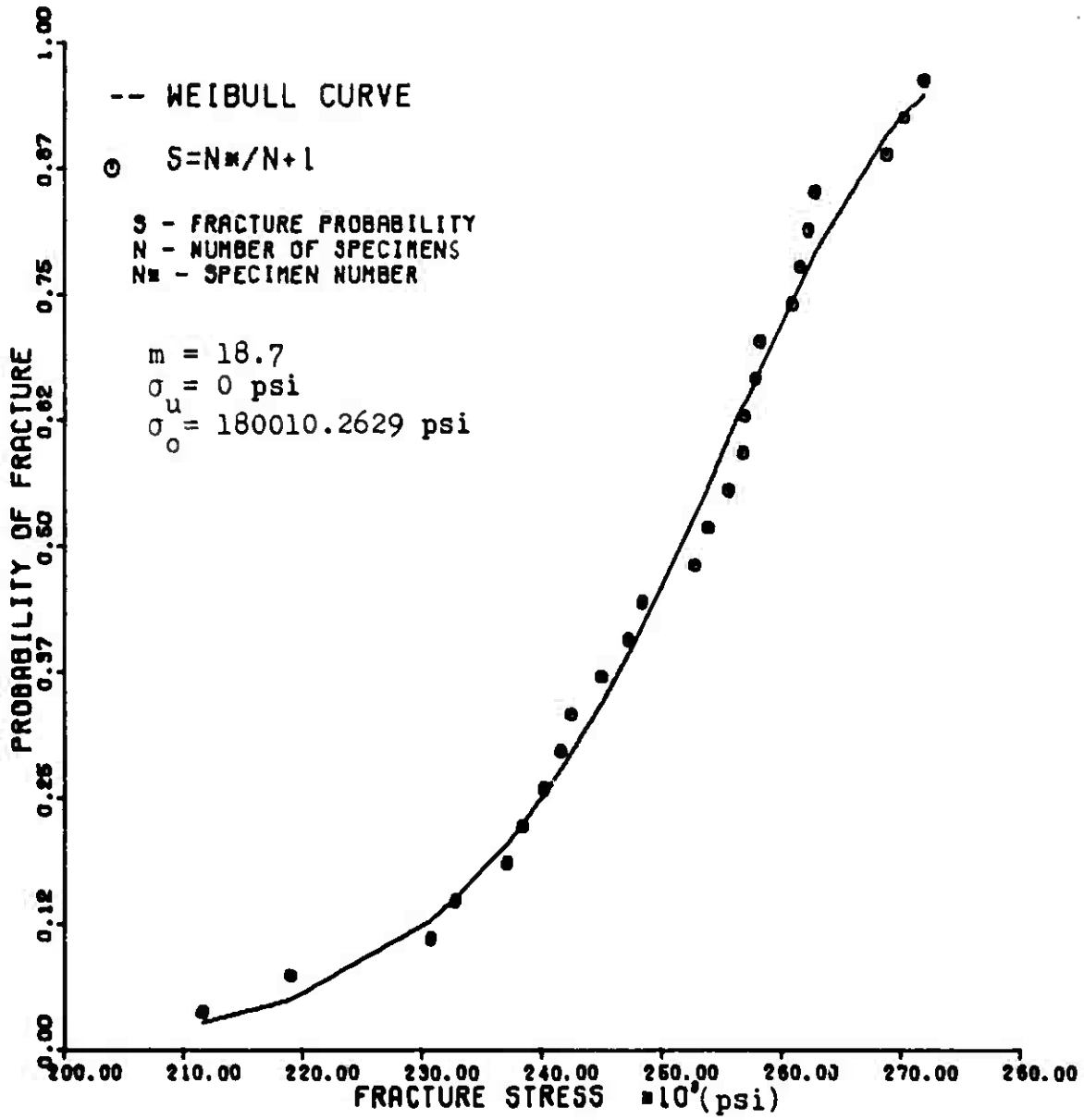

Fig. 22. Comparison of Experimental Bending Data and Theoretical Cumulative Distribution Function 0-degree Specimen

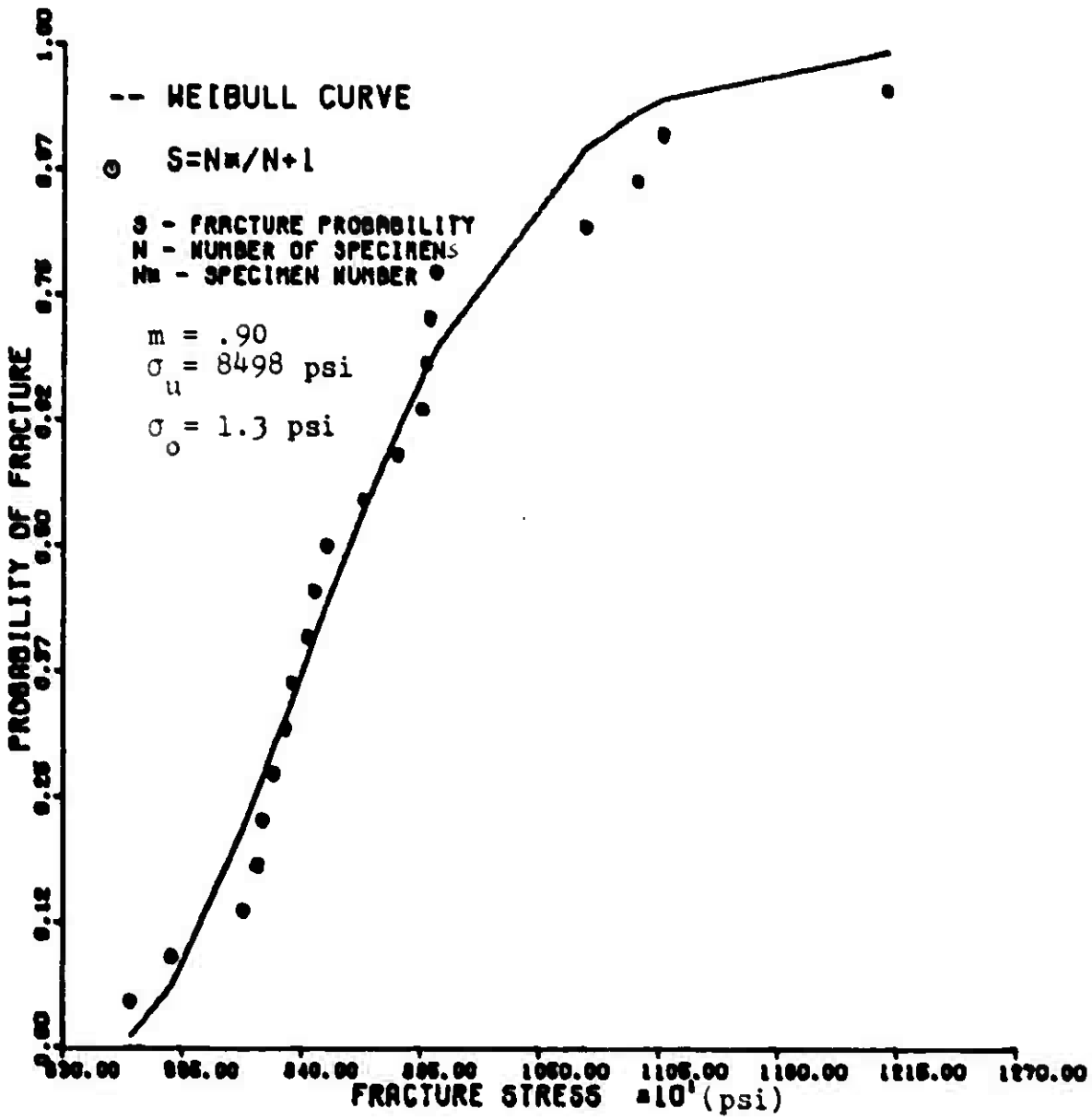

Fig. 23. Comparison of Experimental Bending Data and Theoretical Cumulative Distribution Function 90-degree Specimen*

* without strain gaged specimens

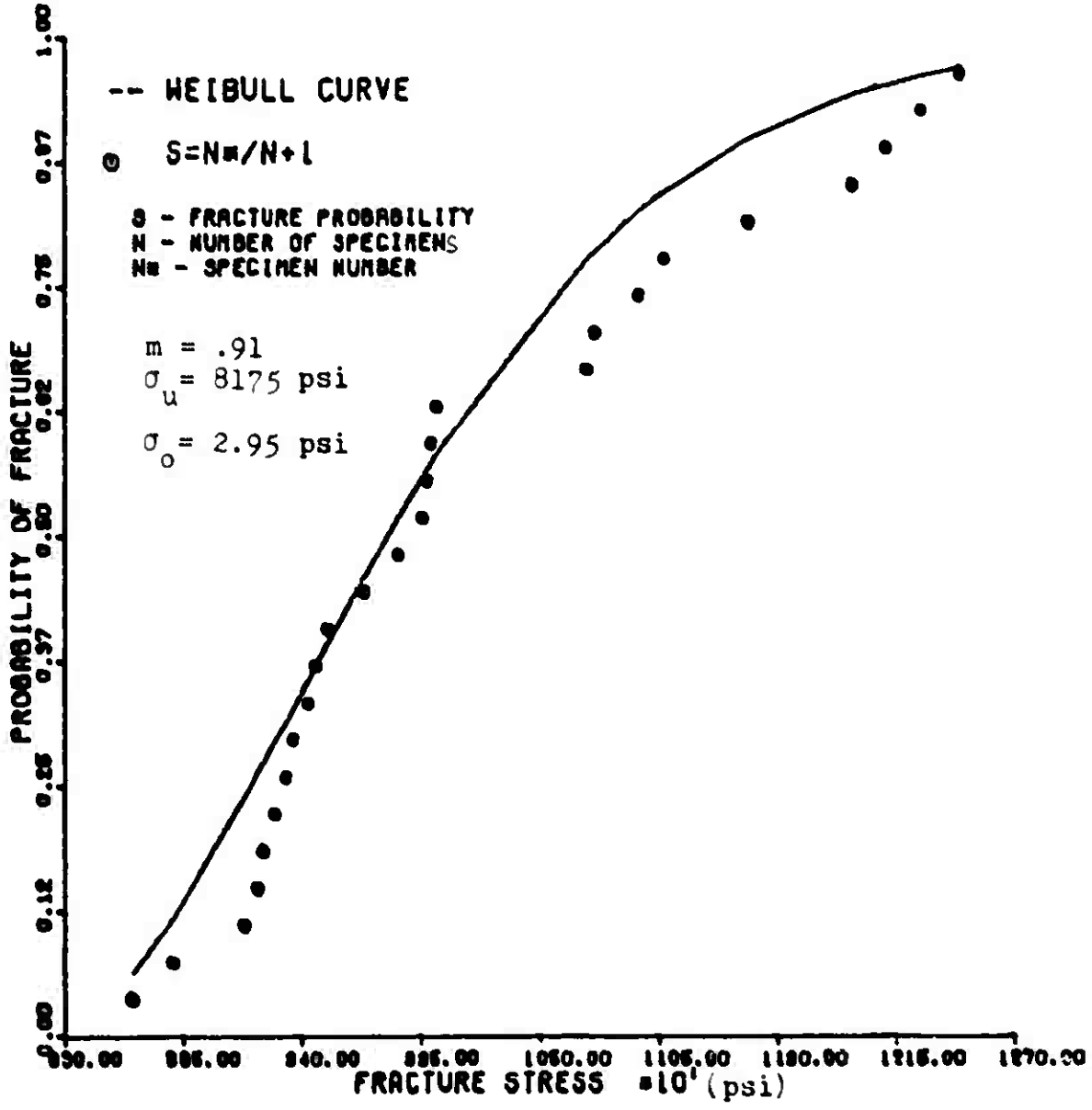

Fig. 24. Comparison of Experimental Bending Data and Theoretical Cumulative Distribution Function 90-degree Specimen*

* including strain gaged specimens

Theoretical Equation Validation

The parameters developed in the previous section now permit the evaluation of the Weibull equations which where derived for tension and three-point loading failure. Based on the premise that the Weibull parameters are material related values, the resulting theoretical distributions should approximate the distribution established experimentally for each failure mode. The specific evaluation results are presented per failure criteria and specimen fiber orientation in the following subsections.

A. Tension equation - 0-degree specimen.

Equation (15) was evaluated in combination with the material parameters derived from the 0-degree bending failure distribution as given in Table II. Direct substitution of this parameter set into Equation (15) resulted in a failure distribution predicting 100 percent failure at stress values above 230,000 psi. This of course does not match the experimental data for 0-degree tension failure as can be seen in Table XI of Appendix B.

Since the derivation of the Weibull equations assumed a volumetric flaw distribution, the volumetric differences between the bending and tensile specimen were normalized using the following relationship

$$\frac{V_b}{\sigma_{ob}^m} = \frac{V_t}{\sigma_{ot}^m} \qquad (81)$$

where b - bending

t - tension

from which a volumetrically normalized σ_o can be defined as

$$\sigma_{ot} = \sigma_{ob} V_t^{1/m} V_b^{-1/m} \tag{82}$$

Equation (15) can now be written as

$$B_t = V_t \left(\frac{\sigma - \sigma_u}{\sigma_{ot}}\right)^m \tag{83}$$

Using this equation and the parameter set established from 0-degree bending specimen, the resulting theoretical distribution function improved slightly, however, the overall data match was still very poor.

Comparison of the experimental failure distributions obtained for bending and tension indicated that the basic failure stress extremes are nearly the same. Therefore, based on this characteristic, a theoretical curve similar to that obtained for bending should also provide very adequate predictions for the experimental tension distribution. The modification of the tension equation under these circumstances can now be accomplished as follows; since the parameter set being evaluated has a σ_u value equal to zero, the bending risk of rupture equation can be written

$$B_b = \frac{V_b}{2(m+1)} \left(\frac{\sigma}{\sigma_{ob}}\right)^m \tag{84}$$

The tension risk of rupture equation under the same conditions is

$$B_t = V_t \left(\frac{\sigma}{\sigma_{ot}}\right)^m \tag{85}$$

Similar risk of rupture values are obtained for a given stress level only under the conditon where

$$\frac{V_b}{2(m+1)\sigma_{ob}^m} = \frac{V_t}{\sigma_{ot}^m} \tag{86}$$

therefore, defining

$$\sigma_{ot}^* = \left[\frac{2V_t(m+1)}{V_b}\right]\sigma_{ob} \tag{87}$$

σ_{ot}^* is used to differentiate this σ_o from that used in the expression normalizing the volumes. By substituting this expression into the tension risk of rupture equation, the resulting form of this equation is

$$B_t = V_t\left(\frac{\sigma}{\sigma_{ot}^*}\right)^m \tag{88}$$

for the specific set of experimental data being evaluated. This equation yields very good failure predictions for the experimental data, as is shown in Figure 25. For graphite-epoxy specimen with 0-dgree fiber orientation it is therefore possible to predict the probability of failure in tension using a set of Weibull parameters which have been established using experimental flexure data. However, the σ_o parameter must be modified to account for the differences in the nature of the two types of risk of rupture equations. The method utilized to modify the tension equation has also been used by Hahn and Knight [12] in studying short fiber composites.

B. Tension equation - 90-degree specimen.

Equation (15) was evaluated using both the set of ma-

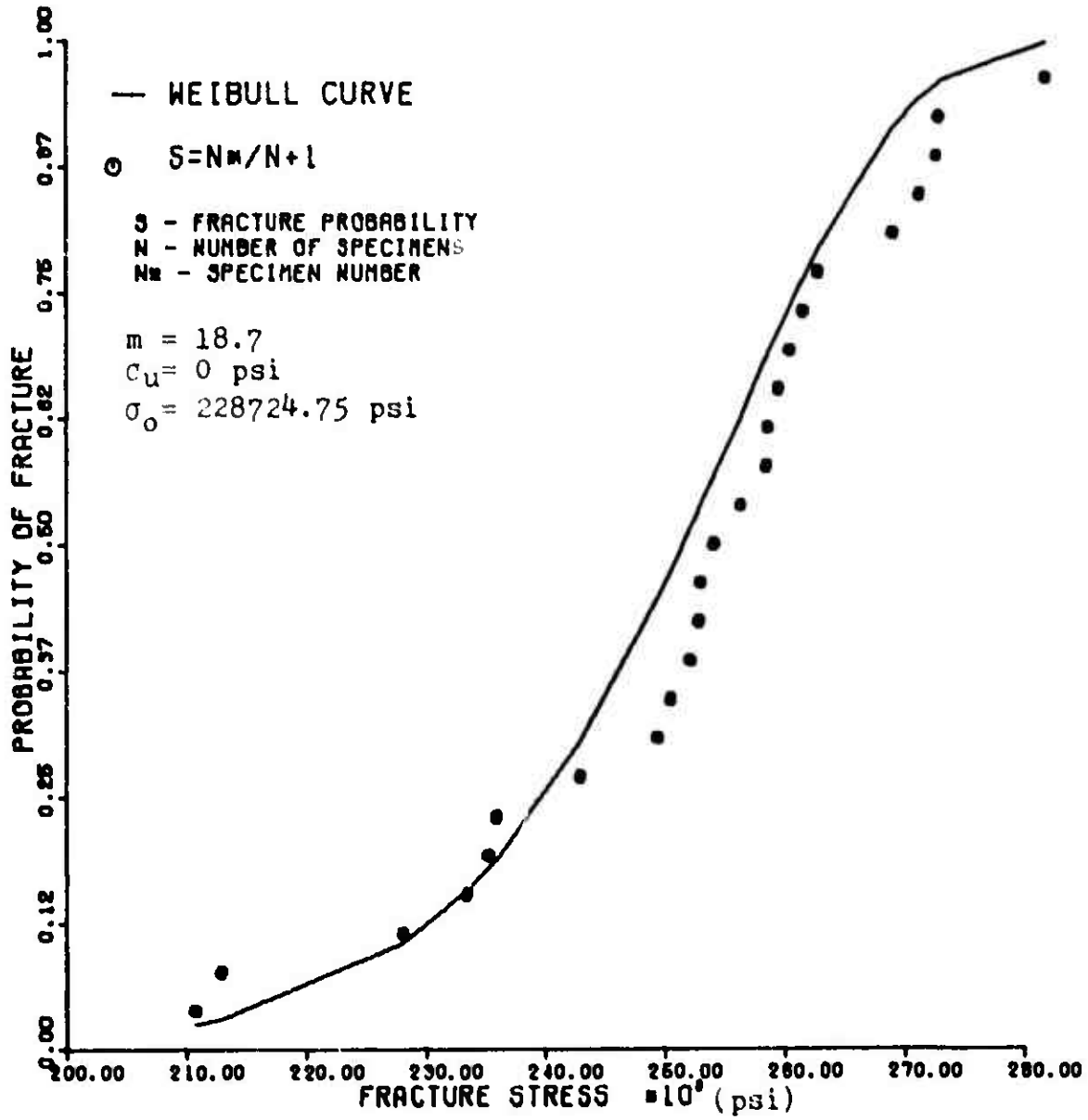

Fig. 25. Comparison of Experimental Tension Data and Theoretical Cumulative Distribution Function 0-degree Specimen - using Bending Parameters

terial parameters defined using the 90-degree flexure data which included the strain-gaged specimen data points as well as the set which was established using only noninstrumented specimen data. Even after manipulations of Equation (15) in the manner described for the 0-degree tension data, no approximation of realistic failure probabilities could be obtained using the parameters from either flexure data. The immediately obvious reasons for this are the values of σ_u. These values are greater than 80 percent of the experimental data points. As a result, a negative exponentiated term appears in the risk of rupture equation.

Various combinations of Weibull parameters with σ_u values lower than the lowest failure stress data point, obtained using Figures 18 and 20, were analyzed but no suitable combination could be established. Due to the significant differences in the failure characteristics in the 90-degree fiber oriented graphite-epoxy specimen when subjected to tension as compared to pure bending failure, no correlation was found in the use of a single set of Weibull parameters for failure probability prediction across these failure modes.

C. Three-point loading equation - 0-degree specimen.

Equation (oo) was evaluated using the Weibull parameters defined using the 0-degree experimental pure bending data. Since the value of σ_u in this set of parameters is equal to zero, Equation (oo) can be rewritten in a much simpler form as follows:

$$B_{3Pt} = \frac{V_{3Pt}}{2(m+1)^2}\left(\frac{\sigma}{\sigma_{o3Pt}}\right)^m \qquad (89)$$

where σ_{o3pt} is normalized for volume.

Substitution of the parameters shown in Table II into this form of the risk of rupture equation yielded failure predictions far too low. For example, replacing σ with the highest experimentally obtained failure stress for this failure mode resulted in a probability of failure of less than .22. Manipulation of Equation (89) in the manner described for the evaluation of the tension equation, allows the adjustment of the σ_o parameter as follows

$$\frac{V_b}{2(m+1)\sigma_{ob}^m} = \frac{V_{3Pt}}{2(m+1)^2\,\sigma_{o3Pt}^m} \qquad (90)$$

from which

$$\sigma_{o3Pt} = \left[\frac{V_{3Pt}}{(m+1)V_b}\right]^{\frac{1}{m}}\sigma_{ob} \qquad (91)$$

using this value for σ_o in the three-point loading risk of rupture equation provides the best correlation attainable for this set of parameters. The resulting curve is shown in Figure 26. As is evident, this curve provides a poor correlation to the experimental data and therefore, it is concluded that theoretical prediction of a 0-degree three-point loading failure mode using 0-degree bending parameters is not possible.

D. Three-point loading equation - 90-degree specimen.

Evaluation of Equation (66) was attempted using both

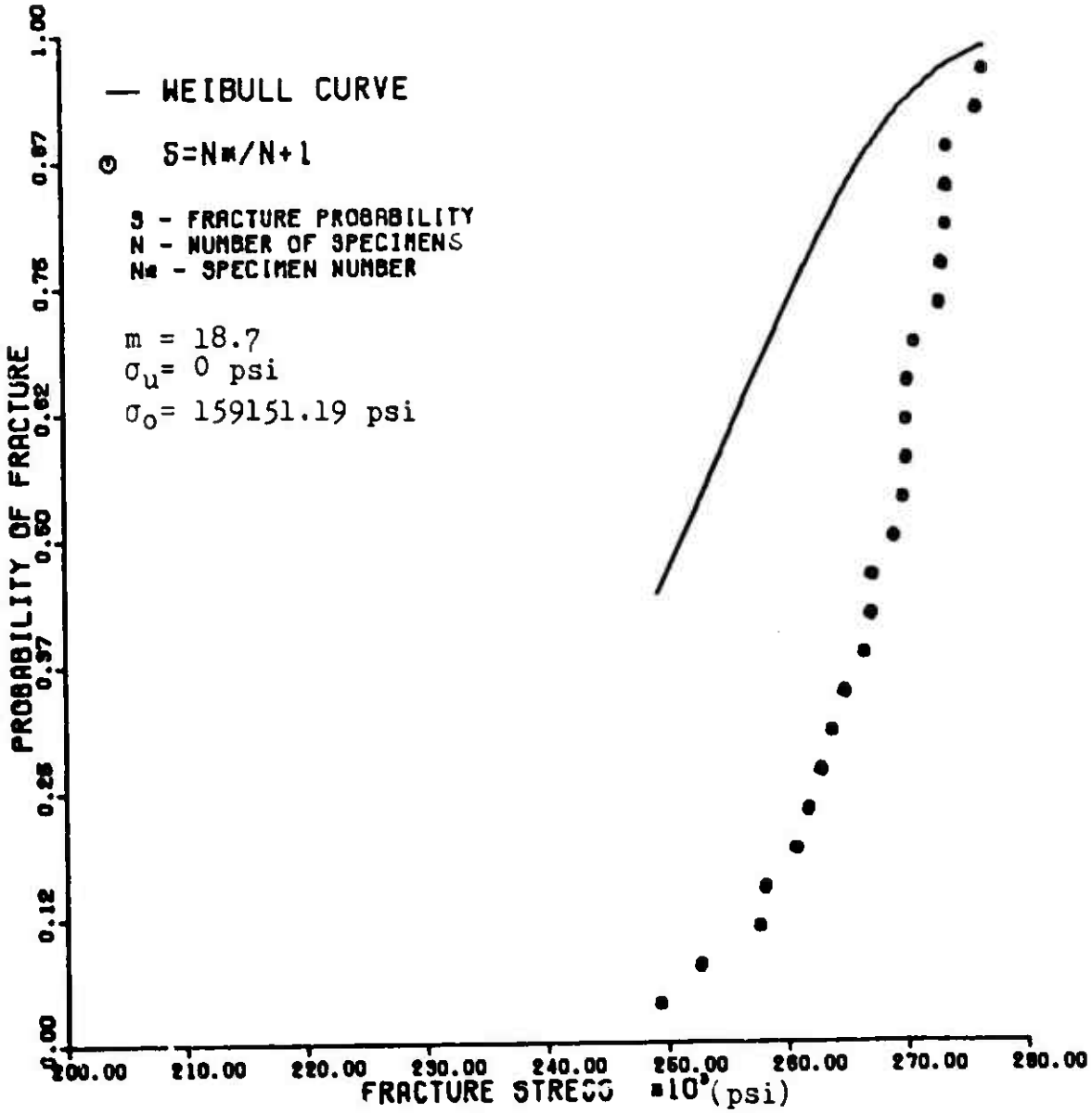

Fig. 26. Comparison of Experimental Three-point Loading Data and Theoretical Cumulative Distribution Function 0-degree Specimen - using Bending Parameters

sets of 90-degree bending parameters. Due to the complexity of the basic form of Equation (66), no solution could be obtained using the values as listed in Table II. However, since the criteria for establishing Figures 18 and 20 is that all sets of the listed m, σ_u and σ_o values provide a fit with the corresponding error, then utilizing the set of values corresponding to $\sigma_u = 0$ should provide an adequate measure of whether correlation between the experimental 90-degree three-point loading and the three-point loading equation given in Equation (89) exist. The resulting theoretical curves are shown in Figures 27 and 28. As can be seen in Figure 28, the theoretical prediction curve using the parameters derived from the 90-degree flexure data without the instrumented specimen is fairly good. However, the useability of the theoretical data in Figure 27 is questionable. The reader should be aware that these curves were plotted by direct substitution of the material parameters from the flexure analysis into Equation (89) using Equation (87). Manipulation of Equation (89) as shown in Equation (91) was not necessary. This of course means that the parameters are true material parameters for the 90-degree bending to 90-degree three-point data. The reader should recall that for the 0-degree data, the nature of the failure distribution had to be considered in order to achieve correlation. A point should be made at this time, and that is that the three bending derived material parameters are not common to

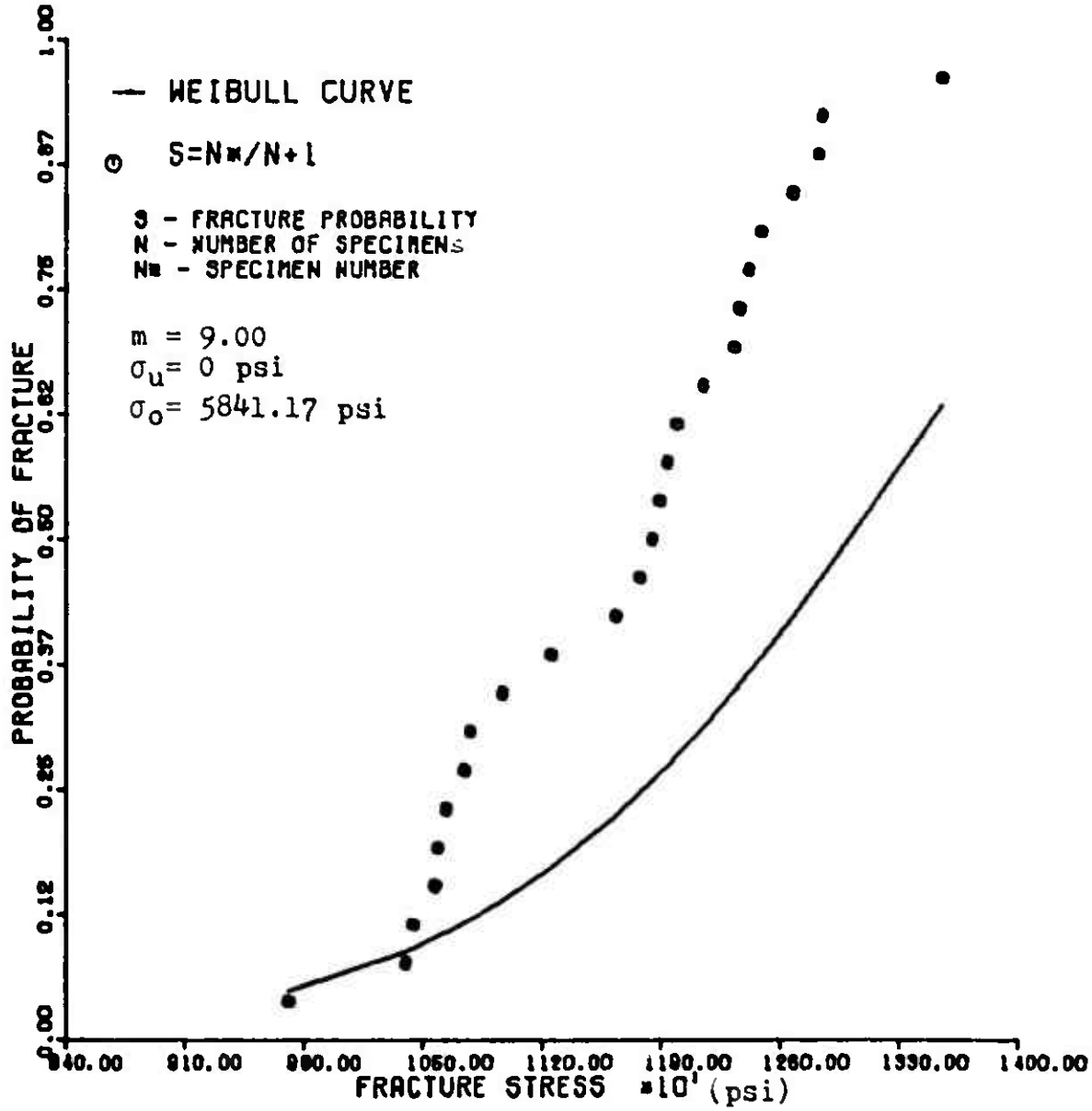

Fig. 27. Comparison of Experimental Three-point Loading Data and Theoretical Cumulative Distribution Function 90-degree Specimen - using Bending Parameters*

* 90-degree data - including strain gaged specimens

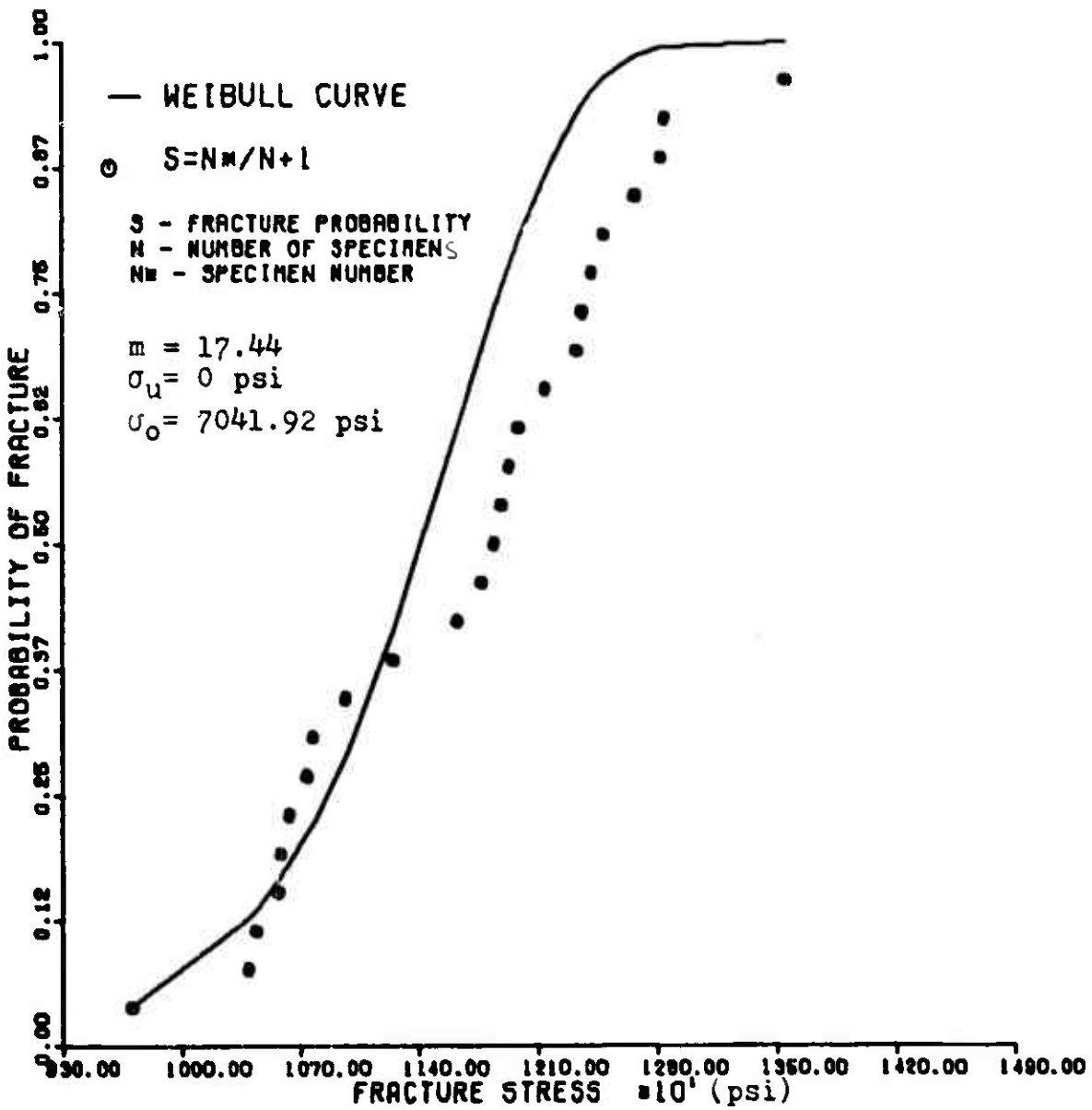

Fig. 28. Comparison of Experimental Three-point Loading Data and Theoretical Cumulative Distribution Function 90-degree Specimen - using Bending Parameters*

* 90-degree data - without strain gaged specimens

this group of experimental data, but are more oriented to the type of test. As a summary of this section the following correlation overview is provided.

Table IV.

Correlation Results - Bending Parameters

Equation	Data	Fit Obtained
Bending	0-degree	Excellent
	90-degree*	Excellent
	90-degree**	Excellent
Tension	0-degree	Good
	90-degree	None
Three-Point	0-degree	None
	90-degree	Poor using 90 flexure*
		Good using 90 flexure**

** not including strain-gaged specimens.

* including strain-gaged specimens.

Alternate Parameter Determination Methods

The problems encountered in obtaining correlation between the experimental data and theoretical predictions using bending parameters led to the evaluation of using an alternate parameter determination method. Since Equation (15) could easily be rewritten in the form of Equation (75), it could therefore be used in the same manner as the bending equation for parameter determination. The total param-

eter determination effort was therefore reaccomplished using the tension data. Figures 29 and 31 provide the values for m and σ_u while Figures 30 and 32 provide the values for σ_o which resulted from this analysis. Table V provides a listing of the best fit values contained on these charts. Table VI lists the fit error corresponding to the parameters shown in Table V.

Table V.

Weibull Parameters Using Tension

Specimen Type	m	σ_u psi	σ_o psi	σ_m psi Experimental/ Theoretical
0-degree	17.53	0	229965.27	251869.99 252128.76
90-degree	4.95	2120	3604.64	7228.64 7222.43

Table VI.

Tension Data Fit Error

Specimen Type	Fit Error
0-degree	.03782
90-degree	.03316

Figures 33 and 34 show the resulting theoretical curves overlayed on the 0-degree and 90-degree specimen tension data points. Evaluation of parameter correlation to the

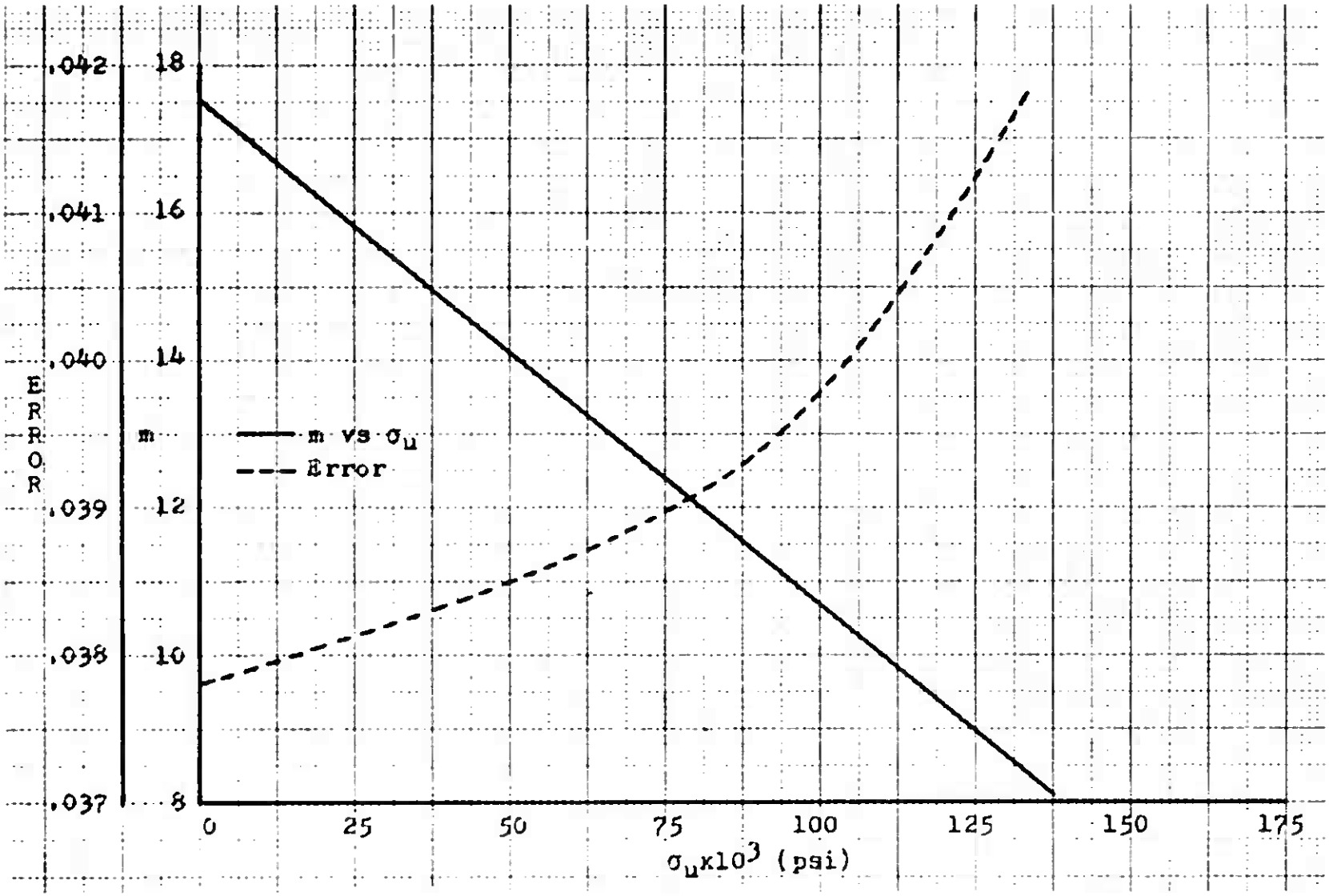

Fig. 29. 0-degree Tension Parameters

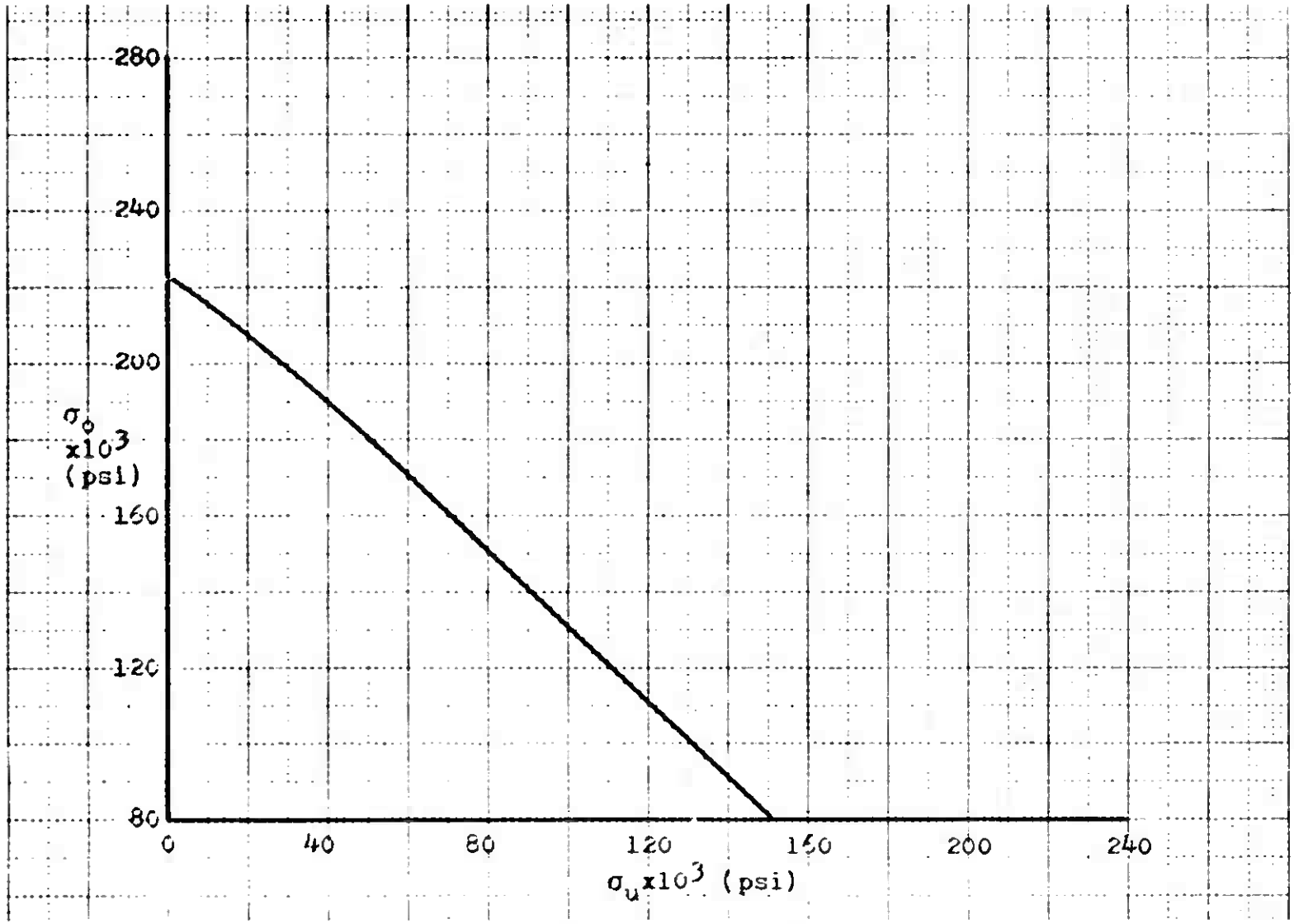

Fig. 30. 0-degree Tension Parameters

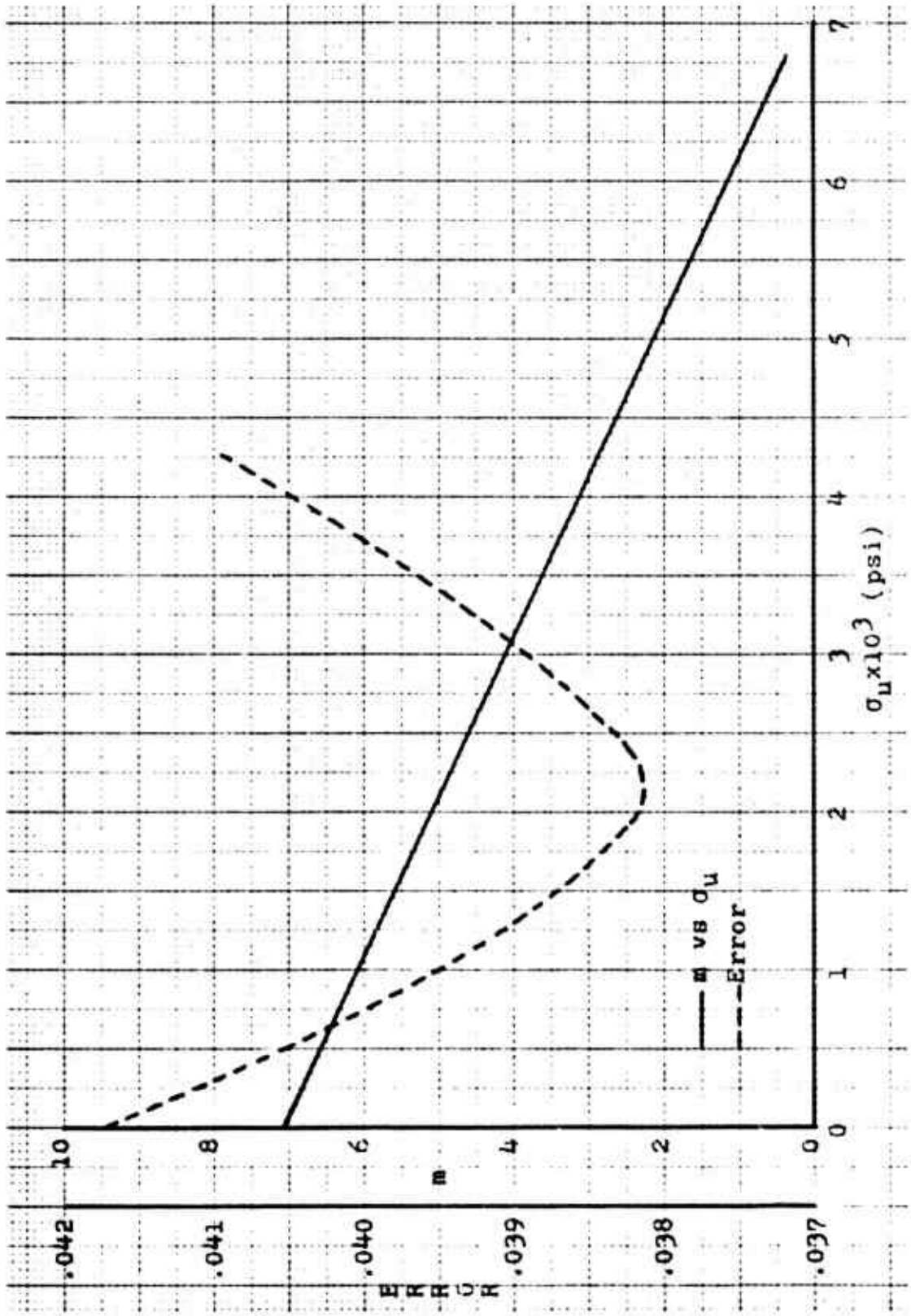

Fig. 31. 90-degree Tension Parameters

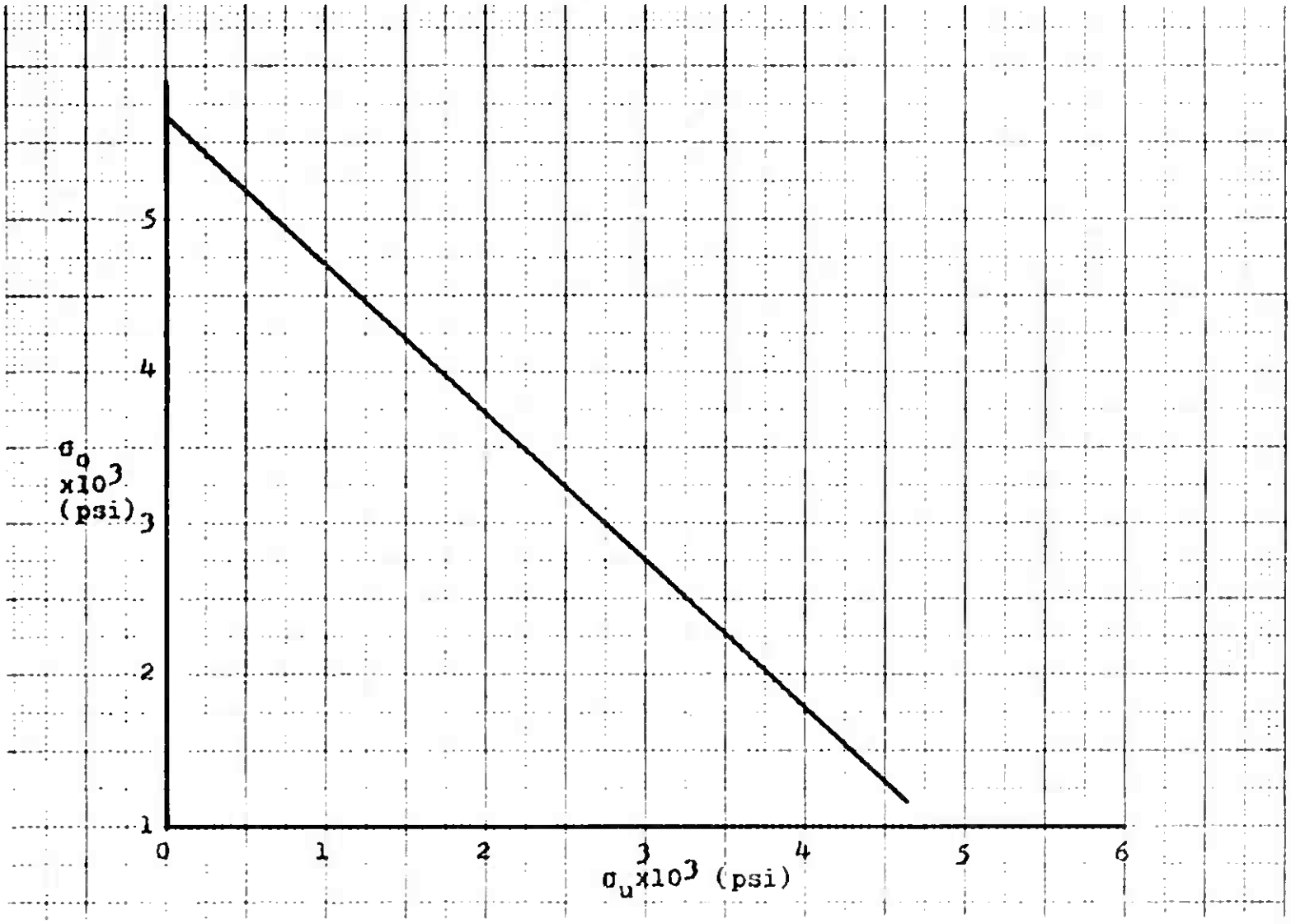

Fig. 32. 90-degree Tension Parameters

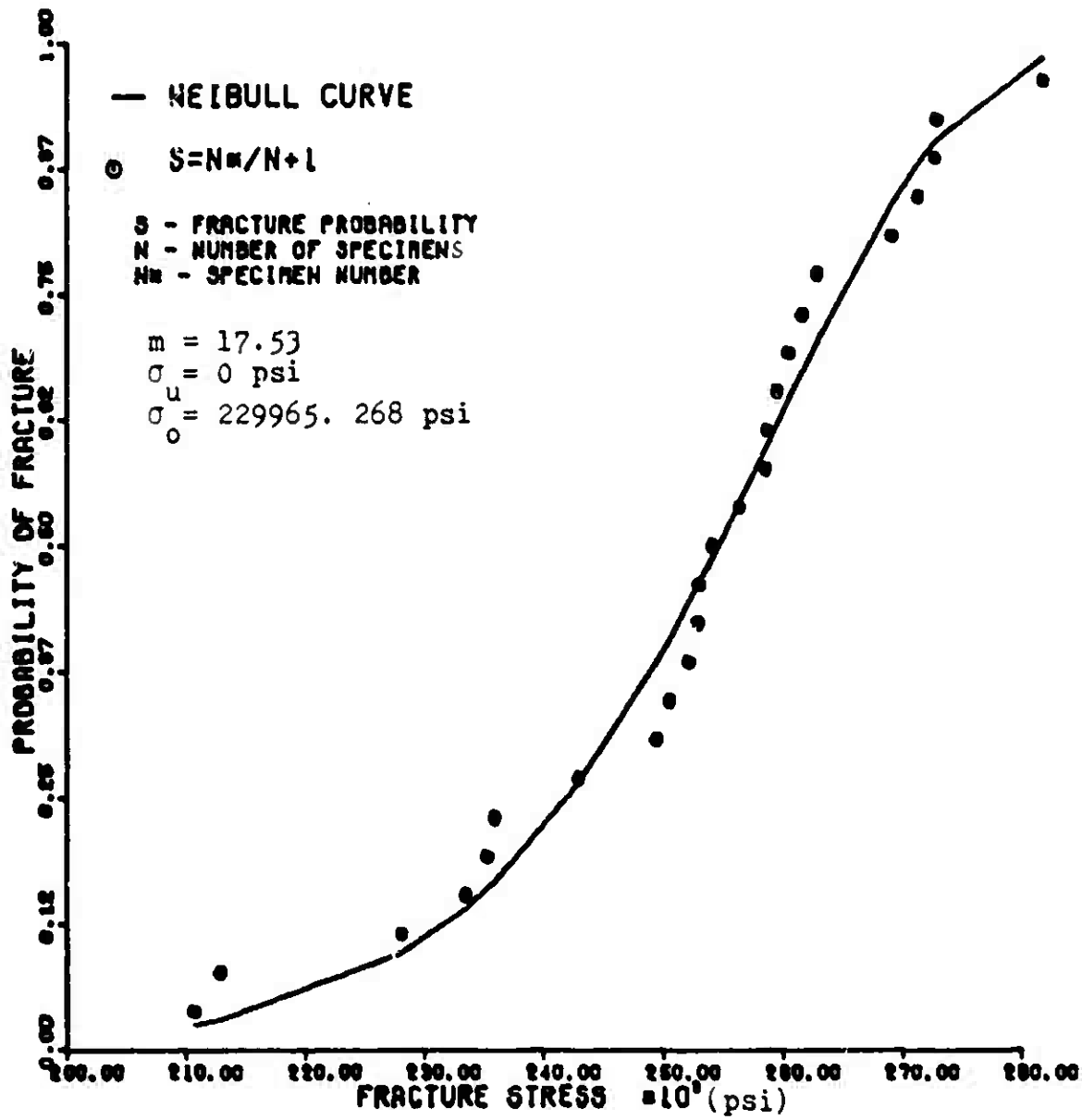

Fig. 33. Comparison of Experimental Tension Data and Theoretical Cumulative Distribution Function 0-degree Specimen

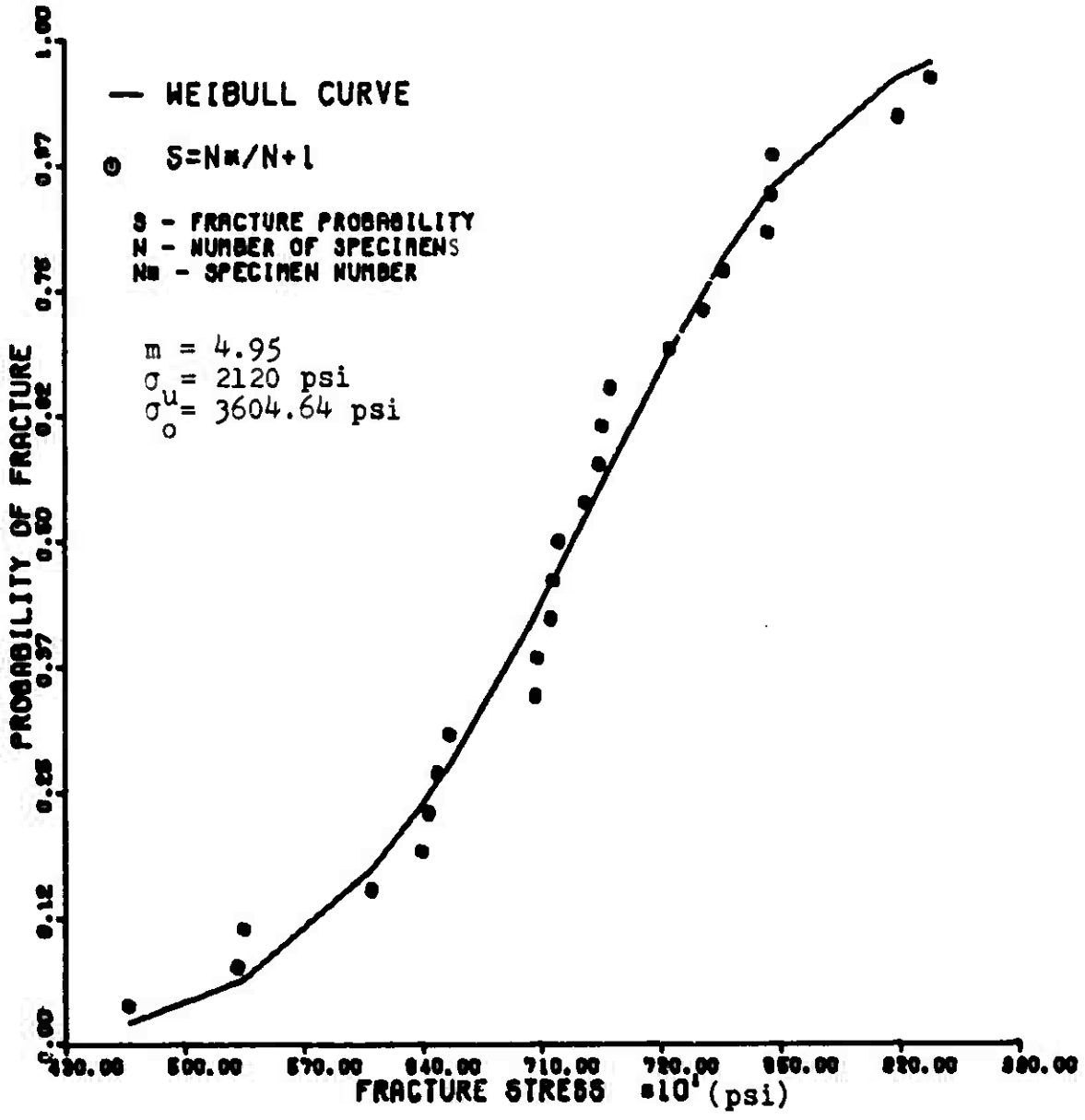

Fig. 34. Comparison of Experimental Tension Data and Theoretical Cumulative Distribution Function 90-degree Specimen

other failure modes for each specimen type is presented below.

A. Bending equation - 0-degree specimen.

Equation (6) was evaluated using the 0-degree parameters presented in Table V. Results similar to those obtained for the previous discussed analysis correlating bending to tension using the bending parameters were obtained in this effort. Using the definition provided in Equation (87) and solving the equation for σ_{ob}, the following expression results

$$B_b = \frac{V_b}{2(m+1)} \left(\frac{\sigma}{\sigma_{o_b}^*}\right)^m \qquad (92)$$

The theoretical curve obtained using this expression is shown in Figure 35. This result show that parameters derived from either tension or bending yield favorable comparisons to either theoretical equation.

B. Bending equation - 90-degree specimen.

Both of the 90-degree bending data samples were evaluated in this analysis. Poor correlation resulted for all equation manipulations attempted. This is further substantiated by the fact that the parameter sets in Figures 18, and 20 compared to those in Figure 31 for a given value of σ_u do not agree. The resulting best theoretical curves attained are shown in Figures 36 and 37.

C. Three-point loading equation - 0-degree specimen.

Equation (66) in the form of Equation (89) was evalu-

ated. No correlation was obtained using the 0-degree tension parameters from Table V. This is expected based on the results of the previous analysis using the bending parameters. A distribution with a very small range of maximum to minimum failure stress values would be expected to require a high value for the flaw density exponent (m) in order to establish correlation between the theoretical curve and experimental data.

D. Three-point loading equation - 90-degree specimen.

Equation (89) was evaluated using Weibull parameters corresponding to $\sigma_u = 0$ from Figure 31. Poor correlation, as shown in Figure 38, resulted. This is expected since the 90-degree bending and 90-degree tension produced poor correlation, while 90-degree bending compared favorably with 90-degree three-point loading.

In summary, the results obtained in this section also did not produce a set of parameters which allowed fracture prediction through the range of desired failure modes. The resulting set of tension data derived parameters proved to be even less suitable than those derived from the bending data. An overview correlation summary is in Table VII.

Since the general results of this thesis were unable to produce a singular set of Weibull parameters from which suitable theoretical failure probabilities could be established for the range of failure modes investigated, the author felt that it would be interesting to at least estab-

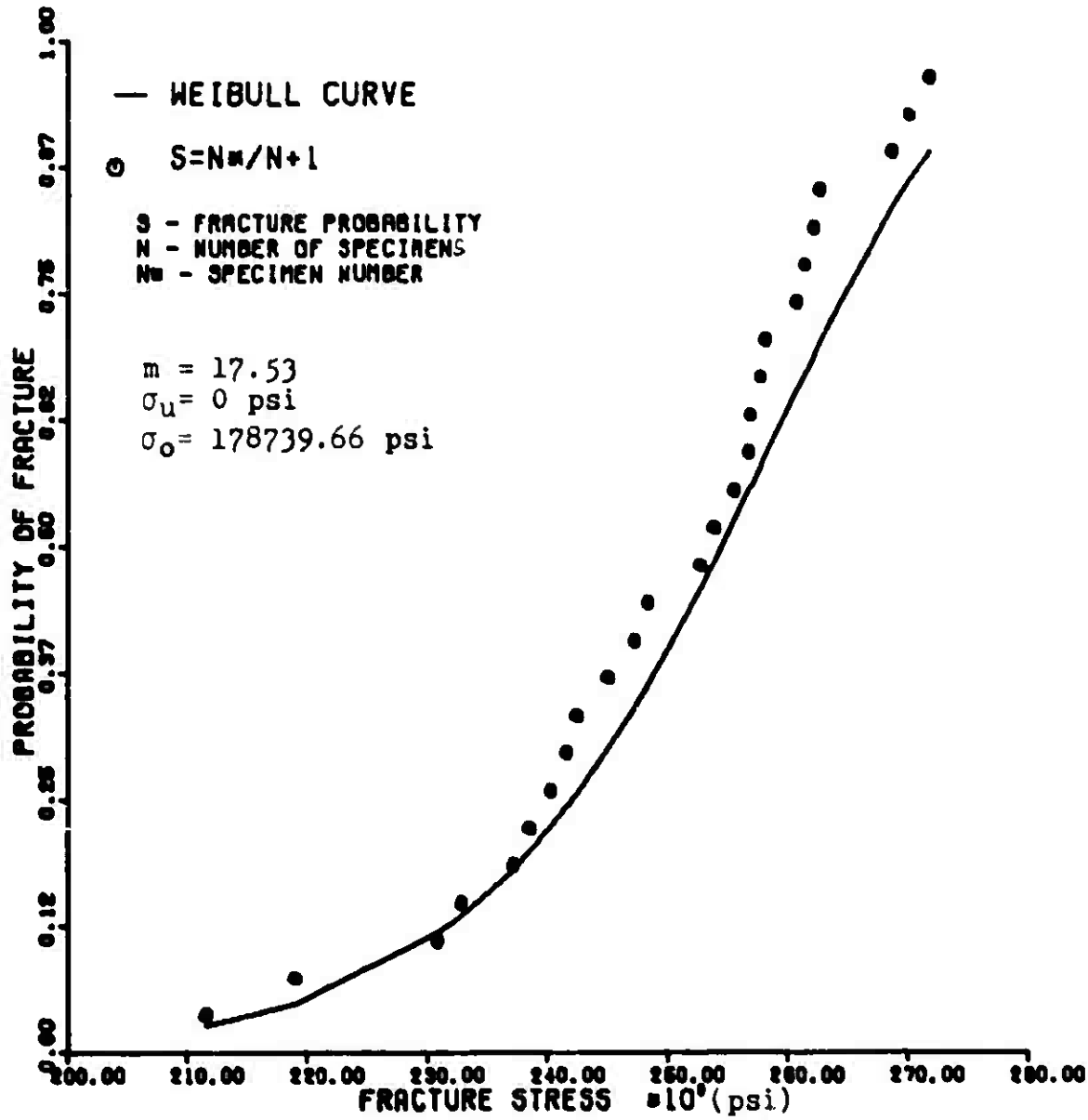

Fig. 35. Comparison of Experimental Bending Data and Theoretical Cumulative Distribution Function 0-degree Specimen - using Tension Parameters

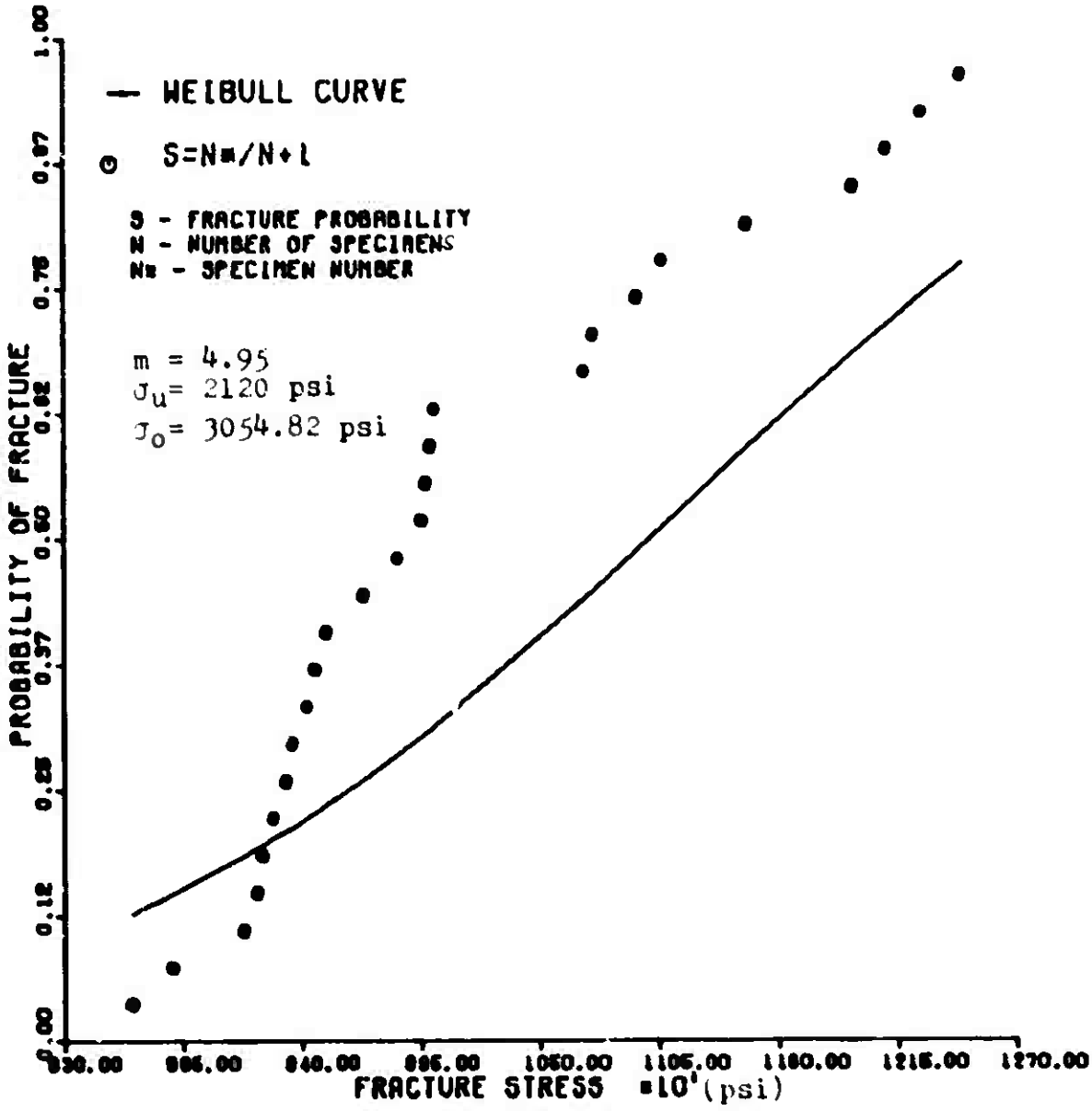

Fig. 36. Comparison of Experimental Bending Data and Theoretical Cumulative Distribution Function 90-degree Specimen* - using Tension Parameters

* including strain gaged specimens

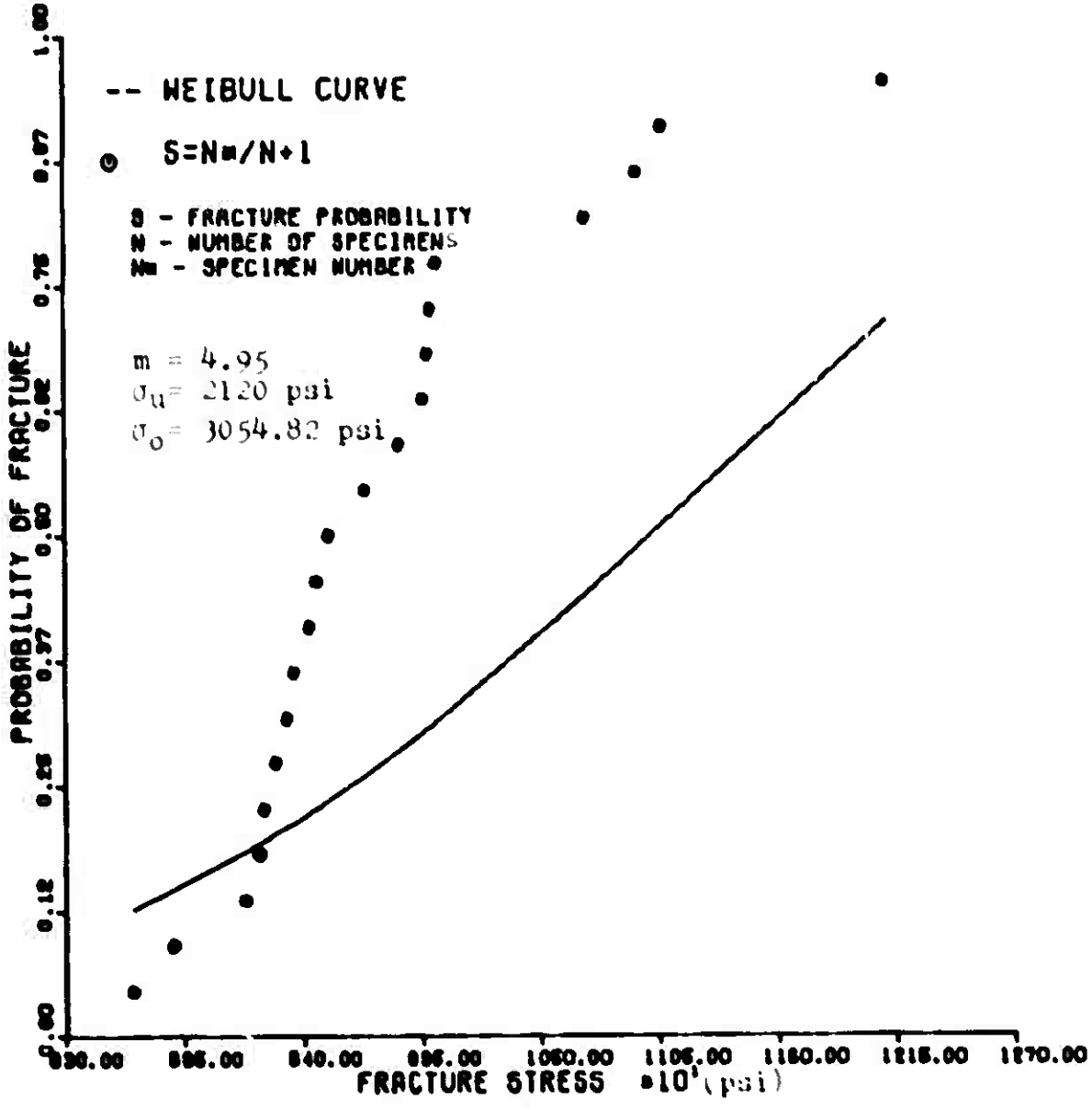

Fig. 37. Comparison of Experimental Bending Data and Theoretical Cumulative Distribution Function 90-degree Specimen* - using Tension Parameters

* without strain gaged specimen

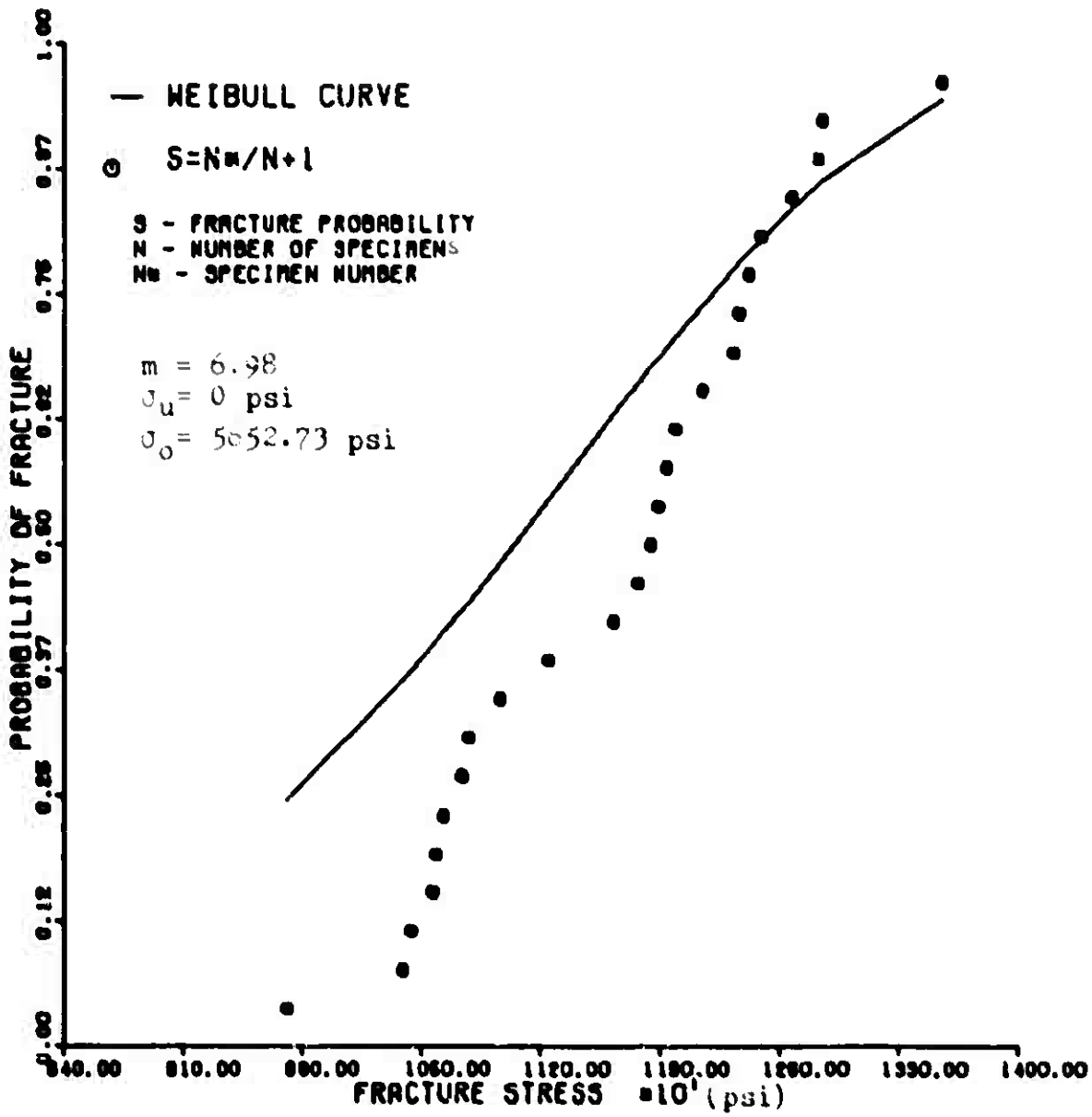

Fig. 38. Comparison of Experimental Three-point Loading Data and Theoretical Cumulative Distribution Function 90-degree Specimen - using Tension Parameters

Table VII.

Correlation Results - Tension Parameters

Equation	Data	Fit Obtained
Bending	0-degree	Good
	90-degree*	None
	90-degree**	None
Tension	0-degree	Excellent
	90-degree	Excellent
Three-Point	0-degree	None
	90-degree	None

* without strain.

** with strain.

lish one set of parameters for each experimental failure distribution which allowed accurate theoretical duplication of that distribution. Parameter sets to provide excellent theoretical curves for both bending and tension have already been established, however, no set for the three-point loading data has as yet been determined. Equation (66) is not suited to the manipulation conducted in Equation (75), however, the special case of Equation (66) presented by Equation (89) can be rearranged into a similar form. This then allows the determination of a best set of m and σ_o for σ_u = 0 and as such represents best theoretical prediction of the three-point loading data obtained in this thesis. The resulting values are shown in Table VIII.

Table VIII.

Weibull Parameters Using Three-Point Loading

	m	σ_u	σ_o	Error
0-degree	42.97	0	211702.27	.023202
90-degree	12.01	0	6150.49	.041770

The corresponding distribution functions are shown in Figures 39 and 40.

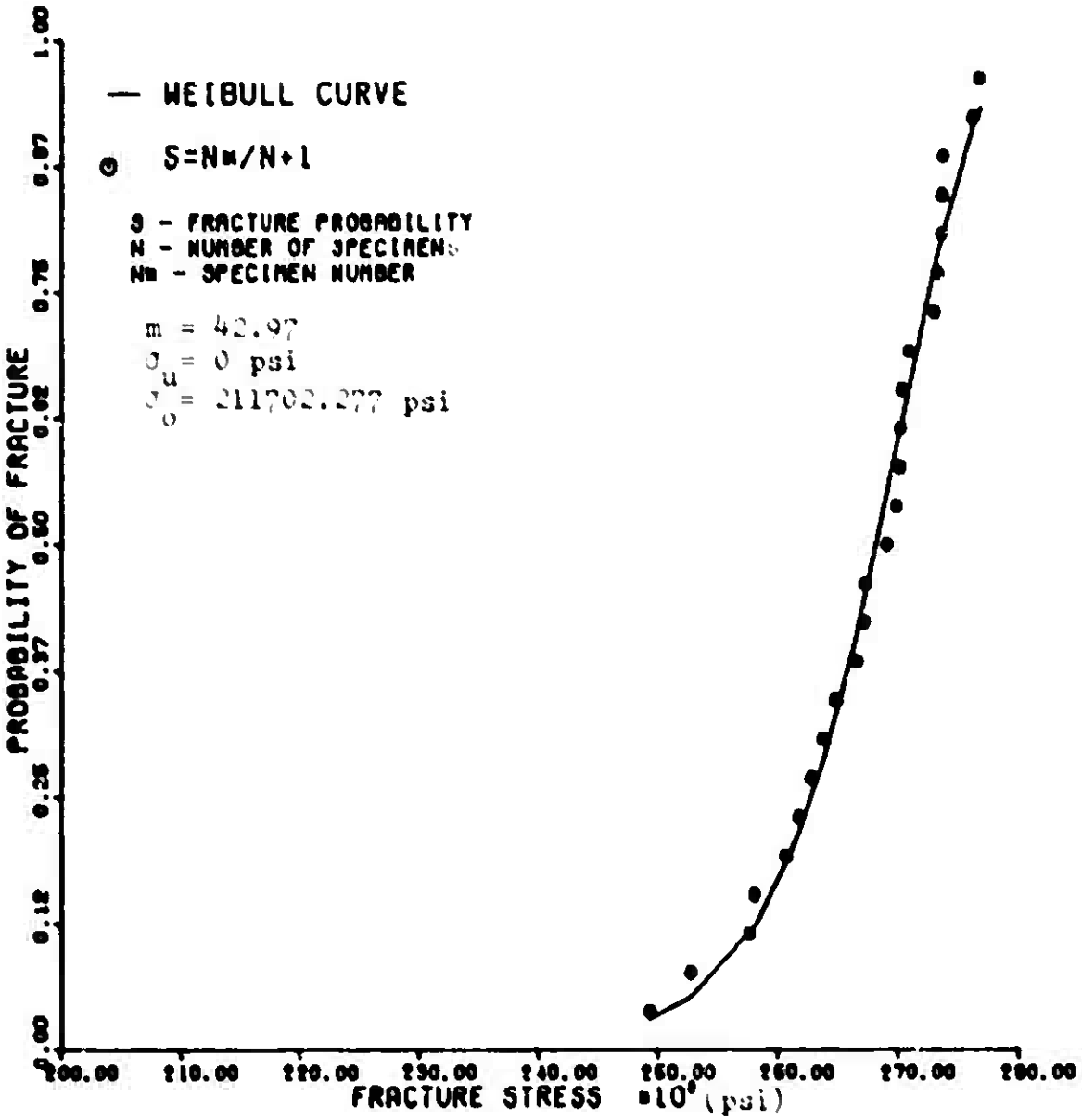

Fig. 39. Comparison of Experimental Three-point Loading Data and Theoretical Cumulative Distribution Function 0-degree Specimen

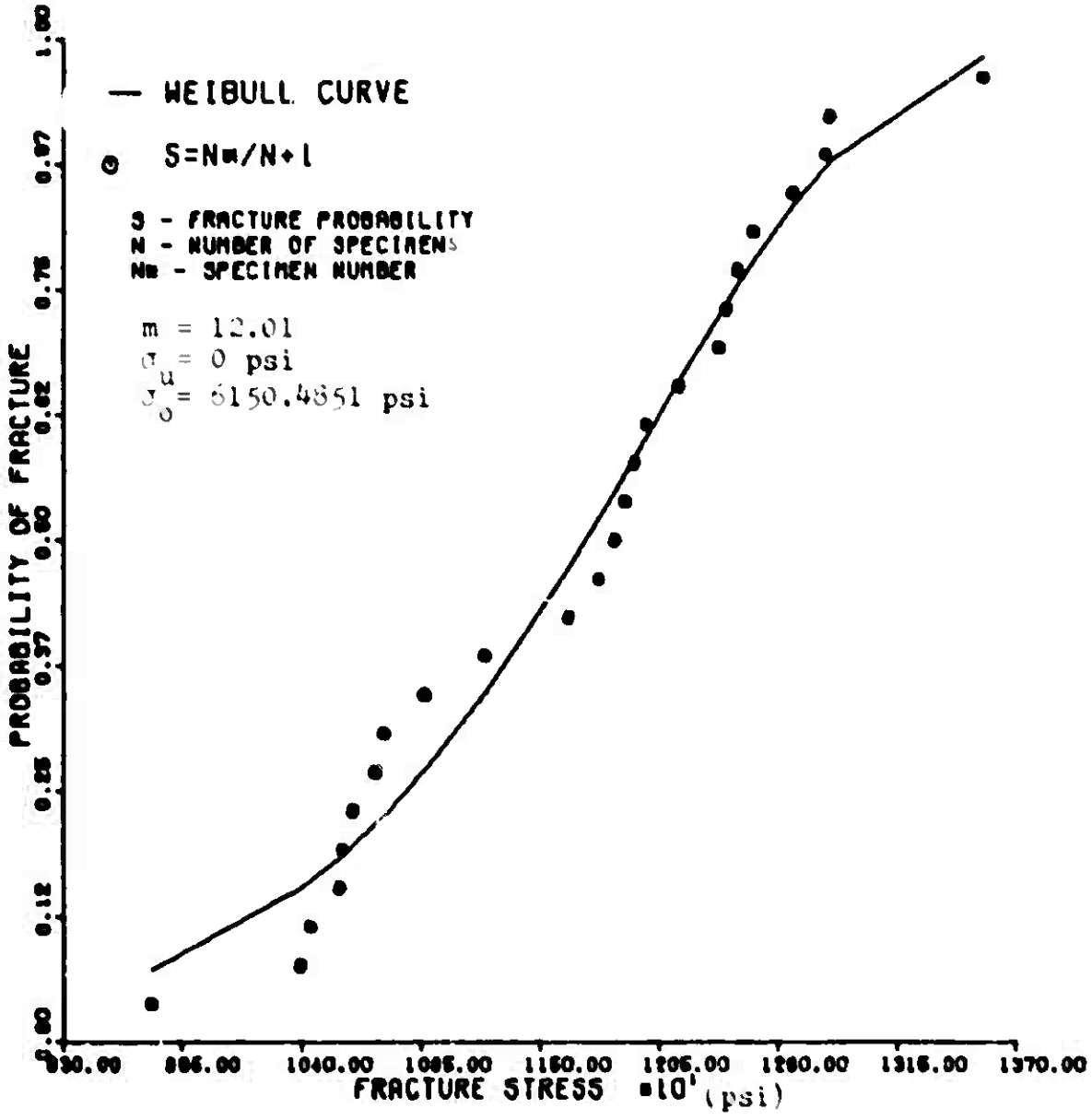

Fig. 40. Comparison of Experimental Three-point Loading Data and Theoretical Cumulative Distribution Function 90-degree Specimen

V. Conclusions and Recommendations

The objectives of establishing a set of Weibull parameter using experimental data and then correlating these parameters to other data samples was accomplished. As a result of the methodology used in the parameter determination, comparisons of various values of m, σ_u and σ_o are available for all data samples analyzed. Listed below are some specific conclusions derived from this thesis:

(1) The graphical procedures for parameter determination described by Weibull and modified by Daniel and Weil are not reproducible. The procedures result in approximations of the material parameters. These approximations can easily be replaced by parameter sets with equal failure prediction ability.

(2) The use of the above mentioned procedure does provide a fair initial guess at a linear distribution of parameter values from which, after mathematical refinement, a best set of values can be isolated through the use of a mathematical fit difference routine like the least square method.

(3) The determination of the σ_o parameter is not mathematically possible when a best fit is desired. The parameter must be determined through a trial and error process in which σ_u is fixed and combinations of m and σ_o are allowed to vary. Accu-

rate fit becomes very sensitive to the σ_o parameter.

(4) The overall analysis was found to be very sensitive to data sample size. Large variations of data points in any specific section of a distribution was found to have significant effect on all parameters. Random variations of a few data points, however, have little impact on m and σ_u but tend to affect σ_o. Addition or deletions of data points from a distribution also tended to alter the resulting best fit set of parameters at the sample size being used in this thesis. The linear representation of m and σ_u, however, was generally insensitive to this. As a result of this characterization, a minimum sample size should be determinable for which fit error convergence starts to occur.

(5) Except for the 0-degree tension and 90-degree three-point loading data the Weibull equations using a single set of material parameters were not correlatable through the three loading conditions studied for graphite-epoxy. Possible causes for these results could be attributable to the relatively small data samples used and possibly poor 90-degree tension data. However, the nature of the discrepancies does not totally support this.

(6) A check of parameter sets other than those providing the best fit per σ_u was not accomplished due to time constraints. It is conceivable that a parameter set of poorer accuracy, not falling on the linear m versus σ_u presentation exists which would allow better correlation between several failure modes.

(7) The physical interpretation generally placed on σ_u is felt not to exist. This is demonstrated by the mathematical improvement which results in the 0-degree bending data when negative values of σ_u are used.

(8) Using the three parameter form of the Weibull equation was found to provide better fit than the two parameter (σ_u assumed zero) form. For the data used in this thesis, an assumption of $\sigma_u = 0$ would have resulted in a significantly increased fit error.

(9) There are a great number of limitations in the use of the Weibull equations. For the composite studied and sample size used, the Weibull theory is only useful if the parameters are derived based on specific experimental data. Correlation was established between 0-degree tension and bending only after manipulation of the Weibull equation based on the characteristics of the available experimental data. Thus, the use of the Weibull

equations does not lead to a reduction in test requirements and the associated cost savings for composite materials. From the available data used in this study, it is appropriate to say that the only true correlation may have between the 90-degree three-point loading and 90-degree bending without instrumented specimen data samples. However, a more conclusive evidence could be developed with additional experimental information.

(10) It is recommended that the experimental data established in this study be extended with additional test data to investigate the variability of the Weibull parameters as additional data is added. Care must however be taken to insure specimen homogeneity in both geometry and material. Once a substantial sample size has been obtained, the error to parameter sensitivity can be investigated by random deletions or additions of data points within this sample.

Bibliography

1. Ashton, J. E., J. Halpin, and P. Petit. Primer on Composite Materials: Analysis. Westport, Conn.: Technomic Publishing Company, Inc., 1969.

2. Bortz, S. A. and Weil, N. A., Effect of Structural Size: The "Zero Strength." ASD-TR-61-628 Part II, 11-74. Wright-Patterson Air Force Base, Ohio: Aeronautical Systems Division: April 1963.

3. Brooks, G. A General Study of Hybrid Composite Laminates. Thesis. Wright-Patterson Air Force Base, Ohio: Air Force Institute of Technology, December, 1977.

4. Carnahan, B., Luther, H. A. and J. O. Wilkes. Applied Numerical Methods. New York: John Wiley & Sons, Inc., 1969.

5. Chou, P. C., Wang, A. S. D. and J. Awerbuch. "Statistical Failure Analysis of Composite Materials." Mechanics of Composites Review. Wright-Patterson Air Force Base, Ohio: Air Force Materials Laboratory, Air Force Office of Scientific Research and Air Force Flight Dynamics Laboratory: October, 1977.

6. Daniel, I. M. and Weil, N. A. "Analysis of Fracture Probabilities in Nonuniformly Stressed Brittle Materials." Journal of the American Ceramic Society, 47: 268-274. (June, 1964).

7. Daniel, I. M. and Weil, N. A., "The Influence of Stress Gradient upon Fracture of Brittle Materials." American Society of Mechanical Engineers, 63-WA-228, 1963.

8. Hahn, H. T. and R. Y. Kim. "Proof Testing of Composite Materials." Journal of Composite Materials, 9: 297-311 (July, 1975).

9. Halpin, J. C., Kopf, J. R. and W. Goldberg, "Time Dependent Static Strength and Reliability for Composites." Journal of Composite Materials. 4: (October, 1977).

10. Jones, R. M. Mechanics of Composite Materials. New York: McGraw-Hill Book Company, 1975.

11. Kaminski, B. E., "Effects Of Specimen Geometry On The Strength of Composite Materials," Analysis Of The Test

Methods For High Modulus Fiber And Composites, ASTM STP 521, ASTM, pp. 181-191. (1973).

12. Knight, M. and H. T. Hahn. "Strength and Elastic Modulus of a Randomly-Distributed Short Fiber Composite." Journal of Composite Materials, 9: 77-90 (January, 1975).

13. Kopf, J. R. Application of the Fracture Properties of a Composite Material to the Development of a Reliability Plan. Thesis. Wright-Patterson Air Force Base, Ohio: Air Force Institute of Technology, June, 1970.

14. Tsai, S. W. and H. T. Hahn. Composite Material Workbook. AFML-TR-77-33. Wright-Patterson Air Force Base, Ohio. March, 1977.

15. Weibull, Walloddi. A new Method for the Statistical Treatment of Fatigue Data. Linkoping, Sweden: Aircraft Company. May, 1954.

16. Weibull, W. A., Statistical Theory of the Strength of Materials. Stockholm: Generalstabens Litografisk Anstalt Forlag, 1939.

17. Whitney, J. M., Browning, C., and Mair, A., "Analysis of the Flexure Test for Laminated Composite Materials." Composite Materials Testing and Design (Third Conference), ASTM STP 546, pp. 30-45 (1974).

18. Young, H. D. Statistical Treatment of Experimental Data. New York: McGraw-Hill Book Company, Inc., 1962.

APPENDIX A

Three-Point Loading Equation Derivation

This appendix provides the detailed steps required to obtain the form of the risk of rupture equation shown for Equation (11).

Starting with Equation (8)

$$B = \frac{2}{\sigma_o^m} \int_0^b \int_{x_u}^{L/2} \int_{z_u}^{h/2} \left(\frac{4\sigma_b}{hL} XZ - \sigma_u \right)^m dV \tag{1A}$$

where $$x_u = \frac{\sigma_u hL}{\sigma_b 4Z} \tag{2A}$$

and $$z_u = \frac{\sigma_u h}{\sigma_b 2} \tag{3A}$$

Integrating with respect to Y yields

$$B = \frac{2b}{\sigma_o^m} \int_{x_u}^{L/2} \int_{z_u}^{h/2} \left(\frac{4\sigma_b}{hL} XZ - \sigma_u \right)^m dx\, dz \tag{4A}$$

Integrating with respect to X yields

$$B = \frac{2b}{\sigma_o^m} \int_{z_u}^{h/2} \left[\frac{\left(\frac{4\sigma_b}{hL} XZ - \sigma_u \right)^{m+1}}{\frac{4\sigma_b}{hL} Z (m+1)} \right] \Bigg|_{x_u}^{L/2} dz \tag{5A}$$

taking out the constants

$$B = \frac{(hbL)^2}{4\sigma_o^m \sigma_b (m+1)} \int_{z_u}^{h/2} \frac{1}{Z} \left(\frac{4\sigma_b}{hL} XZ - \sigma_u \right)^{m+1} \Bigg|_{x_u}^{L/2} dz \tag{6A}$$

substituting the integration limits yields

$$B = \frac{V}{2(m+1)\sigma_o^m \sigma_b} \int_{z_u}^{h/2} \frac{1}{Z} \left(\frac{2\sigma_b}{h} Z - \sigma_u \right)^{m+1} dz \tag{7A}$$

Defining

$$I = \int_{z_u}^{h/2} \frac{1}{Z} \left(\frac{2\sigma_b}{h} Z - \sigma_u \right)^{m+1} dz \tag{8A}$$

The integration of this integral is now addressed separately in the following manner.

Defining $$\sigma = \frac{2\sigma_b}{h} \tag{9A}$$

then

$$I = \int_{z_u}^{h/2} \frac{1}{z} (\sigma z - \sigma_u)^{m+1} dz \tag{10A}$$

Integration of this term results in the following

$$I = \frac{(\sigma z - \sigma_u)^{m+1}}{m+1} \Big|_{z_u}^{h/2} - \frac{(-\sigma)(m+1)}{(m+1)} \int_{z_u}^{h/2} \frac{1}{z} (\sigma z - \sigma_u)^m \tag{11A}$$

Further integration of the resulting integral leads to a form which can be expressed in series notation

$$I = \left\{ \sum_{r=0}^{N} \frac{(\sigma_b - \sigma_u)^{m+1-r}}{m+1-r} (-\sigma_u)^r \right\} + (-\sigma)^{N+1} \int_{z_u}^{h/2} \frac{1}{z} \left(\frac{2\sigma_b z}{h} - \sigma_u \right)^{m-N} dz \tag{12A}$$

using the following definitions

$$m = \bar{m} + \alpha \tag{13A}$$

$$N = \bar{m} \tag{14A}$$

leads to the form defined in Equation (11)

$$I = \left\{ \sum_{r=0}^{\bar{m}} \frac{(\sigma_b - \sigma_u)^{m+1-r}}{m+1-r} (\sigma_u)^r \right\} + (-\sigma_u)^{\bar{m}+1} \int_{z_u}^{h/2} \frac{1}{z} \left(\frac{2\sigma_b z}{h} - \sigma_u \right)^{\alpha} dz \tag{15A}$$

Substitution of this final expression for I into the risk of rupture equation will result in the form of this equation shown in Equation (11).

$$B = \frac{V}{2(m+1)\sigma_b \sigma_o^m}\left\{(\sigma_b-\sigma_u)^{m+1}\sum_{r=0}^{\bar{m}}\frac{1}{m+1-r}\left(1-\frac{\sigma_b}{\sigma_u}\right)^{-r}+\left(-\sigma_u\right)^{\bar{m}+1}\int_{z_u}^{h/2}\frac{1}{z}\left(\frac{2\sigma_b z}{h}-\sigma_u\right)^{\bar{m}+1}dz\right\} \tag{16A}$$

APPENDIX B

Experimental Data

This appendix provides a compilation of the experimental data gathered for this study.

Table IX.
Four Point Loading Data - 0-degree Specimen

Specimen Number	Thickness (in)	Width (in)	Volume (in^3)	Load (lb)	Stress** (lb/in^2)
1A	.0779	.4993	.0512	373.0	242449.12
2A	.0805	.4999	.0531	394.5	240208.92
3A	.0782	.4985	.0513	399.0	258173.25
*4A	.0783	.4995	.0514	340.0	218996.37
5A	.0810	.5003	.0533	429.0	257794.57
6A	.0792	.5002	.0521	416.0	261526.86
8A	.0810	.4996	.0532	427.0	256952.25
9A	.0796	.4986	.0522	420.0	262233.33
10A	.0775	.4986	.0508	372.0	245021.54
11A	.0803	.4989	.0527	394.0	241584.26
13A	.0784	.5000	.0515	387.0	248385.28
14A	.0809	.4999	.0532	421.0	253815.96
15A	.0810	.4990	.0532	393.5	237077.95
16A	.0809	.5009	.0533	420.0	252767.56
17A	.0815	.4973	.0533	430.0	256774.44
*18A	.0817	.4994	.0537	390.0	230775.11
19A	.0815	.4993	.0535	414.0	247220.04
20A	.0814	.5008	.0536	430.0	255606.76
21A	.0797	.4988	.0523	434.0	270186.51
22A	.0784	.4995	.0515	406.0	260840.74
23A	.0785	.5007	.0517	411.0	262749.52
24A	.0811	.4988	.0532	447.0	268754.89
25A	.0783	.4998	.0515	414.0	271885.71
*32A	.0793	.4999	.0521	380.0	238435.60
*40A	.0769	.5001	.0506	349.0	232773.16
*42A	.0774	.4979	.0507	328.0	211613.29

* Strain-gaged Specimen. ** Calculated - using $\sigma = Mc/I$

Table X.
Four Point Loading Data - 90-degree Specimen

Specimen Number	Thickness (in)	Width (in)	Volume (in^3)	Load (lb)	Stress** (lb/in^2)
1B	.0779	.4982	.0510	13.2	8612.16
2B	.0785	.5040	.0520	15.5	9844.16
3B	.0789	.5041	.0523	15.9	9994.09
4B	.0784	.4954	.0511	14.1	9133.73
6B	.0777	.5025	.0513	14.9	9687.80
7B	.0776	.4899	.0499	14.1	9427.69
8B	.0790	.5361	.0560	15.6	9196.90
*9B	.0780	.5049	.0518	18.6	11943.60
10B	.0773	.4950	.0503	13.9	9269.74
11B	.0789	.5040	.0523	14.0	8801.58
12B	.0780	.5033	.0516	17.0	10950.90
13B	.0775	.4987	.0508	14.0	9219.39
14B	.0791	.5035	.0524	15.2	9517.18
16B	.0771	.4964	.0503	18.1	12099.16
*17B	.0789	.5038	.0523	19.5	12264.21
18B	.0778	.5034	.0515	17.1	11069.82
19B	.0772	.4968	.0504	14.0	9326.72
21B	.0785	.5020	.0520	16.8	10712.30
22B	.0772	.4952	.0503	14.0	9356.85
23B	.0790	.5037	.0523	15.9	9976.73
24B	.0790	.5014	.0521	15.9	10022.49
25B	.0772	.4967	.0504	14.2	9461.86
*26B	.0790	.5028	.0520	19.8	12446.08
27B	.0792	.5022	.0523	15.9	9956.05
*30B	.0786	.5015	.0518	18.0	11459.71
*43B	.0764	.5030	.0505	16.0	10749.35

* Strain-gaged Specimen

** Calculated - using $\sigma = Mc/I$

Table XI.
Tension Loading Data - 0-degree Specimen

Specimen Number	Thickness (in)	Width (in)	Volume (in^3)	Load (lb)	Stress** (lb/in^2)
*0- 1	.0383	.4987	.1146	4785	250520.81
*0- 2	.0395	.4971	.1176	4585	233506.23
*0- 3	.0387	.4999	.1158	5275	272664.35
*0- 4	.0394	.5000	.1182	5300	269035.53
*0- 5	.0394	.4999	.1182	5550	281782.24
0- 6	.0388	.4914	.1146	5010	262767.02
0- 7	.0384	.4996	.1152	4375	228047.02
0- 8	.0396	.5001	.1188	4940	249445.06
0- 9	.0399	.5002	.1198	5050	253031.62
0-10	.0398	.5000	.1194	5430	272864.32
0-11	.0379	.4882	.1110	4840	261582.31
0-12	.0385	.4995	.1152	4930	256360.26
0-13	.0404	.4988	.1212	5465	271195.42
0-14	.0387	.5010	.1164	4710	242925.00
0-15	.0393	.5007	.1182	5125	260449.62
0-16	.0391	.5002	.1176	5075	259487.00
0-17	.0392	.5044	.1188	5000	252876.73
0-19	.0390	.4997	.1170	5040	258616.71
0-18	.0392	.4994	.1176	5060	258473.43
0-20	.0397	.4993	.1188	4220	212892.51
0-21	.0398	.4992	.1194	4675	235301.10
0-22	.0385	.4996	.1152	4850	252149.77
0-23	.0404	.4993	.1194	5075	254105.75
0-24	.0396	.4992	.1188	4670	235352.97
0-25	.0395	.4998	.1182	4150	210717.20

* Strain-gaged Specimen

** Calculated - using $\sigma = P/A$

Table XII.
Tension Loading Data - 90-degree Specimen

Specimen Number	Thickness (in)	Width (in)	Volume (in^3)	Load (lb)	Stress** (lb/in^2)
*90- 1	.0393	.9960	.1173	280	7153.30
*90- 2#	.0392	.9962	.1170	280	7170.10
*90- 3#	.0390	.9943	.1164	274	7065.92
*90- 4#	.0391	.9956	.1167	208	5343.20
*90- 5	.0394	.9948	.1176	368	9388.92
90- 6	.0391	.9993	.1167	237	6093.07
90- 7#	.0387	.9963	.1158	325	8429.12
90- 8	.0395	.9952	.1179	295	7504.38
90- 9	.0395	.9961	.1179	258	6557.22
90-10	.0395	.9956	.1179	255	6484.23
90-11#	.0390	.9956	.1169	328	8447.43
90-12	.0394	.9945	.1176	183	4670.36
90-13	.0385	.9952	.1149	282	7360.00
90-14#	.0393	.9953	.1173	291	7439.55
90-15	.0393	.9954	.1173	331	8461.31
90-16	.0390	.9941	.1164	289	7454.24
90-17	.0395	.9959	.1179	209	5312.92
90-18	.0395	.9961	.1179	309	7853.41
90-19	.0393	.9966	.1176	252	6434.09
90-20	.0395	1.0001	.1185	318	8049.83
90-21	.0393	.9950	.1173	250	6393.29
90-22#	.0397	.9959	.1185	280	7081.93
90-23#	.0393	.9962	.1176	282	7202.94
90-24	.0393	.9964	.1176	320	8171.91
90-25	.0393	.9964	.1176	360	9193.40

* Strain-gaged Specimen # Fractured at tabs
** Calculated - using $\sigma = P/A$

Table XIII.
Three Point Loading Data - 0-degree Specimen

Specimen Number	Thickness (in)	Width (in)	Volume (in^3)	Load (lb)	Stress** (lb/in^2)
* 7A	.0776	.4986	.1018	208.0	273296.85
*26A	.0796	.4994	.1045	210.0	261813.25
27A	.0784	.4994	.1030	208.0	267318.91
28A	.0781	.4998	.1027	211.0	273043.06
29A	.0789	.5005	.1039	211.0	267159.96
30A	.0795	.4988	.1043	213.0	266542.16
32A	.0816	.4987	.1070	233.0	276810.94
35A	.0799	.4965	.1043	207.0	257634.81
40A	.0783	.4961	.1022	213.0	276270.08
42A	.0787	.4980	.1031	214.0	273704.52
43A	.0777	.4982	.1018	206.0	270189.50
*45A	.0776	.4967	.1014	200.0	263790.65
49A	.0768	.4997	.1009	202.0	270375.03
1C	.0772	.4932	.1001	204.0	273791.21
4C	.0775	.5013	.1022	206.0	269906.36
12C	.0789	.5002	.1038	216.0	273654.80
14C	.0822	.4994	.1080	223.0	260711.21
16C	.0784	.4981	.1027	204.0	262862.42
17C	.0807	.5005	.1062	206.0	249323.42
*24C	.0806	.4998	.1059	208.0	252722.56
25C	.0789	.5001	.1038	209.0	264839.30
*32C	.0811	.5020	.1071	216.0	258080.58
34C	.0789	.4995	.1036	213.0	270232.21
36C	.0787	.5007	.1036	213.0	270956.49
44C	.0780	.5011	.1028	208.0	269151.46

* Strain-gaged Specimen

** Calculated - using $\sigma = Mc/I$

Table XIV.
Three Point Loading Data - 90-degree Specimen

Specimen Number	Thickness (in)	Width (in)	Volume (in^3)	Load (lb)	Stress** (lb/in^2)
28B	.0773	.4996	.1016	7.9	10439.81
29B	.0795	.5019	.1049	8.5	10570.96
30B	.0792	.5032	.1048	9.0	11248.60
31B	.0773	.4990	.1014	8.0	10584.67
32B	.0798	.5028	.1055	8.9	10965.69
*33B	.0795	.5028	.1051	10.0	12414.16
34B	.0776	.4990	.1018	8.1	10634.28
35B	.0792	.5036	.1049	10.0	12488.52
37B	.0765	.4999	.1006	7.2	9708.98
38B	.0782	.5026	.1034	9.3	11936.97
39B	.0787	.5025	.1040	8.2	10393.82
40B	.0771	.4987	.1011	8.9	11843.74
41B	.0797	.5041	.1057	11.0	13552.09
42B	.0790	.5045	.1048	8.6	10775.32
43B	.0765	.4995	.1005	9.0	12145.94
*44B	.0796	.5036	.1054	9.7	11992.42
45B	.0781	.5043	.1036	10.0	12824.96
46B	.0787	.4995	.1008	8.0	10740.16
47B	.0800	.5024	.1057	9.5	11630.31
48B	.0787	.5035	.1042	9.4	11891.21
50B	.0793	.5024	.1048	9.9	12361.93
51B	.0784	.5049	.1041	9.7	12330.52
* 5B	.0787	.5025	.1040	10.0	12672.87
*15B	.0782	.5023	.1033	10.0	12843.11
*20B	.0792	.5022	.1046	9.4	11771.93

* Strain-gaged Specimen ** Calculated - using $\sigma = Mc/I$

APPENDIX C

Data Plots

This appendix provides graphical data verifying the linear relationship between the values of m and σ_u. Also, the validity of using the sum of the mean error technique for isolation of the best set of values can easily be seen by plot comparisons of similar data.

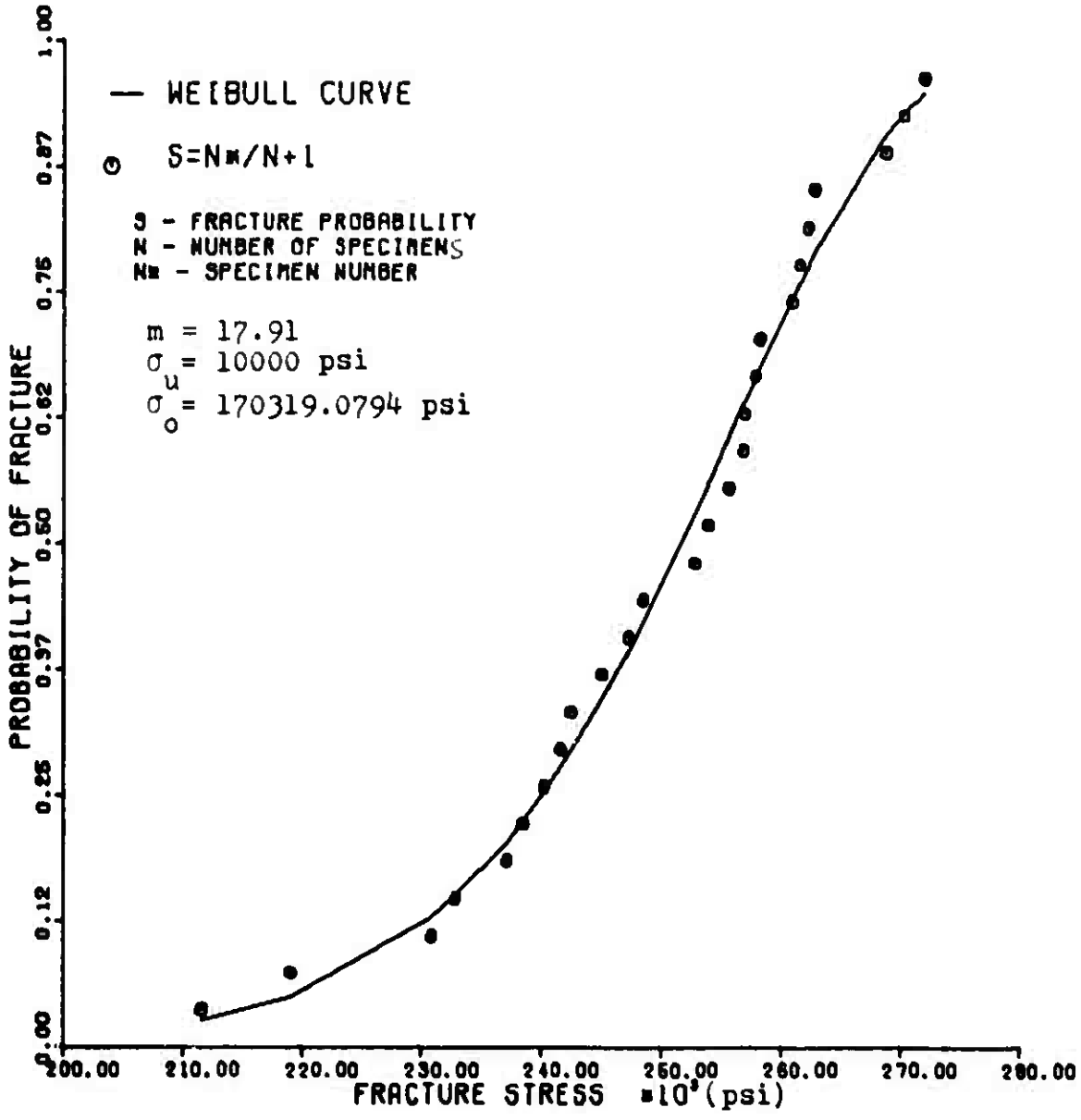

Fig. 1C. Comparison of Experimental Bending Data and Theoretical Cumulative Distribution Function 0-degree Specimen

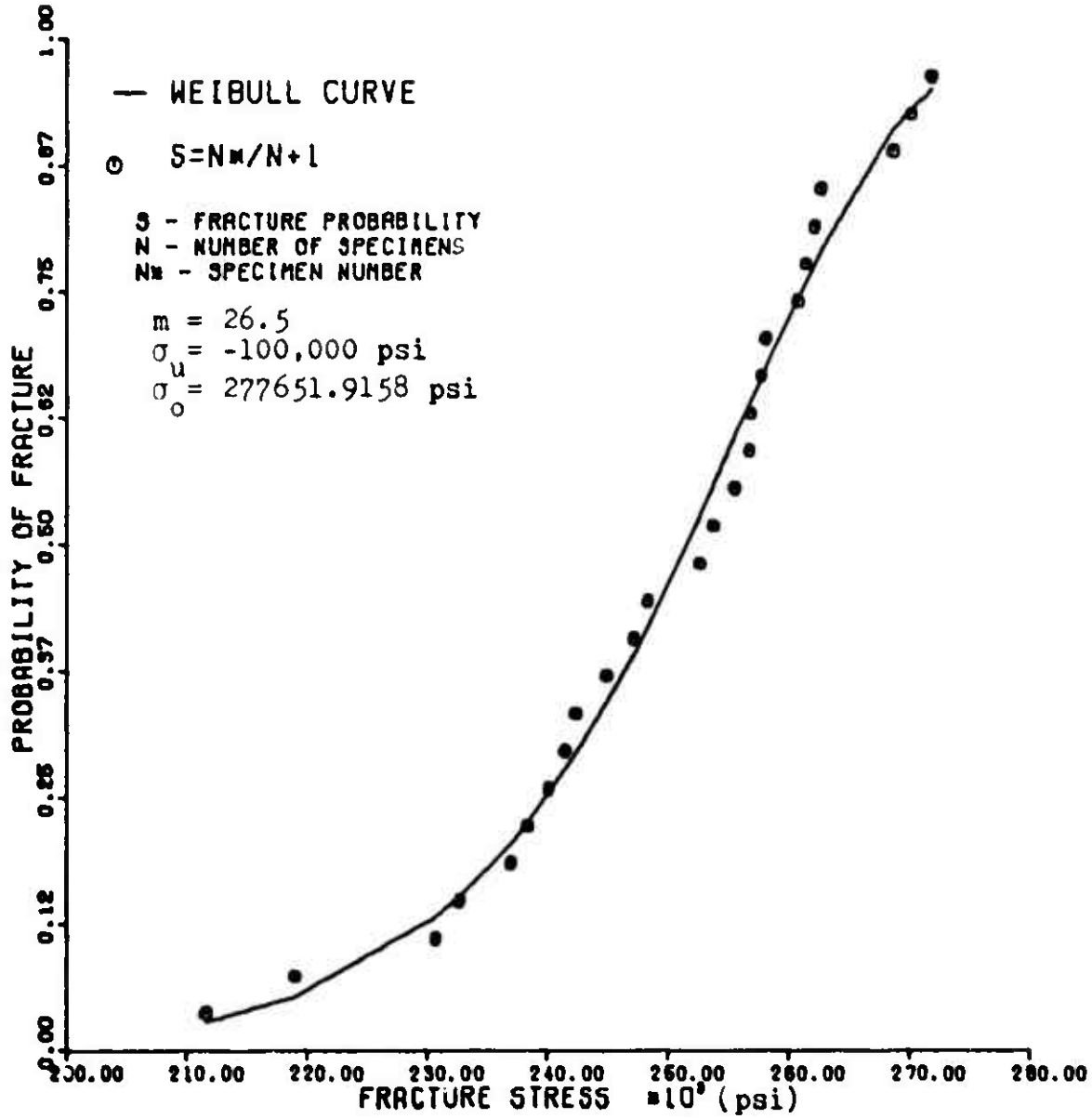

Fig. 2C. Comparison of Experimental Bending Data and Theoretical Cumulative Distribution Function 0-degree Specimen

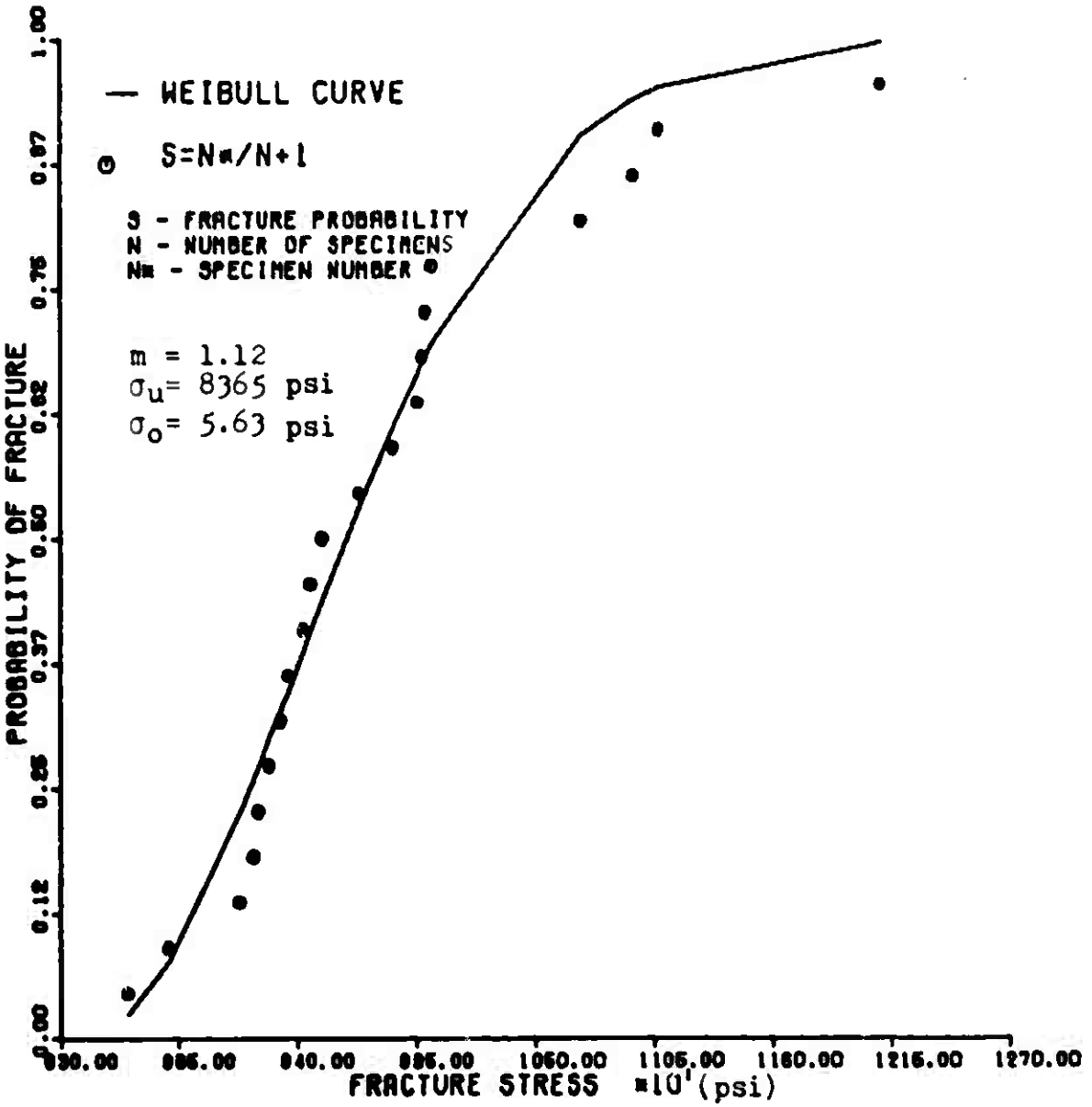

Fig. 3C. Comparison of Experimental Bending Data and Theoretical Cumulative Distribution Function 90-degree Specimen*

* without strain gaged specimens

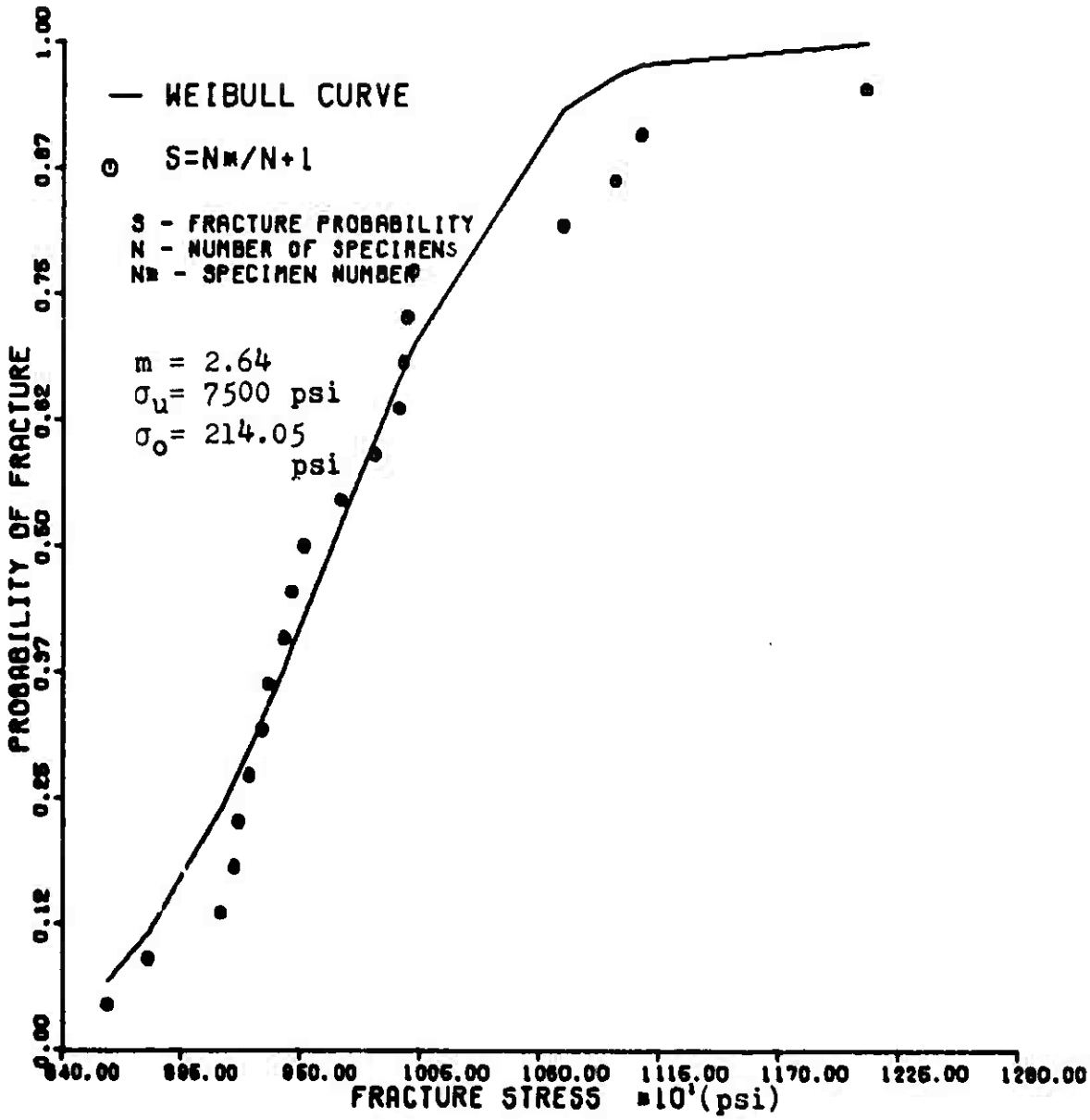

Fig. 4C. Comparison of Experimental Bending Data and Theoretical Cumulative Distribution Function 90-degree Specimen*

* without strain gaged specimens

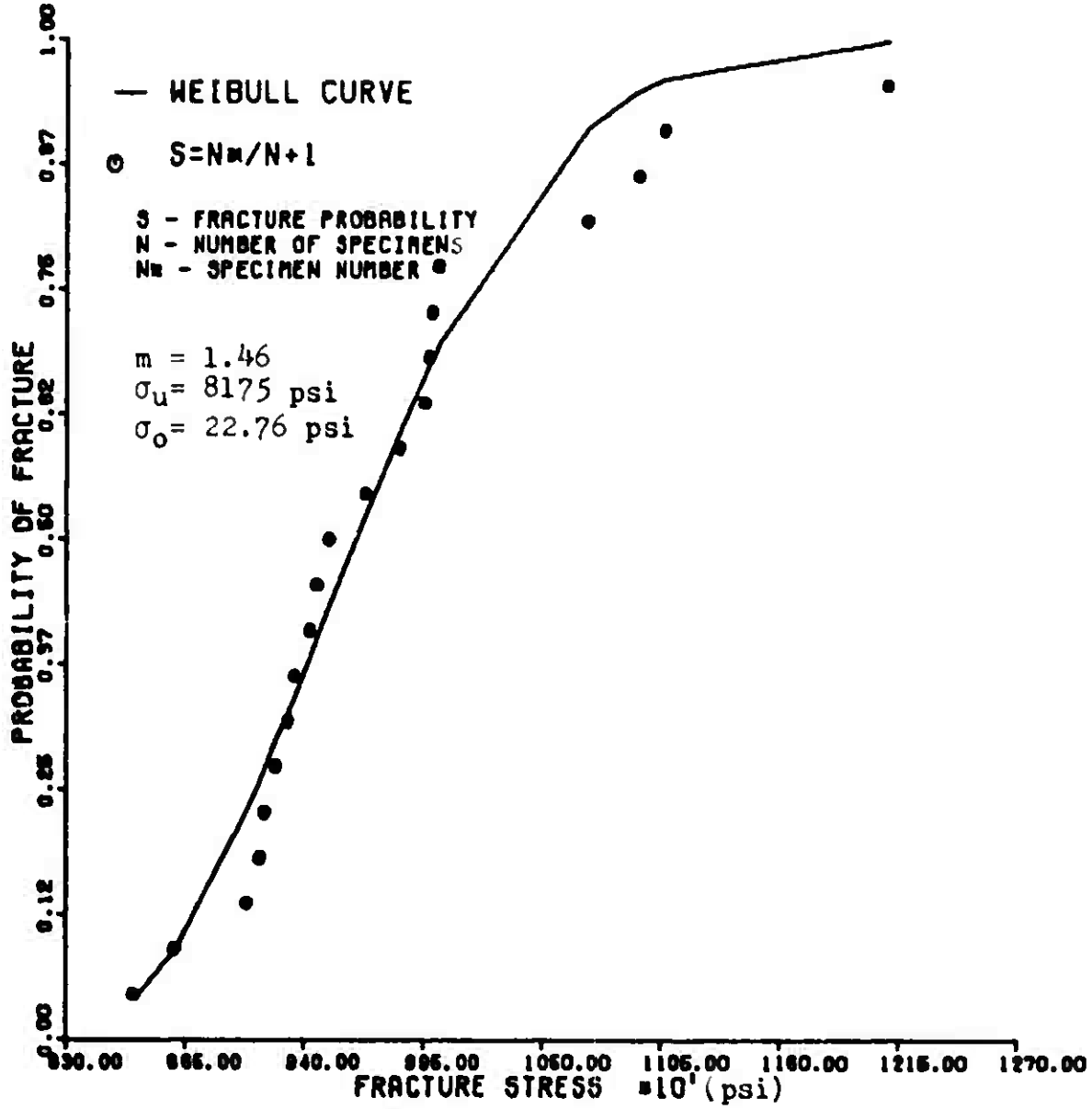

Fig. 5C. Comparison of Experimental Bending Data and Theoretical Cumulative Distribution Function 90-degree Specimen*

* without strain gaged specimens

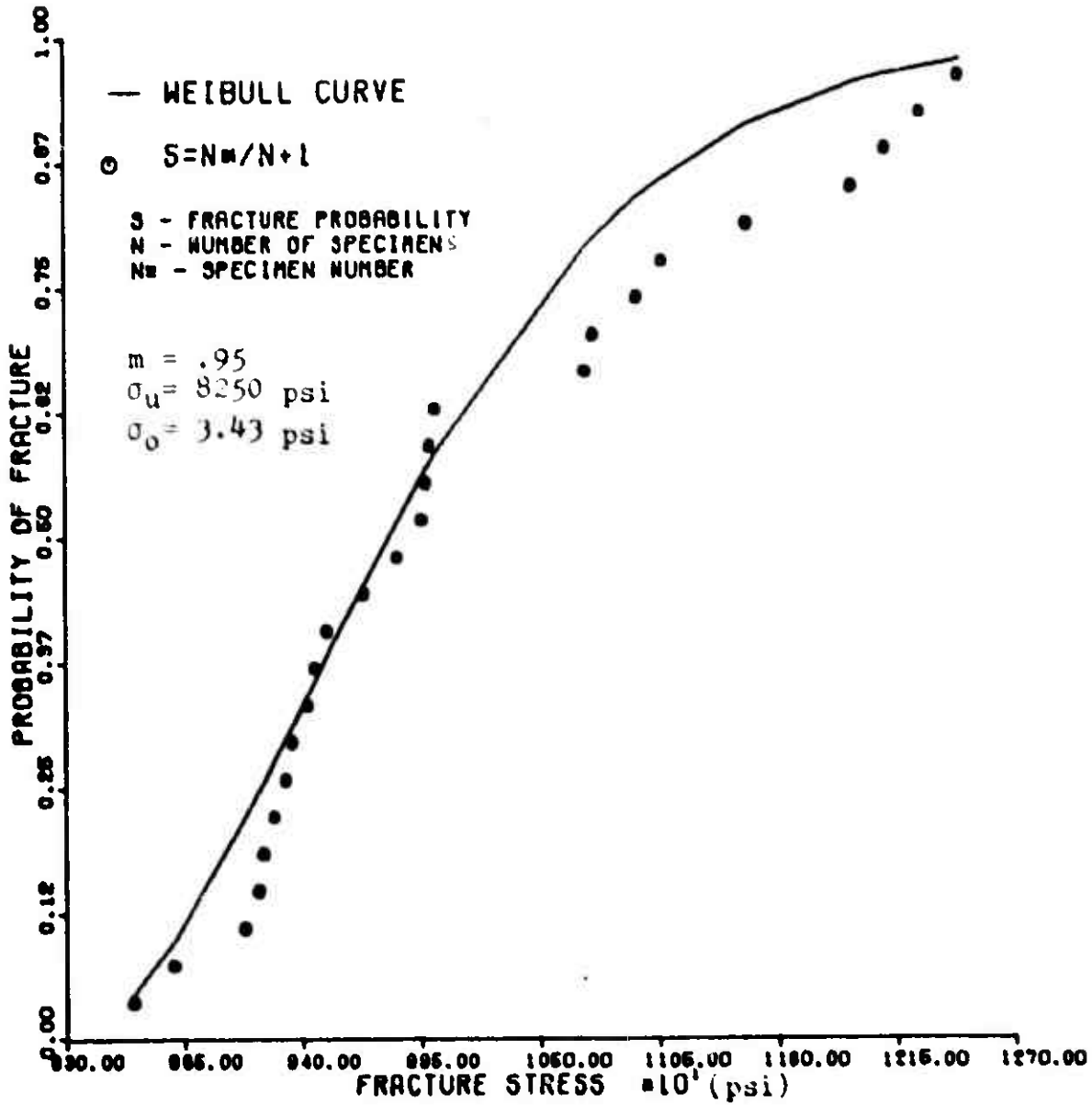

Fig. 6C. Comparison of Experimental Bending Data and Theoretical Cumulative Distribution Function 90-degree Specimen*

* including strain gaged specimens.

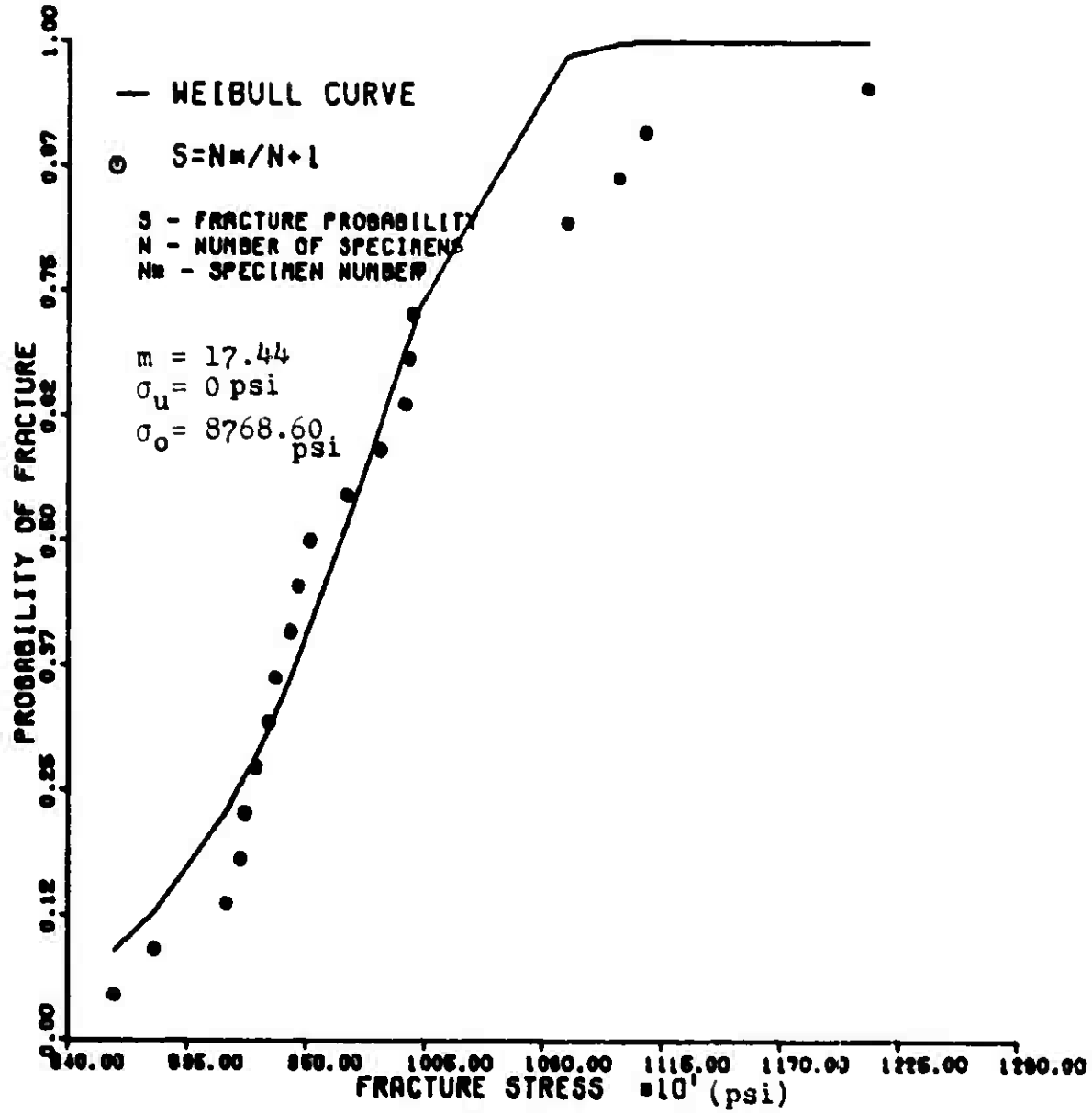

Fig. 7C. Comparison of Experimental Bending Data and Theoretical Cumulative Distribution Function 90-degree Specimen*

* without strain gaged specimens

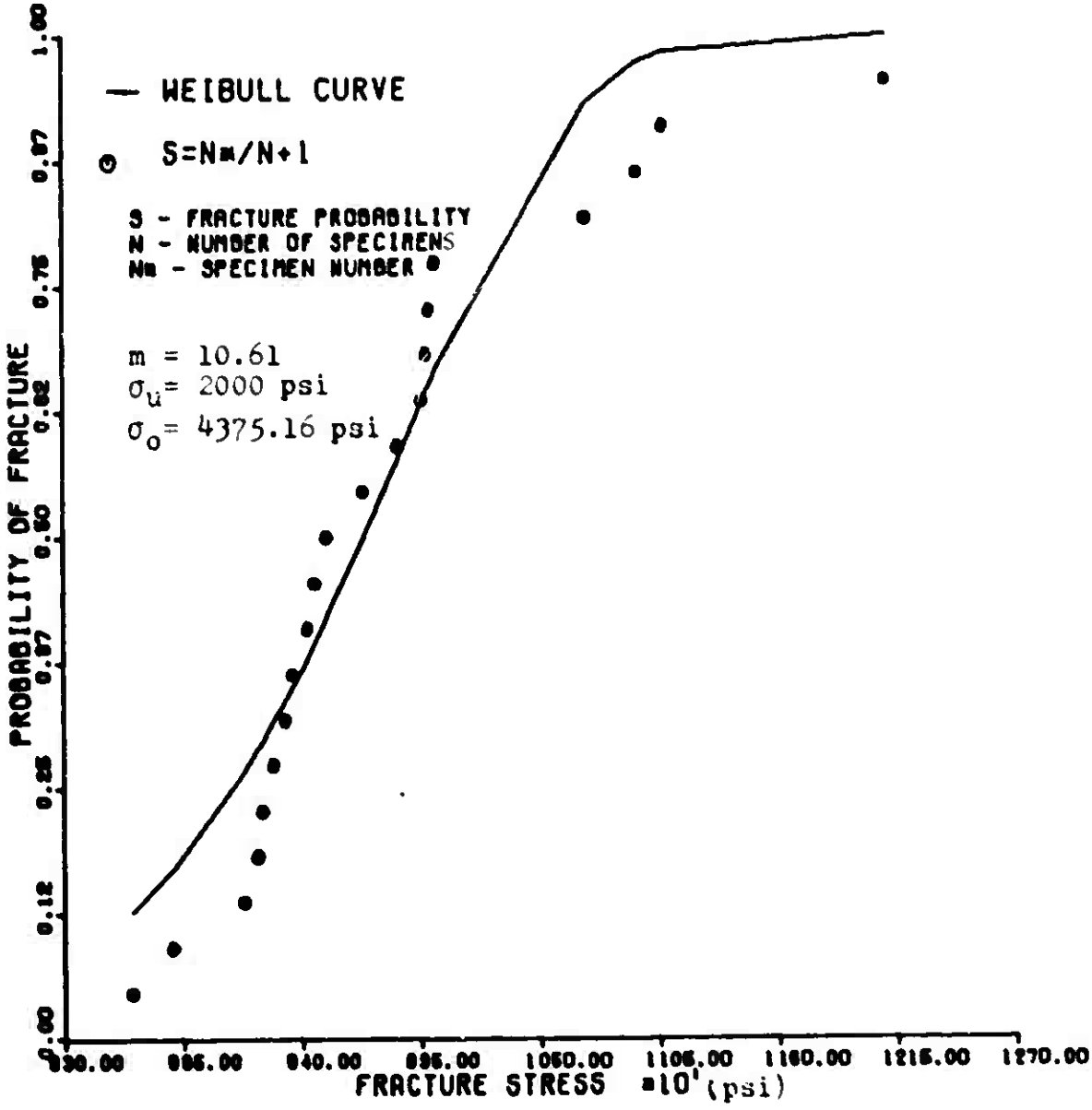

Fig. 8C. Comparison of Experimental Bending Data and Theoretical Cumulative Distribution Function 90-degree Specimen*

* without strain gaged specimens

Vita

Dennis R. Schneider was born on [redacted], in [redacted]. He graduated from [redacted] High School in [redacted]. He graduated from Northrop Institute of Technology in 1967, with a Bachelor of Science Degree in Aeronautical and Astronautical Engineering. He entered the Air Force in 1967 and has served as project officer for advanced strategic missile development projects as well as test manager for target drones, air to air missiles and laser guided bombs. In August of 1975, he enrolled in the Air Force Institute of Technology in the graduate Aeronautical Structures Engineering Program.

UNCLASSIFIED

SECURITY CLASSIFICATION OF THIS PAGE (When Data Entered)

REPORT DOCUMENTATION PAGE		READ INSTRUCTIONS BEFORE COMPLETING FORM
1. REPORT NUMBER AFIT/GAE/AA/78M-14	2. GOVT ACCESSION NO.	3. RECIPIENT'S CATALOG NUMBER
4. TITLE (and Subtitle) EVALUATION OF THE THREE PARAMETER WEIBULL DISTRIBUTION FUNCTION FOR PREDICTING FRACTURE PROBABILITY IN COMPOSITE MATERIALS		5. TYPE OF REPORT & PERIOD COVERED MS THESIS 6. PERFORMING ORG. REPORT NUMBER
7. AUTHOR(s) Dennis R. Schneider Captain USAF		8. CONTRACT OR GRANT NUMBER(s)
9. PERFORMING ORGANIZATION NAME AND ADDRESS Air Force Institute of Technology (AFIT/ENA) Wright-Patterson AFB, Ohio 45433		10. PROGRAM ELEMENT, PROJECT, TASK AREA & WORK UNIT NUMBERS
11. CONTROLLING OFFICE NAME AND ADDRESS Air Force Materials Laboratory (AFML) Wright-Patterson AFB, Ohio 45433		12. REPORT DATE March 1978 13. NUMBER OF PAGES 132
14. MONITORING AGENCY NAME & ADDRESS(if different from Controlling Office)		15. SECURITY CLASS. (of this report) UNCLASSIFIED 15a. DECLASSIFICATION DOWNGRADING SCHEDULE

16. DISTRIBUTION STATEMENT (of this Report)

Approved for public release; distribution unlimited

17. DISTRIBUTION STATEMENT (of the abstract entered in Block 20, if different from Report)

18. SUPPLEMENTARY NOTES

Approved for public release; IAW AFR 190-17

JERREL F. GUESS, Captain, USAF
Director of Information

19. KEY WORDS (Continue on reverse side if necessary and identify by block number)

Composite laminates
Weibull Theory
Composite Materials
Failure
Probability of failure
Weibull distribution function
Failure Stress

20. ABSTRACT (Continue on reverse side if necessary and identify by block number)

This thesis is an evaluation of the three parameter Weibull distribution function for predicting fracture in a composite material subjected to failure under both uniform and nonuniform stress distributions. The specific forms of the three parameter Weibull equations for these failure modes are derived for a general laminated composite and simplified for the special case of a unidirectional composite. An analysis into a parameter determination methodology which is mathematically reproducible is presented.

DD FORM 1 JAN 73 1473 EDITION OF 1 NOV 65 IS OBSOLETE

UNCLASSIFIED

SECURITY CLASSIFICATION OF THIS PAGE (When Data Entered)

The resulting expressions and methodology are applied to experimental bending, tension and three-point loading failure data for 0-degree and 90-degree unidirectionally laminated graphite-epoxy specimen. Weibull parameter sets are derived from both the bending and tension experimental data. Each set is then used to evaluate the theory's ability to predict the probability of failure throughout the three failure modes and thereby to establish a single set characteristic of the material. Although a set of parameters peculiar to each failure distribution was obtained, a characteristic set of values capable of predicting failure across the variety of failure modes was not found for this composite material.